Final work : Impact Damage Modelling on Composite Structures

Auteur : Jerez Sotoca, Irene
Promoteur(s) : Ponthot, Jean-Philippe
Faculté : Faculté des Sciences appliquées
Diplôme : Master en ingénieur civil en aérospatiale, à finalité spécialisée en "turbomachinery aeromechanics (THRUST)"
Année académique : 2022-2023
URI/URL : http://hdl.handle.net/2268.2/18327

UNIVERSITÉ DE LIÈGE - FACULTÉ DES SCIENCES APPLIQUÉES

IMPACT DAMAGE MODELLING ON COMPOSITE STRUCTURES

Academic Promoter
PROF. JEAN-PHILLIPPE PONTHOT

KTH Supervisor and Director of the THRUST Program
PROF. NENAD GLODIC

MASTER THESIS CARRIED OUT TO OBTAIN THE DEGREE OF MASTER OF SCIENCE IN THRUST BY IRENE JEREZ SOTOCA

ACADEMIC YEAR 2022–2023

Members of the jury

Prof. Jean–Philipe PONTHOT, *Academic Promoter*
University of Liège, Faculty of Engineering (Liège, Belgium)
Department of Aerospace & Mechanical engineering
Computational Mechanics Laboratory, MN2L

Prof. Nenad GLODIC, *Academic Promoter*
KTH Royal Institute of Technology (Stockholm, Sweden)
UNIT OF HEAT AND POWER TECHNOLOGY
Brinellvägen, 68

Prof. Ludovic NOELS
University of Liège, Faculty of Engineering (Liège, Belgium)
Department of Aerospace & Mechanical engineering
Computational & Multiscale Mechanics of Materials (CM3)

Abstract

The advanced properties of carbon fiber reinforced composite materials, such as their low strength and stiffness-weight ratios, make them a very attractive alternative for aerospace applications, particularly for fan-blade design. However, their integration is truncated due to its susceptibility to impact phenomena, and the lack of reliable numerical models that capable to predict their damage response. Aircraft components, particularly fan blades, are known to experience harmful foreign impact events e.g. tool-drop, ice ingestion, bird strike, etc. The aim of this project is to provide the necessary theoretical background on the failure mechanisms experienced by a composite during an impact, and to build Foreign Object Impact (FOI) model on a rectangular composite plate for the cases of low and high velocity. The focus of the high velocity model is to validate the ballistic response of a composite rectangular plate by means of experimental and numerical results found in the literature [6, 39], and to analyze the main sources of damage present and the influence of relevant physical properties i.e. thickness, stackup sequence, etc. On the other hand, the low velocity model is focused in delamination modelling. Two different sub-models are developed in this case: (1) ”Elastic Model”, in which only interlaminar damage between the plies is modelled and, (2) ”Failure Model”, where both intra and interlaminar failure are considered. The final goal is to provide an organized numerical methodology to model an impact on a composite structure and to analyze the effect of the projectile velocity on the damage mechanism developed by the composite target.

Keywords: Foreign Object Damage (FOD), Intralaminar failure, Interlaminar failure or Delamination, Tiebreak contact, Residual velocity

Acknowledgement

First and foremost, I would like to express my deepest gratitude to my advisers for this master thesis: *Professor Jean–Philippe Ponthot* and *Professor Nenad Glodic*.

Professor Ponthot, thank you enormously for your valuable feedback on every draft, your flexibility and the interest you have always shown during the development of this project, even coming to KTH University in Stockholm to do follow up meeting in person. Thank you also, for giving me and rest of the THRUST students a little piece of your wide knowledge on Finite Element Methods and Continuum Mechanics. Thanks to teachers like you I have became the engineer that I am today.

Professor Glodic, thank you for the proposal of this Master Thesis, in the frame of a the EleFanT project in partnership with a company like GKN Aerospace. Thank for your time and for giving us your opinion on every follow up meeting, but specially thank you for the trust that you have always put in me and for making KTH University feel like home to me. Thank you also for these two years directing the THRUST program, this program has provided all of us not only with technical but with personal experiences that I will carry during my whole life.

Finally, I would like to warmly thank my parents *Miguel* and *Sonia*, who have been my reference and unconditional support during my whole career. Thank you for giving me your passion to always keep growing professionally. You are the most important people in the world to me, thank you for always having my back.

Contents

List of Figures

List of Tables

List of Acronyms

ATSM American Society for Testing and Materials.

AWG Aerospace Working Group.

BVID Barely Visible Impact Damage.

CFRP Carbon Fibre Reinforced Polymer.

EASA European Aviation Safety Agency.

EleFanT Electric Fan Thruster.

FAA Federal Aviation Administration.

FEA Finite Element Analysis.

FOD Foreign Object Damage.

FOI Foreign Object Impact.

FRC Fibre Reinforced Composite.

MMC Metal Matrix Composite.

VID Visible Impact Damage.

Chapter 1

Introduction

This MSc thesis project is part of the EleFanT [5] (”Electric Fan Thruster”) research program funded by the Swedish Energy Agency and the Heat and Power Technology Division at KTH (Kungliga Tekniska högskolan) Royal Institute of Technology. Under the project, which spans over 1.5 years, GKN Aerospace and KTH will together develop fan technology for small regional aircraft. The project will study aerodynamic design, performance, noise and manufacturing technology for a ducted fan powered by electricity, either from batteries, hydrogen fuel cells or more conventional hybrid propulsion solutions. The proposed propulsion solution, with a ducted fan instead of a conventional propeller, offers significant advantages in three main areas: safety, noise level and engine installation. Through the development of the necessary fan technology for electric aviation, the EleFanT project will accelerate the pace of electric aviation development and position the participants for international aero-engine and aircraft development projects.

This program also aims to explore the feasibility of using carbon fiber reinforced polymers (CFRP) as a material for designing composite fan blades for an electrically driven ducted fan thruster. The integration of carbon fiber reinforced composites for fan blade manufacturing is limited due to its susceptibility to impact phenomena, and the lack of reliable numerical models that are able to predict the materials response in terms of damage.

This thesis project focuses on analyzing the damage caused by Foreign Object Impact (FOI) in a CFRP composite simple component (laminate plate) through robust and feasible models developed by means of the explicit software tool of LS-Dyna. The final models delivered represent accurately the behaviour of a the material during an impact through different layup structures and material formulations. The results from the impact models are to be validated through some experimental and numerical results found in the literature. These models carry out the first step in the composite material design and impact numerical simulation on more complex aircraft components, e.g. fan blades. Thus, in this project

the main goal is to analyze all damage sources that occur during an impact on a carbon fibre reinforced material, to later implement the developed methodology into the fan blade component designed by GKN Aerospace and KTH University for the ElefanT project. Due to resources and time limitations, the introduction of the methodology into the blade design is not done in this project, but reserved for future developments in this line of investigation.

In this first chapter, we provide a brief overview on the integration of carbon fiber composites into fan blade material design. Since this is not the main objective of this study, this part has been summarized to give an introduction to the future development of the project. Firstly, a summary on composite fan blade technology evolution together with a comparison between the use of metallic or carbon fiber materials for this application is given 1.1. On the second section 1.2, the standard regulations on FOD on composite aircraft components specified by the Federal Aviation Administration are described thoroughly. Finally, on section 1.3 the objectives of the project are outlined to provide clarity to the reader.

1.1 Context

Over the past 30 years, carbon fiber composites have become more attractive in aerospace components material design, particularly in fan blade technology, due to their advantages with respect to more classical metallic alternatives, such as Titanium or Aluminum. Thanks to the information provided in [28], a brief historical overview is carried out next.

In 1968, Rolls Royce's first attempt at designing a composite blade for a large commercial turbofan engine failed. The problem arose from the severe bird ingestion environment, and the early carbon fiber composites' lack of ductility and toughness towards impact phenomena of this kind. These materials' lack of strain-to-failure and inferior interlaminar shear strength, made them inadequate for these kind of phenomena. However, the turbofan engine design and fan blade technology development kept evolving in the following years, leading to an increase in the by-pass ratio and eventually driving back to the use of composite materials as an alternative to classical metallic fan blades, to reduce the weight specially then when the blades increased in size.

This progress was aided by the improvements in the constituents of these materials, including carbon/graphite fibers' strength, strain-to-failure, and stiffness modulus, and generating tougher polymer matrix systems. Additionally, the advancement in finite element analysis (FEA) technology enabled the development of linear and non-linear analyses of laminated plates, including those experiencing complex impact events such as bird ingestion. As a result, in 1989 General Electric was able to develop its innovative composite high-by-pass ratio fan blade design (GE90) shown in Fig. 1.1. These blades

were made from molded toughened epoxy resin reinforced with high-grade carbon fibers and had a titanium leading edge to provide protection against bird strikes and other objects.

Figure 1.1: Jet Engine Fan Blade GE90-115B.

In 2005, CFM International also developed a composite blade design for the LEAP engine, manufactured using an out-of-autoclave 3D weaving resin transfer molding technique. Also in 2012, Rolls Royce partnered with GKN Aerospace, a company highly experienced in the field of composite design and analysis, to develop of carbon reinforced composite fan blades and casing. The designed blade was supposed to perform flight testing on the Trent 1000 engine [38].

As a conclusion, the application of composite materials in fan blade design represents a significant milestone in engine technology, improving their efficiency and reliability, while protecting them against environmental threats such as bird ingestion. To carry out the numerical analysis of an impact on a composite blade, it is crucial to first understand what are the failure and damage mechanisms of a composite material during impact.

1.1.1 Comparison of Composite and Titanium materials for Fan Blade Design

The fan is one of the most critical parts of a jet engine, responsible for driving most of the air into the air intake and thus accounting for 70-90% of the engine total thrust force. Inside the fan structure, the fan blades are particularly significant. Over the past years, the diameters and chord lengths of fan blades have progressively increased, leading to larger fans and, as a result, greater thrust for jet engines.

The typical material choice for fan blades has been between three main material families: Titanium, Fiber-Reinforced Composites (FRC) and hybrid metallic structures. Titanium alloys have a unique combination of high strength-to-weight-ratio, together with

a good corrosion, fatigue and high temperature resistance [7]. However, there has been an increasing trend in the aerospace industry to explore the use of carbon fiber reinforced polymers (CFRP) composites for fan blade applications.

First, as explained in [37], fiber-reinforced composites consist of high strength and modulus embedded in, or bonded to, a matrix with distinct interfaces (boundaries) between them. In general, fibers are the principal load-carrying members, while the surrounding matrix keeps them in the desired location and orientation, acts as a load transfer medium between them, and protects them from environmental conditions. The most common form in which fiber-reinforced composites are used in structural applications is called a laminate, which is made by stacking a number of thin layers of fibers and matrix and consolidating them into the desired thickness. Fiber orientation in each layer as well as the stacking sequence of various layers in a composite laminate can be controlled to provide certain physical and mechanical properties for the composite laminate.

Some of the advantages for aerospace applications that composites present compared to metallic classical materials, such as Titanium or Aluminium, are explained in [37]:

- **Weight reduction:** Carbon fiber composites are known for their exceptional strength-to-weight ratio. They offer high strength and stiffness, while being significantly lighter than metals like titanium alloys. By using carbon fiber composites, the weight of fan blades can be reduced, leading to improved fuel efficiency, increased payload capacity, and enhanced performance. This benefit is translated into lower centrifugal loads and stresses.

- **Tailored performance:** Carbon fiber composites offer flexibility in tailoring the mechanical properties of the fan blades. By adjusting the orientation and stacking sequence of carbon fibers, the material can be modelled to have specific mechanical properties to meet the design requirements. In other words, the properties of a fiber-reinforced composite depend strongly on the direction of measurement, and therefore, they are not isotropic materials such as titanium. For example, the tensile strength and modulus of a unidirectionally oriented fiber-reinforced polymer are maximum when these properties are measured in the longitudinal direction of fibers. As a direct consequence, the design of a fiber-reinforced composite structure is considerably more difficult than that of a metal structure.

- **Corrosion resistance:** Unlike titanium alloys, carbon fiber composites are inherently corrosion-resistant. They are not affected by the corrosive environments encountered during flight, such as high humidity, saltwater exposure, or chemical exposure. This corrosion resistance reduces the need for protective coatings or surface treatments, simplifying maintenance requirements and increasing overall durability. However,

each particular composite must be examined as some of them, particularly fibre reinforced, absorb moisture and chemicals and need protective coatings.

- **Fatigue resistance:** Carbon fiber composites have excellent fatigue strength and damage tolerance, in some cases, outstanding metallic alternatives. In general, they can withstand cyclic loading and vibration without experiencing significant fatigue damage. This characteristic is crucial for fan blades that are subjected to repetitive stress cycles during operation.

- **Energy absorption mechanisms:** While metals in general exhibit yielding and plastic deformation, the heterogeneous nature of composite materials provides mechanisms for energy absorption on a microscopic scale, which is comparable to the yielding process. Depending on the type and severity of external loads, a composite laminate may exhibit gradual deterioration in properties, but usually would not fail catastrophically. Mechanisms of damage development and growth in metal and composite structures are quite different and must be carefully considered during the design process of a fiber-reinforced component.

Finally, hybrid-metallic structures combine composite materials with metallic areas to improve the structural integrity of fan blades in specific locations, such as the leading edge (LE) (e.g. the GE90 fan blade titanium leading edge reinforcement). They combine the structural LE stiffness of a titanium fan blade with the lightness of a composite or hollow titanium design. Hybrid-metallic construction makes fan blades more tolerant to complex events such as bird impact strikes and reduces costs.

To summarize, using composite or hybrid materials instead of metals in fan blade manufacturing provides different advantages such as weight reduction, allowing for tighter tolerances and increased efficiency and tailored properties that improve the mechanical performance of the whole component. However, the key limiting factors in using carbon fiber-reinforced epoxy in aircraft structures are their high cost and relatively low impact damage tolerance (from bird strikes, tool drop, etc.).

1.2 Impact on Composite Components Structural Design Standards

There is a clear interest of introducing carbon fiber composites in aerospace applications over the traditionally exploited metallic materials, e.g. titanium, particularly in fan blade design. However, it is well known that the manufacturing of composite fan blades is limited due to their high sensitivity to impact events and the lack of experimental and

numerical tools to evaluate its performance during FOI event. Because of this, the aviation authorities, such as the FAA and the EASA, have established formal regulations and instructions aiming to demonstrate the fan blade resistance to FOI and other relevant impact phenomena, e.g. Fan Blade-Out (FBO), bird strike, etc.

The focus of this project pertains to the analysis of the FOI damage experienced by laminated plate, as a first step of composite fan blade design process. When designing composite fan blades, engine manufacturers follow a combination of regulatory requirements, industry standards, and their own internal guidelines. The specific regulations and standards followed may vary depending on the jurisdiction and the specific application of the engine.

In this section, the regulations for the design and manufacturing of a carbon-fiber composite blade are reviewed. More specifically, it focuses the standards for impact on a composite component in an aircraft. All the regulations and guidelines depend on the application and the regulatory framework followed by the jurisdiction where the aircraft is operated. These requirements are defined by certification authorities, whereas a certification itself is dependent upon the continent an aircraft is manufactured, purchased or operated in [25]. The different organizations that provide standards of type certification for large commercial aircraft, in which there is a section dedicated to the use of composite materials are:

- **European Aviation Safety Agency (EASA)**, in charge of the European type certification. The CS-25 Book 1 contains certification specifications which are standard technical interpretations of the essential airworthiness requirements. The book is divided into a number of sub-parts together with its respective appendices. The CS-25 Book 2 contains what are known as AMC's (Additional Means of Compliance) which are non-exclusive means of demonstrating compliance with airworthiness codes or implementing rules.

- **Federal Aviation Administration (FAA)**, which regulates the standards followed by composite US manufacturers. The FAR-25 contains basic regulations and any additional material is contained within AC's (Advisory Circulars).

Firstly, the requirements that composite materials must full-fill to serve for any aerospace application are introduced. Secondly, some indications are given on the assessment of impact damage on a generic composite aircraft component. In addition, there are specific certification standards to be met for composite fan blade design subjected to FOI, particularly in the case of bird strike. Engine manufacturers must comply with relevant regulations outlined in the Federal Aviation Regulations (FAR) Part 33, "Airworthiness Standards: Aircraft Engines." [18]. This regulation document focuses on engine certifi-

cation with some special sections dedicated to the bird strike, ice, rain and hail ingestion, which are different type of FOI. The strict specifications that concern bird strike have been included in Appendix 8, as this event is within the future developments of this work.

There are very few industry standards that outline the critical damage for particular composite structural applications with enough detail to establish the necessary design criteria or rules for test assessment, so it is the responsibility of individual applicants to perform the necessary development tasks. That is why, it is crucial to understand the recommendations given in documents such as CS-25.603 (AMC 1) (EASA) and FAA-AC 20.107A (FAA). These documents present acceptable means of showing compliance for composite aircraft structures, involving fiber reinforced materials, e.g. carbon (graphite), boron, aramid (Kevlar), and glass reinforced plastics [25].

1.2.1 Composite Materials Airworthiness Requirements

Some of the categories of material related airworthiness requirements are, the static strength (gust, man-oeuvres or ground loads), endurance and other more specific such as emergency landing, ditching, flutter, bird impact, accidental drop tool, etc.

To certificate the compliance of a composite component in an aircraft, it is necessary to demonstrate that structural failure does not occur and that the part has an adequate life during its entire operation. Thus, a fatigue and fracture mechanics analysis is required. These analysis are limited by the availability of material experimental data, which is normally provided by the American Society for Testing and Materials (ASTM). This is not common, as the fracture toughness is a thickness dependent property and structural components with different sizes and thicknesses require numerous fracture toughness tests, which can become costly and time consuming.

Moreover, there is not a common standardization system for manufacturers to assess composite material performance. Hence, each composite material is identified under its own trademark and as a consequence, no exact equivalence can be established between two different suppliers. Any modification of one of these parameters leads to a material change, which needs a new approval procedure. Therefore, any method that can reduce the number of tests, e.g. reliable robust virtual testing tools, will be useful to the industry to avoid unnecessary costs.

1.2.2 Impact on Composite Aircraft Components

In this matter, the FAA AC 20-107B - Composite Aircraft Structure Advisory Circular [19] establishes some ways of showing compliance with the airworthiness type certification requirements for composite aircraft structures involving fiber reinforced materials.

Guidance information is also presented on the closely related design, manufacturing, and maintenance aspects. This document provides descriptive recommendations to assess the damage tolerance on composite structures in the field of aircraft components.

The document includes a disscussion of the **Static Proof of Structure** is discussed, which specifies that the structural static strength validation of a composite design should consider all critical load cases and associated failure modes. It should be demonstrated that that impact damage that can be likely expected from manufacturing and service (low velocity impact cases), will not reduce the structural strength below ultimate load capability. It is specified that the recommendable means to support this is by test evidence of coupons, elements, subcomponents and components. During the tests, the boundary conditions and structural details of the component should be considered and the size and shape of impactors should be representative of impact damage scenarios that may go undetected for the life of an aircraft.

On the next point of the document, the **Damage Tolerance Proof of Structure** is discussed in different generic scenarios (low and high velocity impact damage). First, damage tolerance evaluation starts with identification of components whose failure would reduce the structural integrity of the aircraft. The structural damage assessment must be performed to determine possible locations, types, and sizes of damage considering fatigue, environmental effects, intrinsic flaws, and **foreign object impact** (FOI) that may occur during manufacture, operation or maintenance. FOI is a critical concern for most composite structures, requiring special attention in the damage threat assessment. The damage assessment includes all the damage data collected from service, plus an impact survey. The impact survey consists of impact tests performed with representative structure, which is subjected to boundary conditions characteristic of the real structure. Many different impact scenarios and locations are considered in order to identify the most critical impacts possible (i.e., those causing the most serious damage but are least detectable).

Fig. 1.2 shows the five damage types that can be detected after performing a damage assessment on foreign object impact, depending on the damage source and on the conditions to keep working in service.

1. **Category 1:** This category includes damage that may go undetected by field inspection or allowable manufacturing defects. This damage is validated structurally, based on the reliability on its service life, while retaining ultimate load capability. Some examples include barely visible impact damage (BVID) and allowable defects caused in manufacturing or service.

2. **Category 2:** This type of damage can be detected by field inspections performed at specified intervals. The structural validation is proven by following periodic

inspections, while retaining loads above limit load capability. As an example there are visible impact damage (VID): deep scratches, manufacturing mistakes not evident in the factory, detectable delamination or debonding. This type of damage should not grow or the level of residual strength retained for the inspection interval is sufficiently above limit load capability.

3. **Category 3:** Damage can be detected within a few flights of occurrence, and it must be clearly visible or cause other indications of potential damage that becomes obvious in a short time. The structural validation depends on how quickly the damage can be detected, while retaining critical load capability, e.g. large VID such as fuel leaks, system malfunctions or cabin noise.

4. **Category 4:** A known and discrete damage from an incident. The structure needs to be able to demonstrate its residual strength for loads specified in the regulations. Some examples are rotor burst, bird strikes (as specified in the regulations), tire bursts, and severe in-flight hail.

5. **Category 5:** Severe damage created by anomalous ground or flight events, which is not covered by design criteria or structural validation procedures, such as service vehicle collisions with aircraft, flight overload conditions, abnormally hard landings, and loss of aircraft parts in flight. Some Category 5 damage scenarios will not have clearly visual indications of damage, particularly in composite structures.

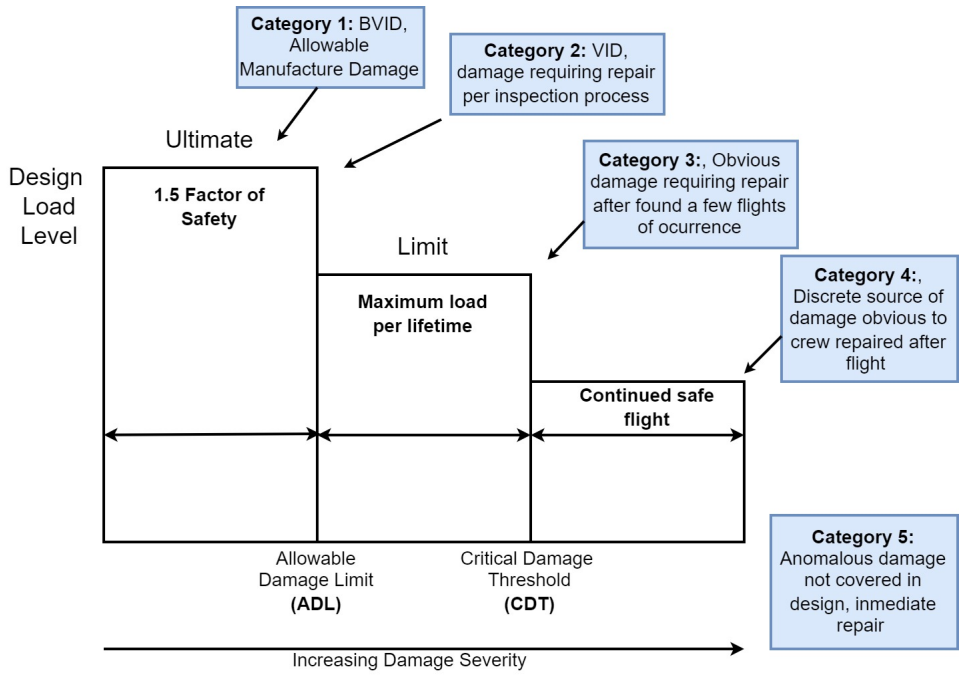

Figure 1.2: Schematic diagram of design load levels versus categories of damage severity. [19]

1.2.3 Other Certification Standards

Apart from the FAA, there are other institutions that provide guidelines on how to perform FOI damage analysis on composites. Indeed, there are not only damage assessment techniques, but also entire material test programs for validation of the composite components.

- National Aerospace Standards (NAS), NAS 412 [51]: The document focuses on ensuring that composite structures meet the required standards for safety, reliability, and performance. It outlines the recommended practices for designing, fabricating, and inspecting composite components. This includes guidance on material selection, layup techniques, curing processes, and tooling requirements. It provides detailed instructions on identifying different types of damage, such as delamination, impact damage, and disbonds, and offers approved repair methods for each type.
- American Society for Testing Materials (ASTM), ASTM-D7136 [26]: Standard Test Method for Measuring the Damage Resistance of a Fiber-Reinforced Polymer Matrix Composite to a Drop-Weight Impact Event. This is a test method which covers the damage resistance of multidirectional polymer matrix composite laminated plates subjected to a drop-weight impact event.

1.3 Objectives

To conclude this first chapter, the main objectives of the project must be summarized. The main goals of this project are to:

- Provide theoretical background on the different failure and damage mechanisms carried out by a composite material during impact phenomenon. Explanation on the effect of **impact velocity** on the composite and description of the most important damage sources and types during different impact phenomena.
- Build a reliable and robust model to represent the Foreign Object Impact (FOI) phenomenon on a composite component with a simple geometry, a composite laminated plate. There are two main case scenarios:

  1. **High Velocity Impact:** Ballistic impact of a cylindrical projectile on a rectangular laminated plate. The numerical model developed is based on a reference study from the literature [39, 6]. Thus, the constructed methodology is compared and validated on the basis of experimental and numerical results.

     The main purpose is to construct a simple and flexible model of a high velocity impact on a composite structure that allows to study the numerical problem:

material formulation, element integration, contact algorithm, etc. This is the first step of modelling an impact problem on a composite structure by means of LS Dyna.

After the model is considered numerically robust and reliable, the physical part of the problem is analyzed. A parametrical physical study is performed and different characteristics of the plate, e.g, constitutive law, thickness, layup sequence, etc. are varied in order to see their effect on the composite failure behaviour.

2. **Low Velocity Impact:** The impact of a hemispherical projectile on a rectangular laminated plate, representing a Drop-Tower test procedure developed by I. Mohammed in [25], is represented through a numerical model based on the previously developed methodology.

   The aim of this part is to deliver a model able to represent accurately the interlaminar failure or delamination phenomenon. The development of two independent models allows to study, first only the interlaminar failure mechanism of the composite plate and second, the evolution of both intra and interlaminar failure mechanisms simultaneously.

For both models we develop a numerical parametric study based on the employment of different element integration methods, hourglass control techniques, material failure properties, contact algorithms, etc. Ultimately, the goal is to construct a reliable model from the numerical point for performing the physical study of the impact and damage on the composite.

The use of these two very distinct dynamics allows to represent the complete range of failure mechanisms that occur within a composite material. The high velocity case is employed to simulate the ballistic properties of a composite component (ballistic limit, absorved impact energy, residual velocity of the projectile, etc.), while the low velocity case focuses on a particularly form of damage known as barely visible impact damage (BVID), which commonly occurs between the plies in the form of delamination and is often overlooked when examining a composite component. As a consequence, low velocity impact induced damage can be equally or even more dangerous than the component being penetrated by a more energetic projectile. Thus, while the high velocity modeling approach adopted proves valuable for the future development of a model pertaining to blade FOI, the methodology employed in the low impact case offers a deeper understanding on the other composite damage mechanisms that are less detectable through visual inspection.

Additionally, to provide the reader with a general perspective on how the objectives are organized and approached, each of them has been linked with one chapter of the present manuscript.

- In **Chapter 2**, an extensive literature overview was carried out on previous works on the analysis of Foreign Object Damage on composite materials. Some additional sources are included in the topic of FOI on CFRP fan blades. This research was focused on numerical studies performed in software tools such as LS-DYNA, validated against reference experimental and numerical results.

- In **Chapter 3**, the necessary theoretical background on the mechanics of high and low velocity impact on a composite plate is provided. This chapter also explains the methodology employed to implement these theories to LS-DYNA.

- In **Chapter 4**, the high velocity impact model is carried out. This chapter is divided in: a of the model, a numerical and a physical parametric studies. The final goal is to validate the ballistic response of the plate to high velocity impact by means of experimental and numerical results carried out in the reference study [39].

- In **Chapter 5**, the low velocity impact model construction and failure analysis is developed. In this case, the focus is set on accurately representing delamination. For this purpose, two different approaches are followed: (1) impact model only representing interlaminar (delamination) failure damage, and (2) alternative impact problem where intra and interlaminar failure mechanisms coexist.

- In **Chapter 6**, the main conclusions delivered in both the high and low velocity impact models on composite laminate plates are collected. In this part, the limitations of both models are presented again and possible enhancements are presented for future research works on this topic. In addition, the main future application of this work is highlighted: the introduction of the constructed methodology into the composite blade designed by GKN Aerospace in the frame of the EleFanT project.

Chapter 2

State of the art

This chapter provides a literature survey on the central topics of the study: composite material modelling, low and high velocity impact on a composite plate and design as well as a brief insight into impact on a CFRP fan blade modelling, considering the future scope of this work. The review is structured by topics and presented in chronological order, to describe the evolution of modelling techniques and tools used to represent high and low velocity impact on composite materials. These techniques have been translated into the study of FOI damage in aircraft composite components, e.g. fan blades. These components are known to experience various harmful impact events, among them, the particularly dangerous bird strike phenomenon, which has come to be one of the main research themes in the frame of composite fan blade design and manufacturing.

To sum up, the literature survey on this topic is very wide, and for the sake of clarity can be divided into two parts:

1. Ballistic impact on composite plates, along with its failure and damage mechanisms modelling. This is the main topic of study in this project.

2. Foreign Object Impact by soft-bodies on CFRP manufactured fan blades. Although this theme is less relevant for this project, it provides a good introduction to one of its main future applications.

The review begins with a detailed overview of **ballistic impact on composite plates** experimental and numerical studies. Inside this main topic, there are relevant subjects to highlight:

- The problem of an impact on a composite component can be divided into the **high and low velocity impact**. The response of the composite component and its damage mechanisms change radically from one case to the other and that is why a special distinction between these two problems must be emphasized. This chapter includes

some sources which reviewed experimental and numerical models representing and comparing these two phenomena.

- The **rigid or elasto-plastic** material laws are used alternatively for the projectiles' modelling. If the projectile is modelled as deformable, this allows an exchange of energy between the projectile and the composite plate.

- The difference between the studies focused on the impact on **unidirectional plied or woven composites**, especially concerning the numerical parameters necessary for the material modelling of the plates.

- **Delamination modelling** is a complex and relevant topic on its own. Accounting for interlaminar failure is not a simple task, as it involves the introduction of either specific tied contact formulations that are able to account for failure (tiebreak contacts) or cohesive element interface layers between the composite plies.

- Numerical aspects of the model, such as the **type of element**, **the through-thickness integration technique**, the **material constitutive model, and the contact algorithm**. These are critical numerical parameters that vary among the selected reference studies, and have an effect on the composite failure and damage mechanisms modelling.

The most relevant works selected as a reference for this study are:

- In 1991, Abrate [1] developed a complete analysis of impact events on laminated composite materials. The **effects of impactor velocity** on the mechanical response and damage mechanisms of composite structures were investigated. The study includes a review on different **experimental methods** employed for impact testing on composite materials, as well as some **analytical models** useful to understand the problem features and reduce the need for experimental testing.

  A further discussion on the analytical methods, its limitations and main applications was carried out in an article published by the same author in 2001, [2]. This study is focused the damage patterns and evolution on composite plates and beams submitted to high and low velocity impact. The article discusses the effect of different physical properties such as the material properties, thickness, stackup sequence and target geometry on the damage mechanisms.

  Similar reviews were carried out in 1996 by Richardson et al. [50] on low velocity impact properties on composite materials, more focused on the failure modes of composites and damage evolution and prediction.

- Yen et al.[14] (2002) and Deka et al.[15] (2006) conducted a **high velocity impact** ballistic impact study on S2-Glass/Epoxy and E-glass/polypropylene laminated composite plates respectively. In both works, the plies were modelled using solid hexahedrons and a material formulation with the Hashin failure criteria to represent **fiber and matrix failure as well as delamination** initiation. The material model also was able to model progressive damage under **high strain rates**. In Deka's et al.[15] work, the final results are the ballistic limit velocities, energy absorption rates, and kinetic energy evolution of the projectiles for different stackups, which are compared against experimental data.

- Heimbs et al. [24] (2008) investigated **low velocity impact** on composite plates. Their work focuses on composite material and delamination modelling, as well as analyzing the effect of **preloading** in composite components. The objective is to analyze the influence of various numerical parameters on the impact response, e.g. element size and type, number of shell element layers employed to model the composite laminate, contact penalty stiffness, material and tiebreak contact parameters, used for delamination. . The study uses **tiebreak contacts** (*CONTACT_TIEBREAK) a specific LS Dyna **tied contact formulation** that allows for including a failure criterion to model **delamination**. The contact force, kinetic energy, interlaminar and intralaminar failure history variables are examined

  This study served as a reference model validated with experimental tests for Dogan et al. [16] (2012). In this paper, three different models representing three different **element types for the composite material layup structure**, with two different delamination modelling techniques were developed and compared. Thick shell and solid elements with a cohesive interface, and thin shell elements with tiebreak contact were the composite layup structures employed. This work provides guidelines for composite and low velocity impact modelling e.g. the element size, number of shell sub-laminates, and contact stiffness scale factors.

- In 2007, Moncayo et al.[40] investigated the available **delamination modelling techniques** for low velocity impact simulations. The purpose was to compare developed simulations with low impact velocity available experimental data, provided by the Institute of Aircraft Design at the University of Stuttgart (IFB), including delamination areas.

  On the same topic, Muflahi et al.[42], explored different methods to model and predict delamination using in-built and user-defined constitutive laws and element formulations. This paper compares the **three possible element formulations with two possible techniques based on cohesive elements and tiebreak contacts for**

delamination. To determine the material and contact parameters this study develops the necessary simulations for material testing, e.g. 3-point bend of a composite coupon and a complete fracture toughness model. The latter includes a Double Cantilever Beam (DCB) problem for opening mode (I) and a 3-point End-Notched Flexure (ENF) for in plane shear mode (II). The best option found to model delamination in terms of the stability and accuracy are either solid or thin shell element formulations, instead of thick shells, with a cohesive material model or a tiebreak contact with a damage law.

- In 2008, Loikkanen et al. [39] conducted a study on **high-speed** ballistic impact on composite panels, shown in Fig. 2.1. The study explored the influence of plate thickness, stacking sequence, impact speed, and projectile shape on the material damage response. A **new advanced material formulation** was used to model the composite plate. The main feature of the new material formulation is the progressive failure model, explained more deeply in 2015 by Haque et al. in [22]. The model was validated against experimental tests which measured the residual velocities a cylindrical and hemispherical projectiles. Moreover, delamination was modelled through **tiebreak contacts** based on fracture toughness material parameters computed through mechanical testing simulation. The tiebreak option employed in this study emulates the behaviour of cohesive elements, for full fracture mechanics-based capabilities.

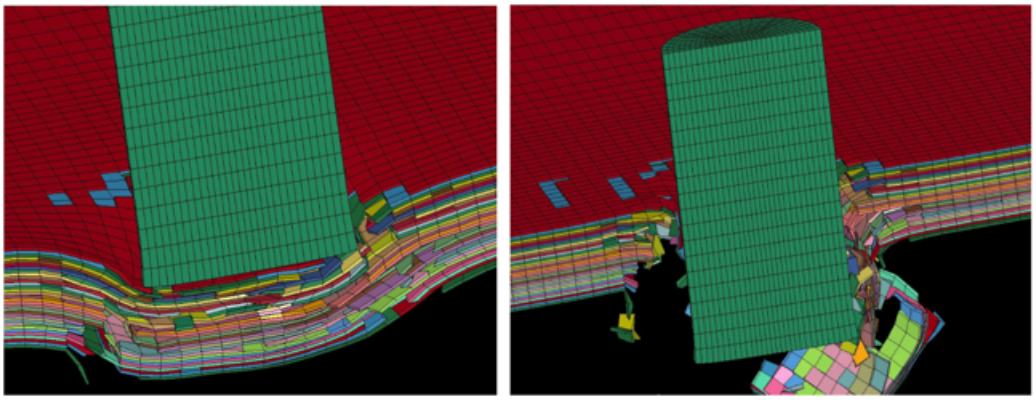

Figure 2.1: High velocity impact model, penetration failure. [39]

- In 2010, I. Muhammad [25] developed a numerical model for a low velocity rigid impact on a composite plate modelled with an advanced progressive damage material model, explained on [22]. Delamination evolution is represented using tiebreak contacts. The focus is to record the displacement at the center of the plate, the contact load, impact energy absorved by the composite, delaminated area, and

energy release rate (G_I, G_{II}) in each interface of the laminate. The results were validated with the experimental test data from Drop Tower tests conducted during this research. In 2.2, a stage of the low velocity impact simulation where delamination failure mechanism is clearly observable is presented.

Maamar et al.[36] continued the development of this model but employing a simpler material formulation that only accounts for the onset of failure through a stress-based failure criterion.

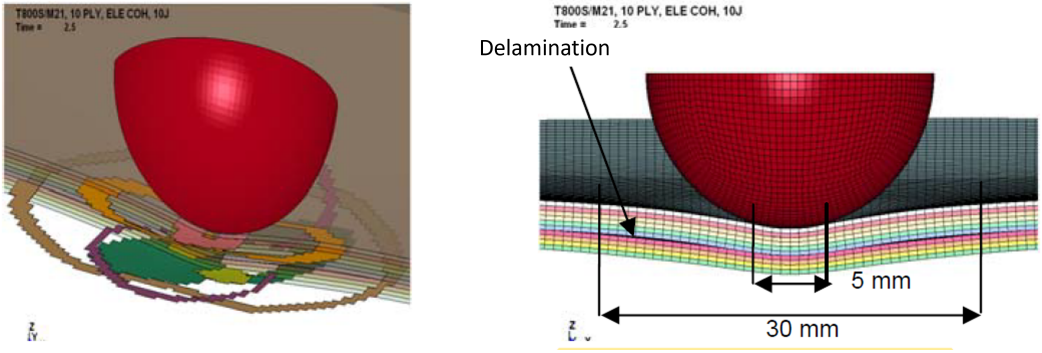

Figure 2.2: Low velocity impact model, delamination failure. [25]

The second relevant topic of the review is **soft-body impact on a fan blade** although the focus is not modelling an impact on a composite blade, but analyzing the composite damage mechanisms during impact.

The work done in 2021 by Sun et al. [55] is one of the most relevant analysis of the damage caused by bird impact on composite plates. The soft (bird) projectile was modelled using a particle method (SPH) and the composite material model failure initiation is predicted by the Hashin failure criterion. The impact location, boundary condition, and impact velocity were varied to obtain the optimal impact damage distribution. The most favorable damage distribution was chosen as the one that provides the least damage in the blade root. This study proves the value of plate-level experimental and numerical impact tests, to investigate the damage mechanism and the impact loading capability of the material, before using the real blade for analysis of the composite material. In Fig. 2.3, the role of the plate level study on the analysis of the bird-strike event on the final composite blade model is presented graphically.

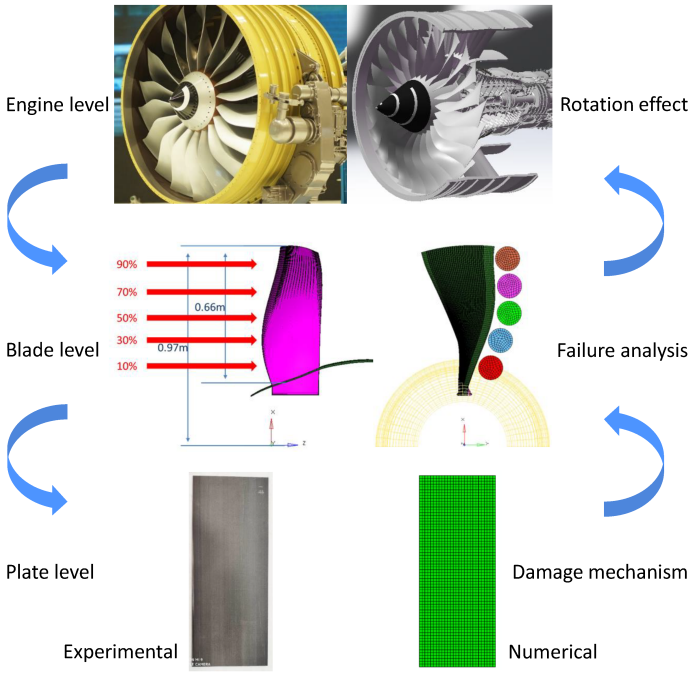

Figure 2.3: Role of plate-level study for bird-strike analysis of aeroengine fan blades. [55]

The **main conclusion** of this review is that FOI on composite structures of any type, plates, beams or blades creates various types of external or internal damage that reduce the strength of the structure significantly. The study of such impacts requires understanding the dynamics of the event, predicting the extent of the damage, and the residual properties of the structure. Damage examination is not always possible through visual inspection, and that is the main drive for developing numerical models that are able to represent the damage response of the composite specimen to impact.

The studies included in this review have been the basis to understand the key aspects of an impact problem on a composite component, e.g. element type for ply layup structure, intra and interlaminar damage model in the material formulation, and delamination modelling technique, contact algorithm, etc. In particular, two representative reference models are used as the first steps to model impacts of different velocity charateristics:

- The **High Velocity Impact on a Composite Plate** developed in [39, 6], served as a reference to develop the methodology recommended to solve the ballistic impact problem and to predict the penetration characteristics of the projectile through the composite.

- The **Low Velocity Rigid Impact on a Composite Plate** models in [36, 25] were the initial step towards the development of a full and complete analysis and prediction of the failure and damage patterns involved in an impact problem on a composite.

Chapter 3

Composite Plate Impact Model

This chapter provides the necessary theoretical background to build a robust numerical model representative of an impact on a composite component. To provide a complete overview on this problem, both a high and a low velocity impact models are going to be employed. To carry out this goal, two reference numerical studies, validated through experimental results, are used as a basis to solve the impact problem. The models have already been mentioned in the previous chapter 2 in **??**, but a remainder is included next to facilitate the reading:

- **High Velocity Impact on a Composite Panel**, developed by the LS Dyna Support Aerospace Group and Loikkanen et. al. in [6, 49, 39].
- **Low Velocity Impact Model** on a composite rectangular plate carried out by Muhammad in his Phd. Thesis work [25] and later by Maamar and his co-workers in [36].

The reference models propose material models to simulate the intralaminar and interlaminar damage in the composite target. The models are based on numerical parameters that were calibrated with the necessary standard and non-standard material testing procedures. The two reference models are explained in detail and compared with the authors' approach in the next two chapters.

The use of these two very distinct dynamics in an impact model has a clear purpose, to account for the complete range of failure mechanisms that occur within a composite material. The high velocity case is employed to simulate the ballistic properties of a composite component (ballistic limit, absorved impact energy, residual velocity, etc.), while the low velocity case focuses on a particularly form of damage known as barely visible impact damage (BVID), which commonly occurs between the plies and is often overlooked when examining a composite component. As a consequence, low velocity impact induced damage can be equally or even more dangerous than the component being penetrated by a more energetic projectile. To conclude, while the high velocity modeling

approach adopted proves valuable for the future development of a model pertaining to blade FOI, the methodology employed in the low impact case offers a deeper understanding on the other composite damage mechanisms that are less detectable through visual inspection.

In the first section of this chapter, an introduction into composite failure and damage mechanics is given. The different types of failure mechanisms, the failure criteria employed to predict the initialization of damage and the consequent degradation of the material properties are some of the relevant topics of this first part. On the second section, a review of the physical concepts involved in an impact problem is performed. The third section is dedicated to explain the different steps followed during the numerical model construction. During the description of the models, the examination methodology of the impact physical properties is explained, and complemented with a discussion about the choice of the numerical aspects of the model constructed in LS Dyna: element type, the material formulation, the contact and hourglass algorithms and the failure, damage evolution and erosion techniques.

3.1 Composite Failure and Damage Model

This section provides an introduction to the main failure mechanisms of composite materials. In general, the developed methods for predicting brittle damage in composite structures subject to severe static or impulsive loading can be divided broadly into four areas [29]:

- **Failure criteria**: Employed to predict the onset of damage in composites through formulations based on stress or strain values. The use of these stress based failure criteria comes with a major disadvantage, known as the ”scale effect”. This issue is related to the length of cracks subject to the same stress field, which cannot be modeled correctly. A more detailed description and the complete formulation is specified in the second part of this section 3.1.1.

- **Fracture mechanics**: This approach is used to model delamination and is based on the computation of energy release rates and critical crack sizes. In most models, a stress or strain based failure criterion is used to predict the onset of damage, followed by a fracture mechanics approach requiring an initial crack size.

- **Damage mechanics approach including softening models**: This methodology can predict accurately the range of degradation in a composite material, from the initial state material to the full damaged state, allowing also strain-rate sensitivity. This is the most complex approach as it requires parameters that can only be determined through specific material testing procedures, as well as advanced material formulations not always compatible with the basic LS Dyna license.

3.1.1 Failure Mechanisms: Classification

There are many different type of failure mechanisms inside composite materials, which are engendered by the complexity of its structure and manufacturing processes. These different types of damages are always the same whatever the loading. However, their proportion and localization highly depend on the loading rate and phenomenon that the composite structure is exposed to. The main failure mechanisms in composite structures are represented in Fig. 3.1 and can be described as follows [25]:

- **Fibre breaking:** Intralaminar mechanism occurs due to a high tension along the fiber direction. The initiation of this phenomenon can be characterized by uniaxial tension tests.

- **Decohesion fibre-matrix:** Intralaminar failure mode which appearance depends highly on the fabrication process for the unidirectional tapes. Its characterization through experimental tests is more complex than in fibre failure.

- **Matrix breaking:** Intralaminar failure model that occurs due to the existence of cracks or voids between the fibers within a ply due to tension in the transversal direction of fibers.

- **Fiber buckling:** Intralaminar failure mechanism that occurs during compression in the fiber direction. It hardly drives to complete failure of the material, but it can drive to fiber-matrix debonding or delamination.

- **Delamination:** Interlaminar mechanism based on the separation of internal layers of a laminate with **different orientation**, normally due to high stress concentration in the interface.

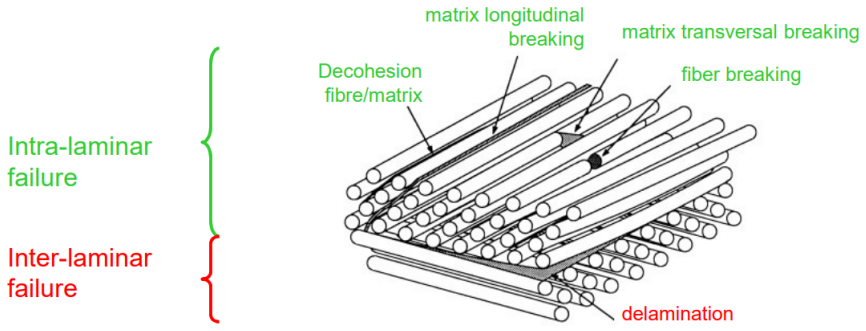

Figure 3.1: Failure modes in composite structures. [10]

3.1.2 Failure Criteria

In this section, the different failure criteria that represent the initiation of composite intralaminar failure are described. These criteria are implemented in the material formulation inside the numerical model of the plate, which is more detailed in 3.3.3. There are multiple available failure criteria in the literature that have been introduced into the LS Dyna composite material formulations. The failure criteria can be classified in basically two types:

- Specific criteria for the various damage mechanisms, such as the Hashin [23] or Chang Chang [13] criteria.

- Polynomial based criteria which describes the failure surface in stress or strain space. Various mechanisms interact with each other, as it occurs in the Tsai-Wu [56].

The mathematical formulations for the mentioned failure criteria are provided next. Note that, γ is the symbol employed for the stress distribution and ϵ for the strains. In this particular section e represents the failure threshold function and the letters X, Y , Z and S represent strengths in fiber, matrix, out of plane and shear directions. The subscripts a, b and c refer to the fiber, transverse and out of plane directions, and finally, f, m, t and c denote fiber, matrix, tension and compression respectively.

The first criterion is related to **fibre failure**, which is due to accumulation of individual fibre breakages in a ply. To cumulate fibre breakage and fibre-matrix debonding, Hashin, Chang-Chang and Tsai-Wu used quadratic interaction criterion involving in-plane shear. Note that, the shear stress weighing factor β, which appears in the following equation, represents the influence of shear in the tensile fibre mode. Thus, by adjusting this parameter the failure criteria is able to be switched: for $\beta = 1$ the Hashin criterion is employed and for $\beta = 0$ the maximum stress criterion is used.

- For the tensile fibre mode,

$$\sigma_{aa} > 0 \text{ then } e_{f,t}^2 = \left(\frac{\sigma_{aa}}{X_t}\right)^2 + \beta\left(\frac{\sigma_{ab}}{S_c}\right) - 1 \begin{cases} \geq 0 \text{ failed} \\ < 0 \text{ elastic} \end{cases}, \qquad (3.1)$$
$$E_a = E_b = G_{ab} = v_{ba} = v_{ab} = 0,$$

The compressive fibre failure is observed to be due to microbuckling and formation of kink bands.

- For the compressive fibre mode,

$$\sigma_{aa} < 0 \text{ then } e_{f,c}^2 = \left(\frac{\sigma_{aa}}{X_c}\right)^2 - 1 \begin{cases} \geq 0 \text{ failed} \\ < 0 \text{ elastic} \end{cases}, \qquad E_a = v_{ba} = v_{ab} = 0. \tag{3.2}$$

The second failure mechanism is **matrix cracking** which is normally generated by through-thickness cracks (perpendicular to fibers or at the fibre-matrix interfaces) and stacking cracks (not cross the overall width and are generally longer along the fiber direction). Through-thickness cracks are considered as a proper damage, while stacking cracks are often not taken into account since they are parallel to delamination, in which the sizes and induced strength reduction are more effective.

- For the tensile matrix mode,

$$\sigma_{bb} > 0 \text{ then } e_{m,t}^2 = \left(\frac{\sigma_{bb}}{Y_t}\right)^2 + \left(\frac{\sigma_{ab}}{S_c}\right)^2 - 1 \begin{cases} \geq 0 \text{ failed} \\ < 0 \text{ elastic} \end{cases}, \qquad E_b = v_{ba} = 0. \rightarrow G_{ab} = 0, \tag{3.3}$$

- For the compressive matrix mode (Chang-Chang/Tsai-Wu),

$$\sigma_{bb} < 0 \text{ then } e_{m,c}^2 = \left(\frac{\sigma_{bb}}{2S_c}\right)^2 + \left[\left(\frac{Y_c}{2S_c}\right)^2 - 1\right]\frac{\sigma_{bb}}{Y_c} + \left(\frac{\sigma_{ab}}{S_c}\right)^2 - 1 \begin{cases} \geq 0 \text{ failed} \\ < 0 \text{ elastic} \end{cases}$$
$$_b = v_{ba} = v_{ab} = 0. \rightarrow G_{ab} = 0$$
$$X_c = 2Y_c \quad \text{for } 50\% \text{ fiber volume} \tag{3.4}$$

- For compressive and tensile matrix failure (Tsai-Wu):

$$e_m^2 = \frac{\sigma_{bb}^2}{Y_c Y_t} + \left(\frac{\sigma_{ab}}{S_c}\right)^2 + \frac{(Y_c - Y_t)\,\sigma_{bb}}{Y_c Y_t} - 1 \begin{cases} \geq 0 \text{ failed} \\ < 0 \text{ elastic} \end{cases} \tag{3.5}$$

In the case of **delamination**, different prediction criteria and methodologies are available in the literature and can be introduced in LS Dyna, this is explained in detail in 3.3. For now, it is important to acknowledge that one of the most common failure criteria for delamination was formulated by Hashin [23] using stress values of each individual ply. Individual ply criteria use combinations of the through thickness tensile and transverse shear strengths in linear or quadratic relationships.

- For delamination prediction (Hashin):

$$\left(\frac{\sigma_{cc}}{Z_T}\right)^2 + \left(\frac{\sigma_{bc}}{S_c}\right)^2 + \left(\frac{\sigma_{ac}}{S_c}\right)^2 \geq 1 \tag{3.6}$$

3.1.3 Damage Modelling

In this section, the damage modelling techniques inside the material formulation are explained. The failure criteria predicts the initiation and the type of failure mechanism inside the composite material, while the damage model represents the progressive degradation of the strength properties of the material between its initiation and the final full damaged state.

As it can be easily deduced, the damage model is one of the most complex parts when developing the material and contact numerical models of an impact problem of any kind. Damage characterization approaches can be generally categorized in two types:

- **Continuum Damage Mechanics:** Introduces the effects of damage as part of the material definition. Inside this general topic, there is the strength based approach, which is one of the most common ones due to its fair simplicity. It is based on one or multiple strength criteria, linear or quadratic laws that combine one or multiple stress terms. However, the damage can also be characterized by other properties such as the strain, displacement, force, etc. This approach has been applied to both intralaminar and interlaminar damage prediction, as done by Muhammad [25].

- **Fracture Mechanics:** This approach is applied specially to represent the evolution of interlaminar damage (delamination). The classical fracture mechanics procedures are based on the assumption of an existing crack and therefore, are used to characterize damage progression. The growth of the crack is controlled by the strain energy release rate (G), which is affected by numerous parameters such as the loading rate, the direction of the crack growth, the orientations of the plies adjacent to delamination and the proportion of different crack modes in the material.

3.2 Impact Mechanics on Composite Structures

This section provides an introduction into the impact mechanics problem on a composite target with a simple geometry, such as a beam or a plate. First, the differences between low and high velocity impact phenomena are described. There are multiple classifications, so only the most relevant that have been of use to this study are included. Secondly, based on section 3.1, in which the principal composite failure mechanisms were described, the

composite failure modes during an impact are described. The location and proportion depending on the impact characteristics of the different failure modes is carefully explained, as well as the interaction between mechanisms. Finally, the effect of some physical parameters on the damage and failure modes is introduced, these parameters are going to be examined further in the physical study performed in the high velocity model in the next chapter 4.

3.2.1 Low and High Velocity Impact: Classification

Due to the relevant changes in energy transfer between the projectile and target and damage propagation mechanisms as the velocity of the projectile varies [52], multiple classifications are available in the literature:

- **Velocity range:** Low velocity impacts are said to occur for impactor speeds less than 100 m/s, and for hypervelocity impacts speeds larger than 1 km/s [1]. Other classifications, [52, 12] characterized the low velocity cases as the ones with a speed up to 10 m/s, intermediate velocity impacts between 10-50 m/s and high velocity between 50-1000 m/s.

- **Deformation area**: The high-velocity impact response can be characterized by a very localized impact area due to the fact that the stress wave does not have time to propagate entirely through the material. As for low-velocity impact, the structural response of the target is described as much more relevant as the contact duration is long enough for the wave to propagate through the entire structure [54].

- **Damage:** The damage pattern can also be a characteristic to classify these phenomena [30]. While high velocity impacts are characterized by penetration-induced fibre breakage damage patterns, low velocity cases are characterized by the presence of delamination and matrix cracking. Also Abrate [1] and López-Puente [33] argued that while for a high velocity impact the response is governed by plugging, which is a combination of local crush and out of plane shear mode, for a low velocity impact, the plate response is dominated by global bending. These previously mentioned failure modes can be observed in Fig. 3.2.

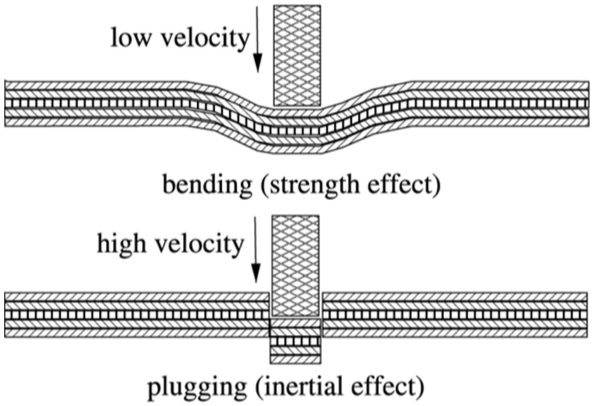

Figure 3.2: Effect of velocity on composite laminate response to impact. [33].

Some analytical models were developed to represent both phenomena [1, 2]. Low velocity impacts are often approximated as a series of spring and masses (spring-mass model). The high velocity cases, the wave propagation method is much more accurate. On another hand, in terms of experimental testing methods, low velocity impacts are normally tested with drop towers or drop weights tests while high velocity impacts are characterized using powder or gas gun tests.

In aircraft components, the low velocity case could represent the impact of a tool during the manufacturing or maintenance process, or the runway small debris impact. The high velocity model is more similar to the bird strike event, which is within the future scopes of this project.

To conclude, it should be noted that for analyzing the impact damage on a composite material, it is highly recommendable to use a low velocity impact model. This can be easily understood by making a comparison with metallic components. While low velocity impact damage of metallic components usually starts from the impacted surface and is detectable by visual inspection, on composite targets, significant amount of permanent damage in the form of subsurface delaminations, matrix cracking and fiber breakage may be present without being detectable by “outside” visual inspection. This damage, which is not usually observable, can result in a significant strength reduction, compromising the safety of the structure and constituting the most difficult challenge on composite material design.

3.2.2 Impact Composite Failure Mechanisms

In this section, the effect of the main impact variables on composite failure and damage mechanisms is analyzed. The focus is set on understanding the location and proportion of the failure modes that are more prone to occur during an impact of certain characteristics. In addition, it is key to understand how these mechanisms interact depending on the impact

velocity.

Many failure modes, such as delamination, fiber fracture, and matrix cracking, can occur during FOI on a composite laminate. It is essential to understand the nature of the damage, the sequence of damage accumulation, and the influence of the impactor velocity, among other variables, on the targets' response.

The different damage mechanisms, that have been already described in 3.1.1, tend to occur in the next order during an impact phenomenon (they are also described from lower to higher impact velocities) [52, 50]:

- **Matrix cracking:** This is the first failure mode that a composite target experiences during an impact. As previously described, it occurs in the transversal direction of fibres due to tension, compression and shearing. It can also be due to debonding between fiber and matrix, induced by property mismatch.

- **Delamination:** The next failure mechanism is one of the most significant failure source in low velocity impacts. Produced by interlaminar stresses, a crack is generated and runs in the matrix area between plies. Experience has shown that it always occurs between two layers of **different fiber orientation**, more likely in the direction of the lower ply [1]. As a result, the compressive strength of the laminate is decreased.

- **Fibre fracture:** Most significant failure source in high velocity impacts. This type of damage generally occurs much later than the previously described ones in the fracture process. Fibre fracture normally occurs due to shear force and bending stress induced by projectile.

- **Penetration:** This macroscopic mode of failure occurs when the fibre failure reaches a critical extent, enabling the impactor to penetrate the material.

There is a strong interaction between the different modes of failure such as simultaneous delamination and matrix cracking as explained in the literature [2, 50]. In fact, delamination does not occur in the absence of matrix cracks, which are known as critical cracks. Initially, in unidirectional composites these matrix cracks are parallel to the fibers and oriented at an angle with respect to the interface. After reaching the interface between differently oriented plies, which have different bending stiffnesses, the crack propagates causing delamination. This source of failure allows the impact energy to dissipate in the interfaces of dissimilar oriented plies. A graphical representation of the interaction just described is shown in Fig. 3.3.

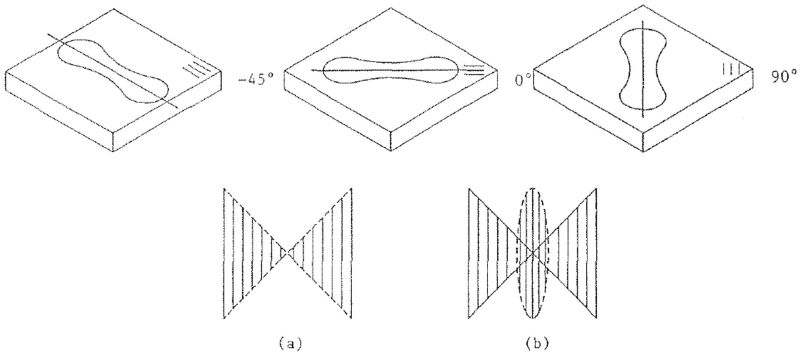

Figure 3.3: Delamination patterns (top) and matrix crack orientation (bottom) developed during low velocity impact.[1]

Fig. 3.3 shows the delamination patterns for different fibre orientation (top), as well as the matrix crack and delamination areas (bottom). In the bottom figure, the three different zones developed during this mechanism are observable. The central zone coincides with the delamination area on the interface, while the other two triangular zones are bounded by the diagonals of the plate. Matrix cracks in the non-impacted surface lamina run parallel to the fibers from one edge of the plate to the other, until they are stopped by the central zone (delaminated area).

3.2.3 Effect of relevant parameters

There are some physical parameters related to the material constitutive law, stackup structure, projectile shape and impact conditions that have a strong influence on the response and damage suffered by a composite plate during impact. It should be noted that this part is based in previous research studies found in the literature [1, 50, 52].

Firstly, the **components material properties** influence on the response is examined. The fibers are the main load-bearing constituent, providing the strength and stiffness to the composite, while the matrix is in charge to transfer the load to the fibers, and protect them from damaging themselves, align and stabilize them. Experimental results [17] indicate that while matrix properties govern the damage threshold and determine the extent of impact damage, the fiber properties, control the penetration resistance. However, for resistance to low-velocity impact, the ability to store energy elastically in the fibres is the fundamental parameter, and it corresponds to the area under the stress-strain curve, which is dictated by the fibre elastic modulus and strain to failure. Note that, the strain to failure for carbon fibres is reported to be normally between 0.5-2.4% [1].

On another hand, the final stiffness achieved by a composite target is mostly controlled by the **thickness and the stack-up sequence of the plies** and it has a relevant effect on the damage pattern of the specimen. In Fig. 3.4, the differences between a flexible or stiff

plate damage behaviour during impact can be appreciated. For flexible targets (top), the response is dominated by bending. This induces high tensile stresses in the lowest ply and thus, causes matrix cracks in this ply which deflect at the lowest interface forming delamination. For stiffer targets, the behaviour is similar but in reverse order. Here, the damage is initiated by contact stresses, and the bending and matrix cracks appear instantly in the top ply followed by delamination on the top interface.

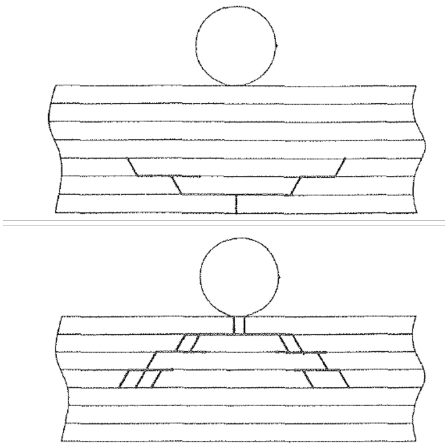

Figure 3.4: Damage development in a flexible (top) and stiff (bottom) composite plate targets during impact.[1]

For low thicknesses, less stiff targets, damage is initiated on the lowest ply. As the thickness increases, more stiffness is introduced into the plate, and a higher energy is required to initiate damage in the lowest ply. The energy required keeps increasing until a maximum is reached, which is the optimal thickness. This critical state is reached when damage is initiated simultaneously on the top and the bottom layer, giving the highest resistance to damage initiation. Above this optimal thickness, failure comes from high contact stresses in the top layer, and increasing the thickness only results in lower damage threshold energies. As for the stackup sequence, in general, laminates having $+/-45\,\mathrm{deg}$ fiber orientation in the first plies are provide a higher stiffness to the plate than $0\,\mathrm{deg}$ plies [8]. The influence of the stiffness conferred by these two variables is studied in more detail in chapter 4 through the two high and low velocity models.

Another relevant parameter is **the shape of the projectile**. For blunt projectiles (hemispherical), the deformation is higher due to the larger contact area. Thus, the failure is shaped as shear plugging, causing tensile stretching after severe indentation and thinning of the target plat. With sharp projectiles (conical) projectiles, the failure mode is most often petaling in thin plates and ductile hole enlargement in thicker plates [52]. In this project, two projectiles are to be tested, a cylinder for the high velocity case and an hemisphere for the low velocity model, so the influence of the projectile shape on the failure mechanism is

also to be examined.

3.2.4 Residual strength post-impact

In the final part of this section, the post impact strength reduction is explained shortly as analyzing deeply the strength reduction requires a higher numerical investment than the one allowed in the scope of this work. Impacts of foreign objects on composite structures can create internal damage that reduces the strength of the structure significantly reaching new residual properties.

Firstly, the **residual tensile strength** of a laminate after impact decreases as the initial kinetic energy of the impactor increases, as shown in Fig. 3.5 [1]. As long as the velocity remains below the threshold value (region I), the strength is kept constant (no damage). When the threshold is reached (region II), the strength decreases as the velocity increases rapidly until a maximum damage size is reached. Then, for higher velocities (region III) complete perforation occurs leaving a hole with a diameter independent of impact velocity so that the residual strength is almost constant. Note that, the last mentioned property is higher than the minimum reached in region II. This is due to the fact damage spreads over a larger area than the one produced at a high velocity impact. Here, the damage is more localized (resulting in a cleaner hole). As the fibres carry the majority of tensile load in the longitudinal direction, fibre damage is the critical damage mode that reduces the tensile strength.

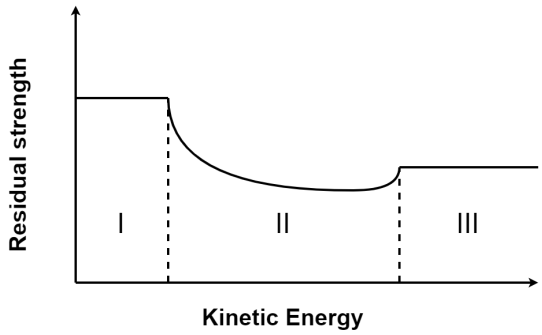

Figure 3.5: Tensile residual strength evolution with projectile kinetic energy for an impact on a composite plate. [1]

On another note, the **compressive strength reduction** is due to local instabilities or buckling effect of the plies. With laminated composites, even low velocity impacts can induce delaminations that reduce the compressive strength and that can buckle under and spread, causing a further decrease in the resistance to compression.

3.3 Numerical Model: Composite Plate Impact

In this section, the different steps to construct the numerical model employed for the low and the high velocity impact problems are explained in detail:

1. **Element type** choice between solid or shell elements, **composite plate layup structure** (one shell elements layer with different integration points or solid element layers with one integration point), and the **integration method**, that can be reduced integration (1-point reduced) or full integration (8 integration points).

2. For reduced integration techniques, an **hourglass algorithm** must be included in the numerical model, to prevent the apparition of these spurious modes of deformation.

3. The **composite material model** employed among all the different available formulations provided by LS Dyna. The intralaminar and, sometimes even interlaminar failure criteria and damage model options, are included in this formulation.

4. The **contact algorithm** that defines the contact interaction between the different parts of the impact problem, e.g. impactor-plies, interlaminar failure or delamination between plies, plies self-contact and contact between not-subsequent plies. This is one of the most tedious parts of any numerical model, and for impact problems, the contact options chosen for each interaction have a big influence on the results.

Any numerical model must include these steps during its development, that is why this section provides an insight into how LS Dyna treats each part of the model. In addition, some indications are given at the end of this section on how to check the numerical validity of the results.

Similarly to other similar software tools, LS Dyna has its own terminology. In multiple parts of this section and in general in this manuscript, some specific LS Dyna terms are employed, so it is strongly recommendable to refer to the Appendix 7. For further understanding, please also refer to the LS Dyna Manuals [31, 32, 43] or to the official support site [46].In fact, before starting to describe the different parts of the numerical model, an introduction into the governing equations that the software solves during the impact problem is included in 7.1 in the Appendix 7.

3.3.1 Element Formulation, Layup Structure and Integration Method

In this part, the element type and the element structure employed to develop the composite plate plies, and the integration technique for computing the stresses on each ply are explained.

Element type

The first point to be discussed is the type of element selected to solve the impacted plate. For both the high and the low velocity impact models, the solid hexahedral or brick element (8 nodes) has been chosen. This is one of the most reliable and robust element type in numerical analysis, particularly for impact phenomena modelling. It is highly recommended because of its geometric flexibility, the capacity to adapt to mesh refinements, the compatibility with contact algorithms and its reliability as this element type is well-documented, and numerous material models and failure criteria are available for accurate representation of different materials. As a conclusion, and although composite materials are also commonly represented through shell element types, solid elements have been chosen as the preferable element type for the reference high and low velocity models.

For more technical information about this element type please refer to 7.2.1 in the Appendix 7.

Composite Layup Structure

There are different ways to define the structure of the layers of a composite plate, depending on the type of element chosen and the number of layers chosen to represent the whole plate as shown in Fig. 3.6. The methodology chosen often depends on the scope of the simulation, the accuracy and the required computational cost. The main techniques are:

- **Single layer of Shell Element:** The composite material structure is defined using one single layer of shell elements with various integration point through thickness, representing the different plies of the laminate. This modelling technique is able to represent intralaminar composite failure but not delamination, as only one layer of elements is modelled. Very simple structure that allows for reduced computational efforts, but not very accurate.

- **Layers of Solid Elements:** This is the structure layup that is going to be employed for both the high and the low velocity models, based on different layers of solid elements, where each one normally is used to represent one entire ply of the laminate. This model allows the introduction of delamination between the plies. An important limitation is found at this point, concerning the number of through thickness integration points. When using 1-point reduced integrated solid elements, although this element provides good properties in terms of stability, reliability and capacity to adapt to the mesh, they normally lack of accuracy particularly in bending deformation. In order to solve this issue, the introduction at least 3 additional integration points through thickness is recommended. Although this is a common practice in

metallic plates, due to the complexity that composite material behaviour and damage evolution introduce in the problem, 1-point reduced integrated solid elements are used to represent each layer without introducing additional through-thickness integration points.

- **Layers of Shell Elements:** The composite material is represented by multiple layers of shell elements. Every layer can be assigned to represent one or various plies of the laminate depending on the accuracy requested, by assigning a number of integration points through thickness. This technique allows to introduce delamination models between the plies.

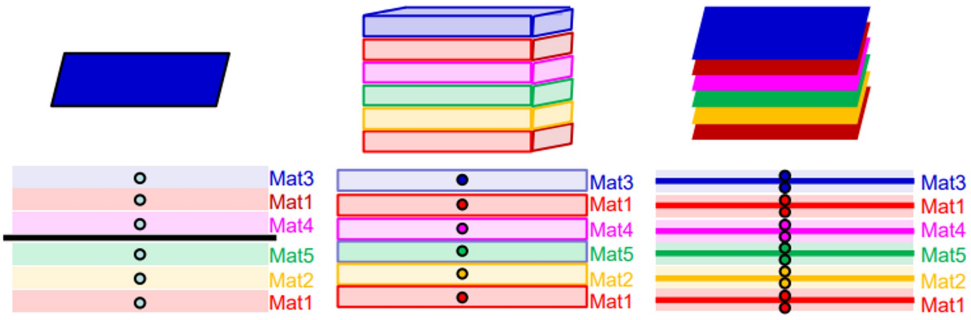

Figure 3.6: Composite Material Structure numerical modelling techniques. One single layer of shell elements (left), layers of solid elements (middle) and layers of shell elements (right) [11]

.

Integration Method

In the case of **solid elements**, which are the elements of interest for this work, the integration technique typically employed is the 1-point reduced integration also known as constant stress solid formulation, ELFORM=1 parameter in LS Dyna. The full mathematical development of the integration procedure that LS Dyna performs is included in 7.2.2 in the Appendix 7.

The main advantage of single point reduced integration is that it is much faster than full integration techniques and avoids the locking phenomenon experienced in fully integrated elements. The solution provided by a full integration technique in plasticity problems and other problems with $\nu \approx 0.5$ locks up in the constant volume bending modes, resulting in an over stiffened response of the structure. However, as it has been proved in most numerical studies of this kind the disadvantage of reduced integration procedures is the apparition of ”hourglass” or spurious modes that require stabilization. The treatment of this issue is discussed in the next part of the section.

In the construction of the reference models discussed further in this chapter, the reduced integration techniques have been generally preferred and employed as the reference configuration. However, full-integration technique is also employed for both models as part of the numerical analysis.

3.3.2 Hourglass Control Algorithm

This section is dedicated to hourglass modes formation and control through different algorithms. Hourglass modes and resisting hourglass methods are a critical part of the numerical problem. All the information for this part of the section has been extracted from the LS Dyna support sources [47, 43]. The objective is to understand the origin of hourglass modes and the computation technique of the correspondant resisting forces in LS Dyna.

Hourglass modes are nonphysical modes of deformation that occur in under-integrated elements and produce no stress. In the case of 1-point reduced integrated hexahedrons, with 24 degrees of freedom, there are in total 12 hourglass modes of deformation, four hourglass for each direction of the coordinate system. The x-components of the hourglass modes are shown in Fig. 3.7; the other 8 hourglass modes can be obtained by replacing the x-axis to the y-axis, and then to the z-axis.

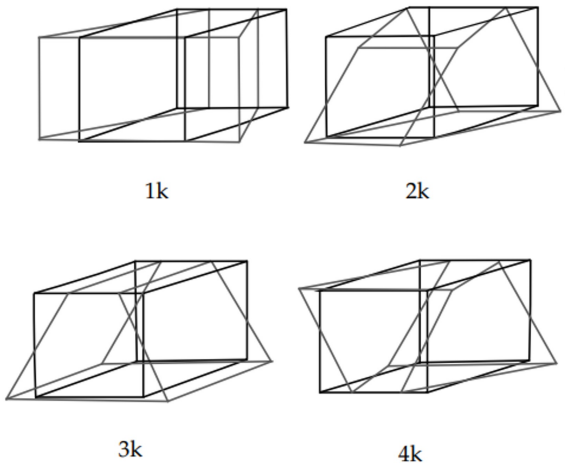

	= 1	= 2	= 3	= 4
j1	1	1	1	1
j2	1	-1	-1	-1
j3	-1	-1	1	1
j4	-1	1	-1	-1
j5	-1	-1	1	-1
j6	-1	1	-1	1
j7	1	1	1	-1
j8	1	-1	-1	1

Figure 3.7: Hourglass modes of an eight-node element with one integration point. [43]

Thus, the formation of hourglass modes occurs whenever diagonally opposite nodes have identical velocities $\dot{x}_i^1 = \dot{x}_i^7, \quad \dot{x}_i^2 = \dot{x}_i^8, \quad \dot{x}_i^3 = \dot{x}_i^5, \quad \dot{x}_i^4 = \dot{x}_i^6$. As a consequence, the strain rates at the integration point of these elements ($\xi = \eta = \zeta = 0$) are zero, as can

be easily deduced from the anti-symmetry property of the strain matrix at the centroid:

$$\dot{\varepsilon}_{ij} = \frac{1}{2}\left(\sum_{k=1}^{8} \frac{\partial \phi_k}{\partial x_i}\dot{x}_j^k + \frac{\partial \phi_k}{\partial x_j}\dot{x}_i^k\right) = 0 \tag{3.7}$$

The hourglass shape vectors, $\Gamma_{\alpha k}$, are orthogonal to the derivatives of the shape functions. Since hourglass deformation modes are orthogonal to the strain calculations, work done by the hourglass resistance is neglected in the energy equation. This may lead to a slight loss of energy. However, the energy dissipated by the hourglass forces reacting against the formations of the hourglass modes should be controlled and kept under a 10% of the internal energy, as is later explained in more detail in this section.

Moreover, the product of the base vectors ($\Gamma_{\alpha k}$) with the nodal velocities, ($\dot{x}_i^k$) known as $h_{i\alpha}$, is zero when the velocity field has no hourglass component, and non-zero when hourglass modes are present. This product can be expressed as,

$$h_{i\alpha} = \sum_{k=1}^{8} \dot{x}_i^k \Gamma_{\alpha k}, \tag{3.8}$$

and it is an important quantity when computing the hourglass resisting force vectors, $f_{i\alpha}^k$. The hourglass control algorithm applies internal nodal forces to counteract hourglass modes:

$$f_{i\alpha}^k = a_h h_{i\alpha} \Gamma_{\alpha k\prime} \tag{3.9}$$

where the coefficient $a_h = Q_{\mathrm{HG}} \rho v_{\mathrm{e}}^{2/3} \frac{c}{4}$, is the product of the element volume, v_e, the material sound speed, c, and the user-defined scale factor Q_{HG}.

The resisting forces can be applied in the form of a viscous damping or elastic stiffness. This leads to a classification of the hourglass algorithms in two types:

- The **viscous hourglass control** technique, computes the resisting forces based on the nodal velocity vector (resists components of the velocity field that are not fully linear). The resisting forces are proportional to components of nodal velocity contributing to hourglass modes, allowing to inhibit additional hourglass mode deformation but not to recover from the previously accumulated. This algorithm is mostly used in high velocity/high strain rate problems.

- The **stiffness hourglass control** resisting forces are proportional to the nodal displacements contributing to hourglass modes. This technique allows to reduce the total accumulated hourglass mode deformation, as the hourglass rates are multiplied by the solution time step to produce increments of hourglass deformation. This control technique is preferred for low rate problems over viscous types as due to

its higher effectiveness. However, artificial stiffness may be introduced in the body more easily than with the viscous technque. This needs to be controlled through the hourglass energy, a measure of the work done by hourglass resisting forces, as explained in the section.

In the Appendix 7 in section 7.3, the mathematical computation of the hourglass resisting forces for both algorithms is explained in detail.

Post-Process: Hourglass Energy Computation

In section, the different checks that should be done in the results to ensure the correct performance of the hourglass algorithm are described. To effectively control hourglass modes appearance, as well as to ensure that there is not an excessive effect of nonphysical hourglass resisting forces on the final solution, it is recommended to check that:

- There are **no hourglass modes present in the simulation**. This can be done by examining the d3plot results in LS Dyna, in which the evolution plots of the system can be observed, as well as the displacement, stress and strain distributions, etc. To facilitate the identification of this spurious modes, the displacements can be scaled by a factor of 2 or 3 by adjusting the settings.

- The **hourglass energy (HGE)** shown in the global energy plot computed by LS Dyna in the glstat file, should always **remain below 10% of the internal energy**. This check should be performed in the global system and in each individual part.

  The work performed by the hourglass resisting forces can be adjusted by employing the correct algorithm and scaling factor. However, the most efficient way of to reduce hourglass modes and deal with hourglass energy control is refining the mesh, as will be seen in the numerical analysis of the results.

3.3.3 Material Formulation

There are multiple composite material models in LS Dyna, so it is key to determine the requirements of each study case. The composite material model employed for both the high and low velocity impact models must be able to represent accurately:

- **Intralaminar failure:** Matrix cracking, matrix-fiber debonding and fiber breakage. For detecting the initiation of these damage modes an adequate stress failure criteria must be introduced into the model. Additionally, as damage is developed, the strength properties of the material should be softened and the fully failed elements must be conferred zero stress, and be deleted from the calculation. Thus, the material model also needs to include strength softening and strain to failure parameters.

- **Interlaminar failure/Delamination:** This part of the model is not included in the material formulation, but in the contact algorithm. Delamination is modelled as a fracture mechanics problem with two modes of failure, mode I (crack opening) and mode II (in-plane shearing). This part of the model is further explained in the section 3.3.4 dedicated to the contact algorithm.

The material models accounts for physical properties of the material that can be measured by experiments e.g. strength, elastic modulus, strain-to-failure, etc. but also include software specific parameters, which, either have no physical meaning or cannot be determined experimentally. The state of the art material modelling requires extensive tweaking and calibration of the material models parameters to reach an agreement between experiments and simulations [4].

Before describing the constitutive law chosen to represent the material, it is essential to know how to model the different ply directions in a composite material structure. In LS Dyna, this is done inside the material definition through a parameter called AOPT. Considering that the layup structure is modelled as a stack of solid element layers and a simple geometry such as a beam or a composite plate this procedure is relatively easy. For more information, please refer to the section 7.4.1 in the Appendix 7.

Material Model 54/55: Enhaced Composite Damage

The specific material formulation employed to model the composite plates in both models is explained in this section. The information is borrowed from different literature sources [41, 32, 57, 53].

The material formulation chosen is called ”Material Model 54/55: Enhaced Composite Damage” or *MAT_054/055 in LS Dyna notation. This model is based on an anisotropic linear elastic behaviour if the material is undamaged, and on damage criteria to model non linearity in the model. It employs the ”ply discount method”, in which the entire ply is discarded (the ply stiffness is set to zero or is reduced to some arbitrary chosen value close to zero) along the damage direction as soon as damage is detected in that particular direction.

This model is based on a series of parameters able to simulate the failure response of the composite, which hould be obtained and calibrated with material test data. In the high and low velocity impact models' construction, most of these parameters were available in the reference studies conducted by the authors. However, because there were some material parameters not recorded during their studies and also due to the necessary adaptation from the reference models to this work, some parameters were approximated, based on other literature sources or on numerical stability and efficiency. This is the most important limitation of the models that have been constructed in this work and it is highlighted again

in the next following chapters. In addition, there is another limitation related to the fact that single ply failures in lay-ups are hardly possible without affecting the neighbouring layers. Thus, it would be desirable to have more information from experiments about strengths in the post failure regime.

The main characteristics of the material formulation are described next. These are described progressively according to the evolution of damage in the material: initiation of damage predicted by failure criteria, the damage model which represents softening of strength properties and finally, the erosion law of elements that are fully damaged.

Before failure starts, the behaviour of the composite material in the elastic region can be described by the following **constitutive law**:

$$\varepsilon_1 = \frac{1}{E_1}\left(\sigma_1 - v_{12}\sigma_2\right) \tag{3.10}$$

$$\varepsilon_2 = \frac{1}{E_2}\left(\sigma_2 - v_{21}\sigma_1\right) \tag{3.11}$$

$$2 \cdot \varepsilon_{12} = \frac{1}{G_{12}}\tau_{12} + \alpha {\tau_{12}}^3 \tag{3.12}$$

To characterize **the onset of damage**, as described earlier in previous section of the manuscript 3.1.1, there are various failure criteria. In the current material formulation, there are basically two available failure criteria: Chang-Chang [13] (*MAT_54) and Tsai-Wu [56] (*MAT_55). The use of either of the criteria must be specified inside the material card, as explained in 7.4.3. These criteria predict the onset of damage in an element of a ply on the composite.

The **evolution of damage** through the composite component is represented through a series of numerical parameters that conform the damage model. These parameters can be classified in: strength reduction parameters and strain to failure parameters.

First, the **strength reduction parameters** are discussed. After failure is reached in an element, the tensile and compressive strengths of the fibre and the matrix components are softened by means of certain parameters (FBRT, YCFAC and SOFT) included in the material formulation. The strength reduction numerical parameters are purely mathematical and cannot be experimentally measured but only through trial and error. These parameters are explained in more detail in section 7.4.3, as they were not available in the reference studies and thus, could not be included in the constructed models.

Secondly, the **strain to erosion parameters** included in the material card need to be described. Note that, in LS Dyna, when any failure criterion is met in an element, the specified elastic properties for that ply element are set to zero, but the stresses carried by the element are not reduced to zero but unchanged from the stress state just prior to failure. This produces a constant stress state in the ply element stress-strain curve following failure

[57]. The resulting 'plastic' behavior is shown in Fig. 3.8:

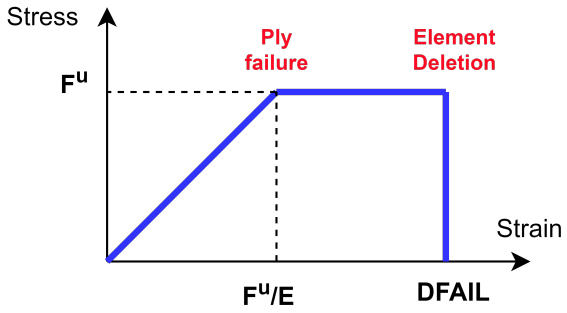

Figure 3.8: Elastic-plastic stress-strain behavior of Enhanced Composite material formulation in LS Dyna (*MAT_54). [57]

In LS Dyna, an element is eroded when the local stresses in that element are zero. This erosion condition is not caused by the composite failure criteria, neither by the previously explained strength reduction parameters. For element deletion, there are specific limit strain values that can be introduced in the material formulation:

- **DFAILT:** Strain to failure in fiber tension.
- **DFAILC:** Strain to failure in fiber compression.
- **DFAILM:** Strain to failure in matrix tension/compression.
- **DFAILS:** Strain to failure in shear.
- **EFS:** Effective failure strain. It immediately reduces the ply stresses to zero when the strain in any direction exceeds the critical value. A critical EFS value can be calculated for any simulation by determining the strains in the principal direction of the composite material: logitudinal (a), transversal (b) and in-plane shear (ab), at element failure, and using them in (3.13). If the computed value of EFS is below the critical one, this will cause premature element deletion. The default value for EFS is zero, which is interpreted by LS Dyna to be numerically infinite..

$$\sqrt{\frac{4}{3}\left(\varepsilon_{aa}^2 + \varepsilon_{aa}\varepsilon_{bb} + \varepsilon_{bb}^2 + \varepsilon_{ab}^2\right)} \geq EFS \tag{3.13}$$

If DFAILT, DFAILC or DFAILM are set to zero, the code ignores the parameters altogether and failure can only occur by the Chang-Chang failure criterion. If DFAILT, DFAILC and DFAILM are non-zero, failure can occur if one of the strains exceeds the strain-to-failure. The four failure strains parameters can be measured through coupon-level tests or one-element numerical simulations. However, most design allowables for material

systems do not include any information about the strain to failure values, and even if they do these parameters are strongly dependent on numerical aspects such as the mesh size employed in the test, so they are highly sensitive to any numerical modification. Thus, there are some authors that recommended to initially approximate them through simple one-dimensional linear stress strain relationships, such as Wade et al. in his work [57].

$$DFAILT = \frac{X_T}{E_a} \tag{3.14}$$

$$DFAILC = \frac{X_C}{E_a} \tag{3.15}$$

$$DFAILM = \frac{Y_T}{E_b} \text{ or } \frac{Y_C}{E_b}, \tag{3.16}$$

where X_T,Y_T,X_C, and Y_C are the fibre and matrix, tensile and compressive strengths respectively, and E_a and E_b are the elastic modulii in the principle and transversal directions. The same values that were employed in the previously described failure criteria 3.1.1 are used in this approximation. The adjustment of the failure strains can be done numerically using results such as the expected strengths, failure strains and energy output as seen in [57].

Althought not included in any of the models, element deletion can also occur if the element time step TFAIL is exceeded, which represents the minimum time step for element deletion. This option is useful only in cases where the computational cost of the simulation is driven up by highly distorted elements that no longer carry load but do not fail from the prescribed element deletion criterion [20].

Lastly, and although this parameter is not used either, the SOFT parameter, or crush front reduction factor, is a numerical factor used to reduce the strength of the elements immediately ahead of the crush front, i.e. the row of elements that will be loaded once the current row is deleted. This parameter is used to avoid instability and to ensure stable crushing. Approaching failure, the load reaches its peak in the active row of elements, and at failure it is suddenly drops to zero. If the SOFT parameter is set to zero this sudden transition may lead to unstable buckling of the structure. If this parameter is defined within the range [0, 1], then the crush front reduction is active. For SOFT = 1, elements at the crush front retain their intact strength and no softening takes place. For SOFT values near zero, the strength is nearly completely reduced. Note that, this parameter cannot be measured experimentally, it needs to be calibrated by trial and error [20].

Post-Process: Material Failure through History Variables

In this section, some indications are given on how to post-process the results related to the intralaminar failure of the composite in LS Dyna. As explained in the previous section,

the failure onset is predicted through the Chang-Chang or the Tsai-Wu failure criteria, depending on the option indicated inside the material formulation.

The failure of the elements is computed in their integration points (centroid) through the four failure variables specified in 3.1.2. These variables were: the fibre tensile and compressive, e_f and e_m, and the matrix tensile and compressive, e_m and e_d, failure history variables. These values are computed for every time step at every integration point. Depending on the result, the integration points are assigned the value of 1 (not failed, elastic) or 0 (failed). The status in each layer (integration point) and element can be plotted in d3plot using the Fringe Plot tool through these history variables.

Note that, these variables are recorded during the simulation only if it is clearly specified in the LS Dyna database card. The number of history variables (for solid elements 17) should be introduced as an input in the card named *DATABASE_EXTENT_BINARY card under the parameter NEIPS. For Models 54 and 55 these additional history variables for solids are tabulated in Tab. 3.1, where i refers to the integration point.

History Variable	Nomenclature	Description	Value
1	$e_f(i)$	Flag for tensile fibre failure	1 (elastic)
2	$e_c(i)$	Flag for compressive fibre failure	
3	$e_m(i)$	Flag for tensile matrix failure	
4	$e_d(i)$	Flag for compressive matrix failure	0 (failed)
5	$e_{fail}(i)$	Total failure max($e_f(i)$)	
6	$dam(i)$	Damage parameter (SOFT)	-1 (intact/elastic) 10e-8 (crashfront/ damaged) 1 (failed)
15	ϵ_a	Local strain a-direction	Strain values reported at ip
16	ϵ_b	Local strain b-direction	
17	ϵ_{ab}	Local strain ab-plane	

Table 3.1: History Variables computed in LS Dyna at the integration point of ply elements for material formulation *MAT_054.

3.3.4 Contact Algorithm

The methodology followed to model the contact interactions involved in an impact on a composite plate in LS Dyna is described in this section. Firstly, the definition of a contact formulation in LS Dyna and some relevant general concepts related to contact search and force calculation are given along with the classification of the main types of contact formulations. The information for this section has been obtained and compared from different LS Dyna support sources such as [45, 46, 43]. The second part focuses

on explaining the basis of penalty based contacts, which are used for defining all the interactions in these work's models. Please refer to 7.5 in the Appendix 7, for more information on contact modelling in LS Dyna.

Introduction and Types of Contacts

Every contact interaction is formed by two sides, the slave and the master. The contact sides can be defined in several different ways (e.g. the slave and the master can be Parts, Part Sets, Segment Sets), but no matter the method used, LS Dyna converts the faces of the elements of the **surfaces involved in the contact into segments**[1] during the analysis.

There are two primary ways to distinguish contact algorithms, the **method used for searching for penetration** and the method of **applying contact forces** after such penetration is found.

- The **contact search methods** are classified between the **node-based search** (non-automatic formulation), the **bucket-sort approach** (automatic formulation) and the **segment-based search**. These three methods are further explained in section 7.5.2 in Appendix 7. The methods involved in the developed models are the bucket sort, which locates the nearest segment to the slave node, and the segment based approach, which searches for penetrating segments instead of nodes penetrating into segments.

- The **contact force calculation** methods in LS-Dyna can be classified in **constraint-based** and **penalty-based**. The constraint-based method is based on a kinematic constraint between slave nodes and master segments. Alternatively, the penalty-based approach, consists of placing normal interface springs between all penetrating nodes and master surface.

Many of the contact formulations available in LS Dyna are penalty-based. In fact, although the tied contacts formulations are usually known to be constraint-based, some can also be defined as penalty-based, e.g. the tiebreak contact (includes failure option) which is used in the model to model delamination. As a consequence, all the contact interactions defined in this study for the high and low velocity impact models are penalty-based options, so obviously the focus of this section is set on this contact type.

Penalty Based Contact

The physics behind the Penalty Based Contact Force calculation method in LS-Dyna are explained in 7.5.3. Basically, the penalty problem starts with a slave node n_s penetrating its corresponding master segment which has a thickness offset value t. The penetration is

[1] Segment: Face of an element included on a contact

detected and its depth l is calculated and counteracted by the application of an interface force, $\mathbf{f}_s$ to the degrees of freedom corresponding to the slave node (n_s). The slave node is projected back up to the surface of the master segment. Finally, a reaction force f_m^i, is applied to the master segment nodes, such that the total force on the master nodes equals the applied slave node force.

The penalty contact theory is based on two relevant parameters: the contact thickness t and the penalty stiffness k_i. The **contact thickness** t, is by default taken as the 40% of the element edge for solid elements. On another hand, the **contact stiffness (k_i)** can be computed through different methodologies. The terms included between parenthesis are specific terminology used in the framework of LS Dyna, for more information please refer to 7.5.3.

1. The **default penalty formulation** (SOFT=0), best suited for contacts between similar materials as the penalty stiffness is based on the material properties of the contact interfaces:

$$k_i = \frac{f_{si} K_i A_i^2}{V_i} \text{ for solid elements} \tag{3.17}$$

   where, f_{si} is scale the penalty factor (SFM/SFS), A_i refers to the area of the contact segment, K_i is the bulk modulus of the material established for the contacted element $K = \frac{E}{1-2\cdot\nu}$.

2. The **segment-based penalty formulation** (SOFT=2), which does not only compute the penalty stiffness differently, but also searches for contact between segments rather than between nodes and segments, as has been represented in Fig. 3.9. This formulation is better suited for dissimilar material interactions like the one in this study, between metallic or rigid impactor and composite material plate. The penalty penalty stiffness is calculated as follows:

$$k_{\mathrm{i}} = 0.5 \cdot f_{si} \left(\frac{m_1 m_2}{m_1 + m_2} \right) \left(\frac{1}{\Delta t_c(t)} \right)^2 \tag{3.18}$$

   In this case, the contact time step Δt_c and the slave and master segment masses, m_1 and m_2 [2] are used for the penalty stiffness calculation. This formulation has the advantage of allowing a more realistic distribution of the penalty contact forces as they are applied to all the nodes of the slave and master segments (remember each segment or element surface in this case is formed by 4 nodes).

[2] Segment mass: Calculated as half of the solid element mass associated to that specific segment.

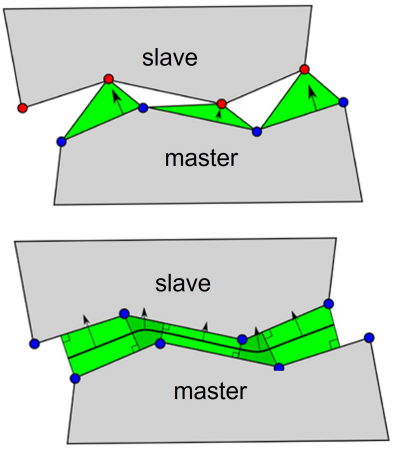

Figure 3.9: Comparison between node-to-segment (SOFT=0) and segment-to-segment (SOFT=2) search contact algorithms. [58]

The last parameter that defines a penalty contact interaction, and that has already been mentioned in the previous paragraph, is the **contact time step**, δt_c. The contact spring stiffness k_i and nodal or segment masses are used to compute a contact timestep Δt_c specific for each artificial contact spring. Depending on the penalty stiffness calculation option, the treatment of the contact timestep also differs:

- The **default penalty formulation** (SOFT=0) calculates the contact timestep independently from the global stability timestep,

$$\Delta t_{ci} = \sqrt{\frac{m_i}{k_i}}. \tag{3.19}$$

  where m_i is the mass associated to the artificial contact spring and k_i the penalty stiffness computed as shown in the previous section.

- For the above described **segment-based penalty formulation** (SOFT=2), the contact time step is initialized as the global solution time step. The contact timestep is then adjusted if the global time step changes, above a limit of 5% of the original, to keep stability through the simulation. As a consequence, the contact stiffness directly depends on the global time step when using this penalty stiffness calculation method.

Relevant Contact Types: Impact on Composite Plate

In this part, the most relevant contact formulations employed in the high and low velocity impact models are described. The main contact interactions involved in a composite plate impact problem are: the contact between the projectile-plies, and the contact between the different plies.

The contact between the **impactor and composite plate plies** is defined through an **eroding surface-to-surface contact**. The choice of contact employs a **two way symmetric treatment** (also called automatic contact), which means that the master and slave nodes are both checked for penetration in every time step. Moreover, the **eroding** option allows for the contact surface to be updated as elements on free surfaces are deleted due to the material failure criteria as discussed previously in the report. The penalty stiffness calculation method chosen is the **segment-based penalty formulation** (SOFT=2), as the projectile and plies are made of very dissimilar materials.

The **contact between plies** is not as intuitive, as there are three possible contact interactions between the plies:

- **Delamination**: Separation of plies with different fibre orientation angle. All the plies are initially tied and delamination is represented by means of a fracture mechanics failure criteria.

- **Contact between not-subsequent plies**: As some of the plies may fail, elements can be eroded from the calculation. As a consequence, plies that are not placed right next to each other could interact, and a contact needs to be defined between them.

- **Self-contact**: Elements of the same ply can also interact, as a direct consequence of the compressive failure mechanism of buckling, a damage mechanism previously explained in section 3.2.

The plies, although having different fibre orientations, share the same material properties. That is why the default penalty stiffness calculation method (SOFT=0) is chosen for defining these interactions, simplifying also the cost of the model.

Tiebreak Contacts for Delamination Modelling

Delamination failure mechanism is represented through a special type of tied contact with failure option, the tiebreak contact. Tiebreaks are penalty based contacts that allow the transmission of both compressive and tensile forces. In penalty-based contacts, when there is an incremental change in the projected distance between slave node and master segment, a penalty force directly proportional to this distance is applied. In most of the classical penalty contacts, the force is only applied if this change in distance is negative (penetration, compressive contact) while in tiebreak, the force applied is irrespective of the sign of the incremental projected distance (penetration and separation). In addition, it is important to note that tiebreak contacts need to be formulated between set of segments and not between parts, in order to preserve stability and easing of the post process of the results.

Thus, tiebreak contacts allow to resist the separation of the slave node from the master segment by a linear artificial contact spring, until a failure criterion is met. After this, the tensile coupling of the artificial spring is removed and the slave node is only allowed to interact with the master segment through the traditional penalty based contact.

The parameters needed to define a tiebreak contact depend on the chosen option and are based on fracture mechanics theory. Depending on the allowable parameters, which are mainly obtained through material tests, it is more convenient to use a different tiebreak option. The principal differing characteristics between the options are the failure criterion used for predicting the initiation of damage and the damage evolution model [9, 31]. For the following contact and failure formulations, $NFLS$ denotes the normal failure stress, $SFLS$ is the shear failure stress computed in the interface between two different plies. The $ERATEN$ and $ERATES$ parameters represent the fracture toughness on the normal (opening, mode I) and shear (in-plan shear, mode II) modes, these values are obtained through standarized material tests, e.g. Double Cantilever Beam (DCB) and the 3 Point End Notched Flexure (ENF). $PARAM$ is a generic parameter that represents different properties in every option as it is explained in the next paragraph.

The three tiebreak options relevant in this work are:

- **OPTION 7:** This option is based on the discrete crack model described by Lemmen and Meijer [29]. The failure criterion for prediction of the onset of damage is:

$$\left(\frac{\max\left(\sigma_n, 0\right)}{NFLS}\right)^2 + \left(\frac{\sigma_s}{\mathrm{SFLS}\left(1 - \sin(PARAM)\min\left(0, \sigma_n\right)\right)}\right) = 1 \qquad (3.20)$$

  Here, PARAM represents the frictional angle that allows to include the possible increase in shear stress due to an increase in the normal stress. However, in the developed models when employing this option this value is not included (set to zero). This tiebreak option allows crack initiation but does include a model of damage evolution, so the stress behaviour post failure follows the profile shown in Fig. 3.10.

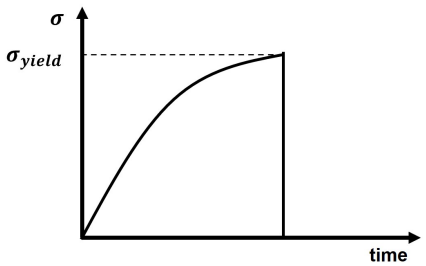

Figure 3.10: Stress profile for tiebreak contact with no damage law after failure onset (OPTION=7). [9]

When the failure criterion is met, the stress in the interface of the plies suffering delamination is driven to zero and the tiebreak contact is deactivated. There is not an evolution on the strength of the interface represented by a damage variable. This is the simplest tiebreak contact option and is taken as the baseline configuration for both models presented in future chapters.

- **OPTION 6:** This model is only applicable for solid elements. The failure criterion for damage initiation is as follows, it has been also represented by means of Fig. 3.11.

$$\left(\frac{|\sigma_n|}{NFLS}\right)^2 + \left(\frac{|\sigma_S|}{SFLS}\right)^2 = 1 \tag{3.21}$$

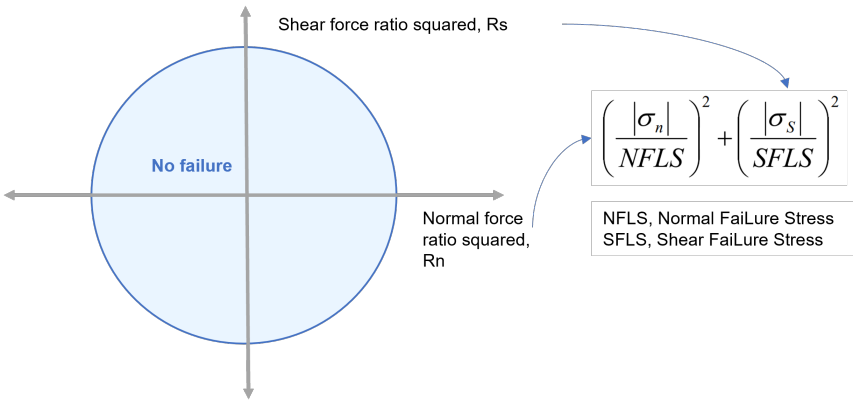

Figure 3.11: Stress based failure criteria for tiebreak contact with linear damage law after delamination onset (OPTION=6).[9]

After the failure stress condition is met, there is a linear function named ”damage” that represents the decrease in the interface’s strength. Damage is a linear function of the the distance between the two points that were initially in contact. When this distance reaches user-defined critical value defined through PARAM (can also be called CCRIT in LS Dyna terminology), damage is considered to be fully developed, and complete interface failure occurs. The stress and damage profiles during failure is presented in the following Fig. 3.12:

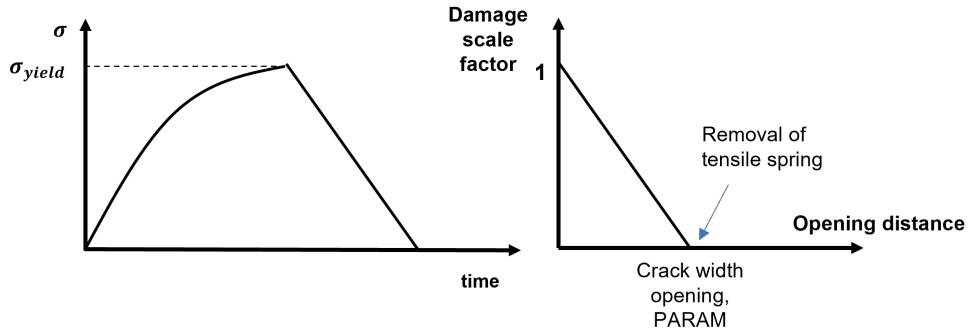

Figure 3.12: Damage and stress profiles for tiebreak contact with linear damage law after delamination onset (OPTION=6). [9]

At the point where damage is fully developed, the energy released due to the failure of the interface can be approximated as:

$$G_{I,II} = \frac{1}{2} \cdot S \cdot CCRIT \tag{3.22}$$

$$S = \sqrt{\max\left(\sigma_n, 0\right)^2 + \left|\sigma_s\right|^2} \tag{3.23}$$

- **OPTION 9:** This option for tiebreak contact modelling is based on the fracture model that is defined inside a cohesive material model also available in LS Dyna (*MAT_COHESIVE_MIXED_MODE). This formulation is based on a bilinear traction separation law with quadratic mixed mode delamination criteria and a damage formulation, which is more detailed in 7.5.4.

  In this section, only an introduction into the basic parameters for the tiebreak contact definition are given. The damage model is based on a traction-separation law and the two individual fracture modes, opening (I) and shear (II), damage onset and evolution laws are connected by means of a new internal parameter, α. This parameter allows the formulation to be fully interactive, as described in [29], allowing to describe a mixed-mode loading condition.

  A graphical representation of this model is included in Fig. 3.13. In this figure, the original model parameters for cohesive elements is shown in black and the corresponding parameters for tiebreak contact are shown in blue.

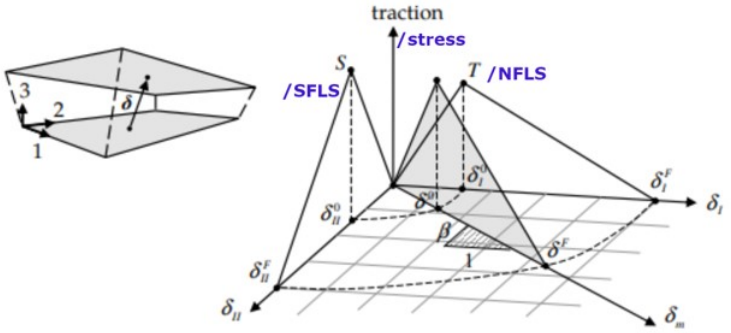

Figure 3.13: Mixed-mode traction separation law for tiebreak contact OPTION=9. [32]

For a better understanding, the description of every parameter and its correspondance between a cohesive element formulation and a tiebreak contact formulation is included in section 7.5.4.

For the high velocity model, the tiebreak option chosen is the simplest one **OPTION=7** as delamination is not the key failure mechanism present at a high velocity impact phenomenon. For the low velocity model, the three described tiebreak options **OPTION=7**, **OPTION=6** and **OPTION=9** were compared inside the parametric numerical analysis in order examine the effects on the accuracy of the results. The contact forces, plate deformation and delamination area were evaluated. The aim of the low velocity impact case was developing a feasible and robust technique for interlaminar failure modelling, by comparing the numerical results with experimental data extracted from the literature.

Interply contact: Contact between not-subsequent plies and Ply self-contact

The other two contact interactions between composite plies have been merged under the same formulation, called ”Interply contact”. These interactions are modelled through an automatic basic penalty-based contact that includes a special feature. This contact, also known as **single surface contact** in LS Dyna, allows to include all parts involved in contact the interaction in the same slave part set. This enables to define the plies self-contact due to buckling and the general interaction between all the plies, subsequent or not in the same contact interaction.

When employing this contact type all the parts are defined as slaves. Thus, the contact force between the contact parts is not computed following the classical approach. An additional LS Dyna feature, called contact transducer, needs to be introduced in the model in order to measure the contact forces between all the plies.

Contact Post Process: Contact Timestep and Sliding Energy

In this final section, the objective is to summarize the main results to be checked to validate the contact algorithm. Two of the main checks to be made in a complex contact algorithm problem, such as an impact on a composite plate problem, are:

- **Contact Time Step**: As described in 3.3.4, this value directly depends on the contact stiffness calculation method employed. LS-Dyna internal algorithm loops through all the slave and master contact surfaces (segments or nodes) of each penalty contact definition and stores the minimum contact timestep encountered. This is performed to check that the contact and the global timestep are not too different. In general, the contact timestep can be an order of magnitude lower or higher than the global timestep. However, if the contact timestep is vastly different, contact breakdowns can occur and the stability and the accuracy of the model is compromised. Particularly for tiebreak contacts, as specified in [9], the contact time step should be within the 10% of the global time step in order to ensure stability.

- **Contact Sliding Energy:** This energy is a numerical artifact, like the hourglass energy, computed by LS Dyna as follows:

$$E_{\text{contact}}^{n+1} = E_{\text{contact}}^{n} + \left[\sum_{i=1}^{nsn} \Delta F_i^{\text{slave}} \times \Delta \text{ dist } t_i^{\text{slave}} + \sum_{i=1}^{nmn} \Delta F_i^{\text{master}} \times \Delta \text{ dist } t_i^{\text{master}} \right]^{n+\frac{1}{2}}, \tag{3.24}$$

  where nsn is the number of slave nodes, nmn is the number of master nodes, $\Delta F_i^{\text{slave}}$ is the interface force between the ith slave node and the contact segment, $\Delta F_i^{\text{master}}$ is the interface force between the ith master node and the contact segment, $\Delta dist_i^{\text{slave}}$ is the incremental distance the ith slave node has moved during the current time step, and Δ dist $_i^{\text{master}}$ is the incremental distance the i th master node has moved during the current time step [43].

The sliding contact energy can be induced by different sources depending on its sign [46]:

- **Positive contact energy:** When friction is included in a contact definition, positive contact energy accumulates due to the dissipative (not recoverable) friction energy. However, in the absence of friction or contact damping, which is the case for both models developed in the next chapter, the positive contact energy is the stored energy in the compressed contact "springs". Thus, as long as there are contact forces being applied, there will be nonzero contact energy. However, as this is a non-physical contact artifact the net sliding contact energy is expected to be small

($E_{\text{contact,}} < 10\%$ peak internal energy [46]. Note that the term "net" refers sum of the slave and master side energy.

- **Negative contact energy:** Negative values on the sliding contact energy appear when relative sliding occurs between parts that have suffered penetration. This sliding is not linked to friction, as it comes from the normal contact forces and normal penetrations, when a penetrated node slides from its original master segment to an adjacent though unconnected master segment.

Delamination Post Process: Contact Gap and Delaminated area

For all tiebreak contact options (OPTION=7,6 and 9), the **delaminated area** can be checked by plotting the **contact gap variable** on the slave side of the contact interface. The "contact gap" is a damage variable that ranges from 0, which accounts for the perfectly tied no damaged condition, to 1, which represents the released and fully damaged status.

In addition, there is a specific file that can be introduced as an output in the input deck, denominated atdout which stands for automatic tiebreak damage output. This ascii file is compatible with automatic tiebreak OPTIONs 7 and 9 and reports time histories of **total delaminated area and energy release rates** for each tiebreak contact interface followed by slave node data on the damage, mode mixity and stress distribution. The information provided in this file is going to be checked and compared with the contact gap data in order to explore the contact tiebreak model capability to accurately represent the delamination phenomenon in a composite plate. The results are validated with experimental and numerical data from previous reference models.

Chapter 4

High Velocity Impact on a Composite Plate

In this chapter the construction and analysis of a high velocity impact model on a composite plate is carried out. The analysis conducted is divided into a numerical and a physical parametrical studies.

The main purpose of developing a high velocity and low velocity models, is to represent the full range of response and damage behaviour of a composite target during impact and the influence that the projectiles' velocity has on the failure mechanisms.

The main interest of this model resides in performing a thorough validation of the authors' methodology through experimentally and numerically validated test cases developed in the literature [6, 39]. The reference model served as a baseline from which some modifications were introduced to adapt it to the scope of this project, and also, to enhance some aspects of its configuration.

4.1 Introduction and Model characteristics

The reference model was developed by the LS-DYNA Aerospace Working Group (AWG) [6] to represent a ballistic impact on a composite rectangular panel. The model provides the baseline to carry out the first step in this work: validating the composite material formulation of interest, that is going to be employed during the rest of this project, for a high velocity impact. Moreover, the studies [39, 49, 27] carried out experimental tests to validate the numerical model developed by the AWG. These experimental results are employed to validate the author's methodology employed in the construction of this project's model.

The high velocity impact is analyzed first because this phenomenon is simpler in terms of material damage modelling than the low velocity case. As it was previously

described in section 3.2, in high velocity impacts the predominant failure mechanism is not delamination, which highly eases the construction of this model. Delamination initiation and evolution modelling are some of the most expensive parts of the numerical model. Thus, by reducing the complexity of the material damage modelling process the focus can be set on other relevant numerical parts of an impact model, e.g. the contact algorithm, the hourglass treatment, etc.

However, this particular reference model [6] came with a challenge: the composite material formulation employed required a commercial license not available for the author (*MAT_162). This is an advanced progressive damage composite material model which main features can be found in the LS Dyna User's Manual [32] or in other relevant studies [22]. The first goal of the High Velocity Model is to translate the material parameters from the baseline material formulation to a composite material option compatible with the author's license. The material formulation employed in this present model was described in section 3.3.4.

A graphical representation of the model is presented in Fig. 4.1.

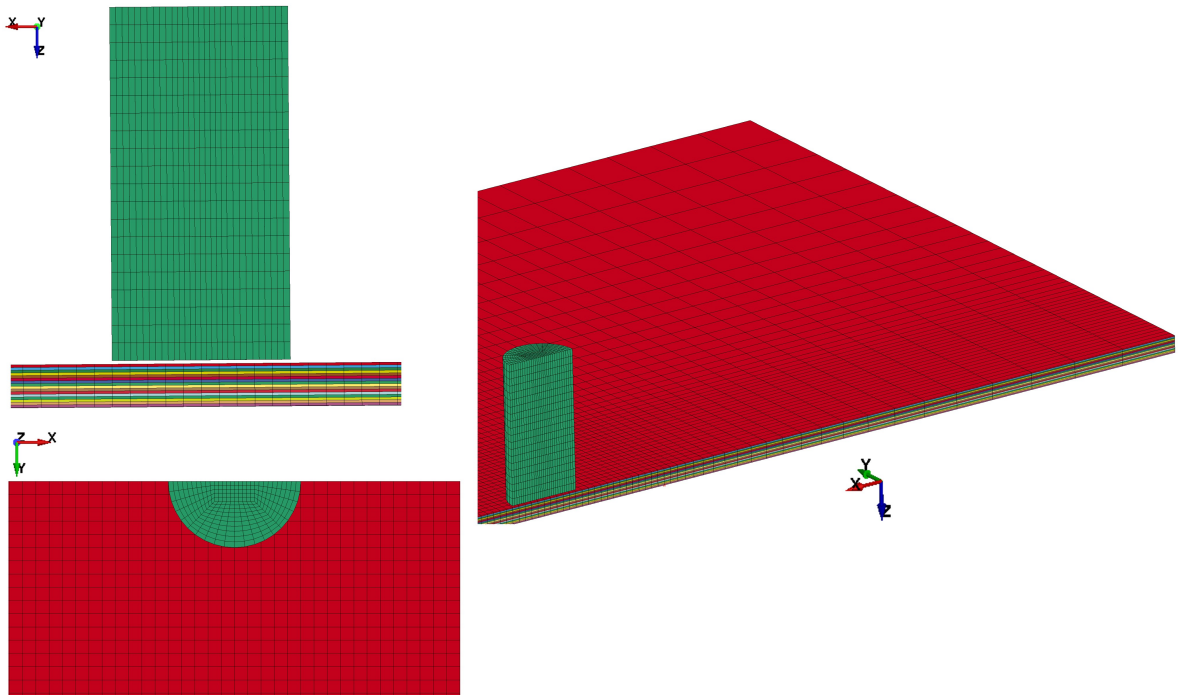

Figure 4.1: High Velocity Ballistic Impact on a Composite Plate Aerospace Working Group Model [6]. Frontal (top left), top (bottom left) and isometric (top right) views of the model in LS Dyna interface.

The principal **characteristics related to the physics** of the problem are the ones related to the plate and projectile material and geometry and the impact conditions, e.g. velocity, location, incidence angle, boundary conditions.

- The **composite panel** has rectangular shape with a XZ symmetry, manufactured in an unidirectional carbon-epoxy composite BMS8-212. The material properties are described later in 4.3.1 inside the numerical model section. The plate is made of 16 plies with a stacking sequence $[45, 90, -45, 0]_{2s}$, and the final thickness of the plate is 3.175 mm. The stackup sequence scheme is shown in Fig. 4.2.

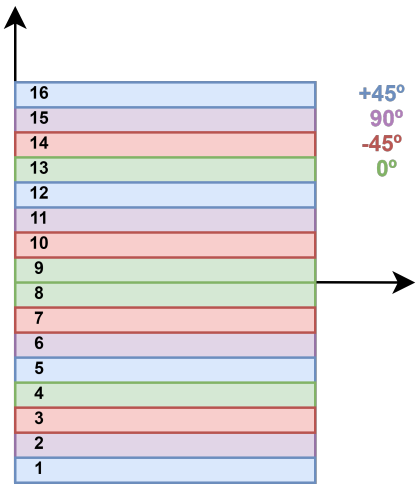

Figure 4.2: Stacking sequence of BMS8-212 composite plate for high velocity impact model.

- **The impactor** is an elasto-plastic steel (ρ=7857 kg/m^3) cylindrical projectile of 25.4 mm of length and 12.7 mm of diameter. The impact occurs at the center of the plate with an initial velocity of $v = 120m/s$, providing an impact energy of $E_{impact} = 184.62J$. Note that the model is reduced to a half by applying the symmetry condition, so in the results the energies correspond to the symmetric model.

The reference model [6] is used as the baseline configuration. However, some modifications were introduced in order to adapt the model to the scope of this project and to the author's license. A comparison between the numerical aspects of the reference model developed by AWG (Aerospace Working Group) [6] and the adapted model, designed as Present Model are presented in the following Tab. 4.1.

4.2 Analysis Methodology

The analysis methodology proposed in this chapter is divided into the numerical and the physical parametrical studies.

<table>
<tr><th>Numerical Model</th><th>Description</th><th>Aerogroup Model [6]</th><th>Present Model</th></tr>
<tr><td>Mesh Density</td><td>Element size impact area</td><td>12.7x12.7x0.2 mm</td><td>12.7x12.7x0.2 mm</td></tr>
<tr><td>Element Type</td><td>Element type and integration</td><td>Hexahedron (8-nodes) with 1-point reduced integration (ELFORM=1)</td><td>Hexahedron 1-point reduced integration (ELFORM=1)</td></tr>
<tr><td>Material Formulation</td><td>Composite LS Dyna type</td><td>Rate dependent progressive damage (*MAT_162)</td><td>Damage evolution by strength reduction, Erosion with failure strains (*MAT_54)</td></tr>
<tr><td>Hourglass Control</td><td>Resisting forces and scale factor (QM)</td><td>Viscous forces (QM=0.1)</td><td>Viscous forces (QM=0.1)</td></tr>
<tr><td rowspan="3">Contact Algorithm</td><td>Projectile-plies</td><td rowspan="2">Single surface eroding (self-contact included)</td><td>Surface-to-surface eroding</td></tr>
<tr><td>Interply</td><td>Single surface</td></tr>
<tr><td>Delamination</td><td>Tiebreak Bilinear damage law (OPTION=9)</td><td>Tiebreak with no damage law (OPTION=7)</td></tr>
</table>

Table 4.1: Numerical properties of High Velocity Impact reference model [6] compared to the present model.

In the **numerical study** the different parts that conform the LS Dyna model, such as the mesh density, the element formulation, the contact algorithm, the hourglass control method, etc are described. The principal outcome of this analysis is a representative, robust and optimized model, in terms of CPU cost and simplicity, from the numerical perspective. Extensive work has been done in the representation of the response of composite laminates to high velocity impact. The purpose of this new model is to contribute to the research of this topic and enhance the current proposed methodology by the AWG [6] and that was validated through experimental tests in different studies [39, 49, 27].

Once a robust and enough flexible numerical solution is provided, the physics of the problem are analyzed in more detail. The aim of this part is to provide an organized methodology to examine the intralaminar damage suffered by the plate and to enhance its performance to impact, by modifying some parts of the configuration, e.g. the plate thickness, the stacking sequence, etc. Besides, the last part of the analysis is focused on the modelling techniques of the failure mechanisms, previously explained in 3.2.1, recommended for a high velocity impact.

4.3 Numerical Parametrical Study

In this section, the numerical results provided in the reference study [6] are employed to check the numerical validity of this project's model. The results of interest are:

- Global (computed for the whole system): Internal (IE), Kinetic (KE) and Hourglass (HGE) energy.
- Projectile: Internal and Kinetic energy and Residual or exit velocity of the projectile after penetration.

These values should remain between the ranges determined in the reference case [6]. Moreover, the methodology for numerical validation developed in this work includes also the following checks:

- Plies: For all plies of the composite plate, the hourglass energy should remain under a 10% of the internal energy peak at all times.
- Global energy plot: Apart from checking that the global energies are within the reference model range of valid results, two additional checks are done in the global energy plot. As it was previously explained in sections 3.3.2 and 3.3.4 the hourglass and the sliding contact energy need to remain under a 10% of the internal energy. Both energies are unphysical artifacts generated by LS Dyna, so they should remain under control at all times during the simulation.

4.3.1 Material formulation

Before examining the numerical results of the model, a note on the material formulation should be done. As indicated previously, the reference model [6] uses an advanced material formulation not compatible with the author's license (*MAT_162). The material parameters introduced in this model were obtained through experimental material tests, e.g. standard ATSM tests, for computing the strength values used in the failure criterion, and non-standard experimental procedures (Hopskison Bar Testing), to measure the failure strains of the composite. These tests were carried out in complementary studies [39, 49, 27] to characterize the response of the BMS 8-212 composite plate under high velocity impact, regarding penetration and delamination of the composite. The details of the material test and parameter calibration process are included in section 8.1 of the Appendix 8.

In the present model, a simpler material formulation was employed (*MAT_54), explained in 3.3.3. Some of the parameters calibrated for the advanced material formulation used in the reference model [6] were borrowed and introduced into the material formulation

of interest. For example, the failure strength properties measured through standard ATSM methods, were directly taken from the reference configuration and introduced into the present model.

As for the rest of the material parameters such as the failure strains (DFAILT/C/M/S), they can measured through coupon-level tests or one-element simulations. However, most material design allowables do not include any information about the strain to failure values, and even if they do these parameters are strongly dependent on numerical aspects such as the mesh size. Considering the resources and time limitations of this project, the strain to failure parameters were adjusted following a very simplified approximation found in the literature [57, 44], shown in 3.3.4 in (3.14), (3.15) and (3.16). This simplification is not very accurate since it is recommended for simulating one-element tests, not full impact models, so it is evident that some error is introduced into the results.

The final material properties and failure parameters that are used in the baseline configuration of the present model are finally shown in Tab. 4.2.

Mechanical Properties BMS 8-212	ρ (kg/m^3)	E_a (GPa)	E_b (GPa)	E_c (GPa)	ν_{ab}	ν_{ca}	ν_{cb}	G_{ab} (GPa)	G_{bc} (GPa)
	1548	117.9	8.825	8.825	0.025	0.025	0.3	5.51	2.53
Failure Parameters	X_T (GPa)	X_C (GPa)	Y_T (GPa)	Y_C (GPa)	S_C (GPa)	ϵ_T	ϵ_C	ϵ_M	ϵ_S
	1.103	1.034	0.055	0.25	0.07	9.35e-3	-8.77e-3	0.028	0.03

Table 4.2: Mechanical properties and failure parameters for material model, BMS8-212 carbon fiber-epoxy composite.[27]

Note that ϵ_T, ϵ_C, ϵ_M and ϵ_S represent the erosion strain parameters to fibre tensile, fibre compressive, matrix and shear failure. In LS Dyna, these are designated as DFAILT, DFAILC, DFAILM and DFAILS.

4.3.2 Contact Algorithm

In this part, the focus is the examination the different contact interactions that are present in the model: projectile-plies, interply and delamination. Note that, the remaining parts of the numerical model, e.g. element formulation, material model, hourglass algorithm, etc. remain as shown in the Present Model in Tab.4.1. The ultimate goal is to test the reference contact algorithm developed by AWG and propose an enhanced and optimized contact model in terms of numerical stability and robustness.

Firstly, the proposed projectile-plies contact option in the AWG study is the single surface eroding contact (*CONTACT_ERODING_SINGLE_SURFACE). The single surface

feature, establishes an interaction between all the parts included in the slave set and also allows the self-interaction. Moreover, the eroding keyword allows a crashfront surface of elements to be created when other elements are eroded due to failure. In this case, the penalty stiffness coefficient was calculated following the segment to segment formulation explained in section 3.3.4, as the projectile and plies are made of very dissimilar materials. Thus, the contact penalty stiffness is independent of the material properties, but depends on the segment masses and the global time step. As a first approach, this option seems like the most efficient, as it englobes all contact interactions in only one formulation with all the necessary features. Nevertheless, this contact option also requires a large computational effort, not only because it englobes all parts, but also because it is of eroding type and the penalty method is developed in the segment-to-segment formulation with the most accurate parameters.

The global energy plot for this reference contact formulation is shown in Fig. 4.3.

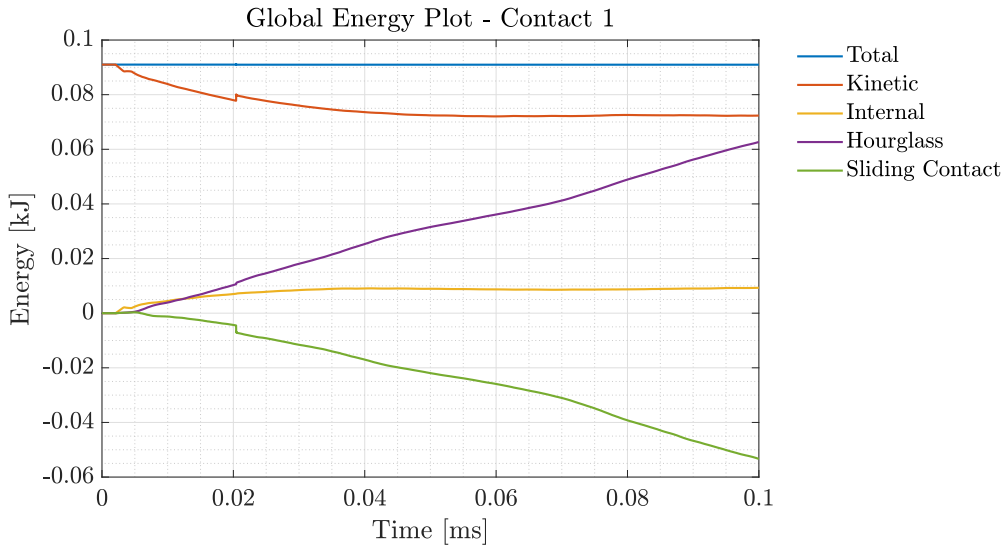

Figure 4.3: Global energy plot of High Velocity impact model with reference contact configuration (*CONTACT_ERODING_SINGLE_SURFACE).

Several issues are visible in this figure and, after a careful examination of every part of the model, it has been found that all of numerical issues come from the same source: contact instability between the different parts of the model.

It is clear that the **contact sliding energy** decreases to high negative values. Note that, since friction is not present in the current model, the negative contact energy indicates that a slave node is sliding from its original master segment to an adjacent though unconnected master segment. As a result, a penetration is detected and the sliding contact energy goes negative. This issue has nothing to do with friction, as negative energy comes in this case from normal contact forces and penetrations [48].

Another issue is the work done by the hourglass resisting forces, which drives the **hourglass energy** to increase above the internal energy. In fact, the hourglass energy seems to be mirroring the contact sliding energy, giving a hint on why the contact algorithm is the first concern of this model.

The hourglass algorithm was modified in order to observe the effect on the internal and hourglass energy with respect to the reference case. Several hourglass configurations were tested: a viscous formulation (IHQ=2) with the scale coefficients recommended in [47] values (QM=0.1-0.05) and a stiffness formulation (IHQ=4) with multiple recommended scale factors (QM=0.03-0.01). As a conclusion, no matter the type of hourglass resisting forces or the scale factor, the contact instability issue was not solved for any case, as it requires a complete reconfiguration of the contact.

To solve these issues a new contact model is developed next. The new contact englobes two separate interactions: the projectile-plies contact is modelled through a surface to surface eroding option (*CONTACT_AUTOMATIC_ERODING_SURFACE _TO_SURFACE) and the interply contact, which accounts for not-subsequent plies and self-ply contact, is modelled with a single surface classical penalty formulation (*CONTACT_AUTOMATIC _SINGLE_SURFACE). The eroding single surface contact was divided in these two contact interactions in order to divide the contact phenomena into two more simple interactions, allowing also to detect where in the model the contact instability occurs as explained before in 3.3.4.

In Fig. 4.4, the global energy plot for the new modified contact formulation is shown.

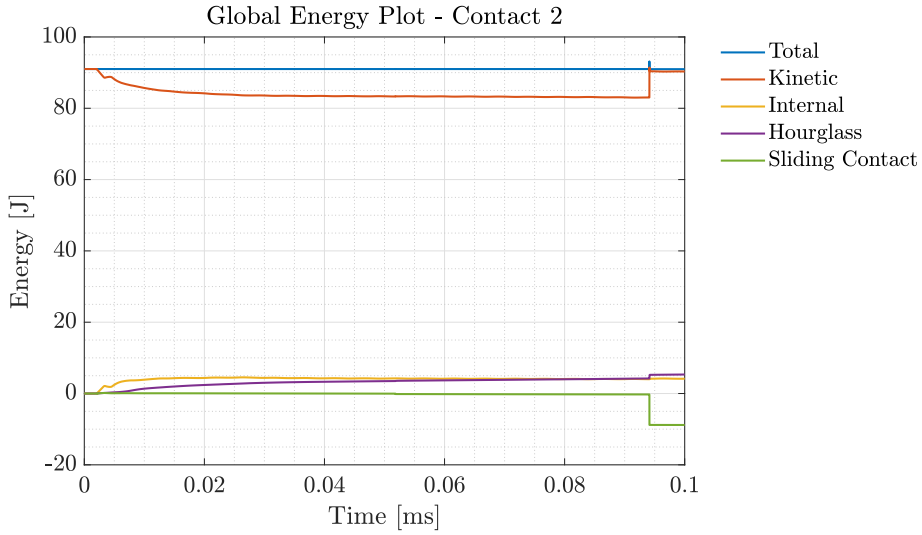

Figure 4.4: Global energy plot of model with modified contact algorithm (*CONTACT_AUTOMATIC_ERODING_SURFACE _TO_SURFACE for projectile-plies and *CONTACT_AUTOMATIC _SINGLE_SURFACE for interply contact).

Although there is a noticeable contact instability in the end of the simulation, the

behaviour of the model with the modified contact algorithm makes much more sense. The sudden drop in the sliding contact energy, induces an unphysical behaviour on the systems' kinetic and hourglass energies, which present a sudden step increase (mirrors the sliding energy).

By examining carefully the sliding contact output file (sleout) the source of the instability can be easily detected. The sudden drop in contact sliding energy comes from only one of the tiebreak contacts (#14-#15) of the plate. The slave and master energies for all contact interactions are shown in Fig. 4.5.

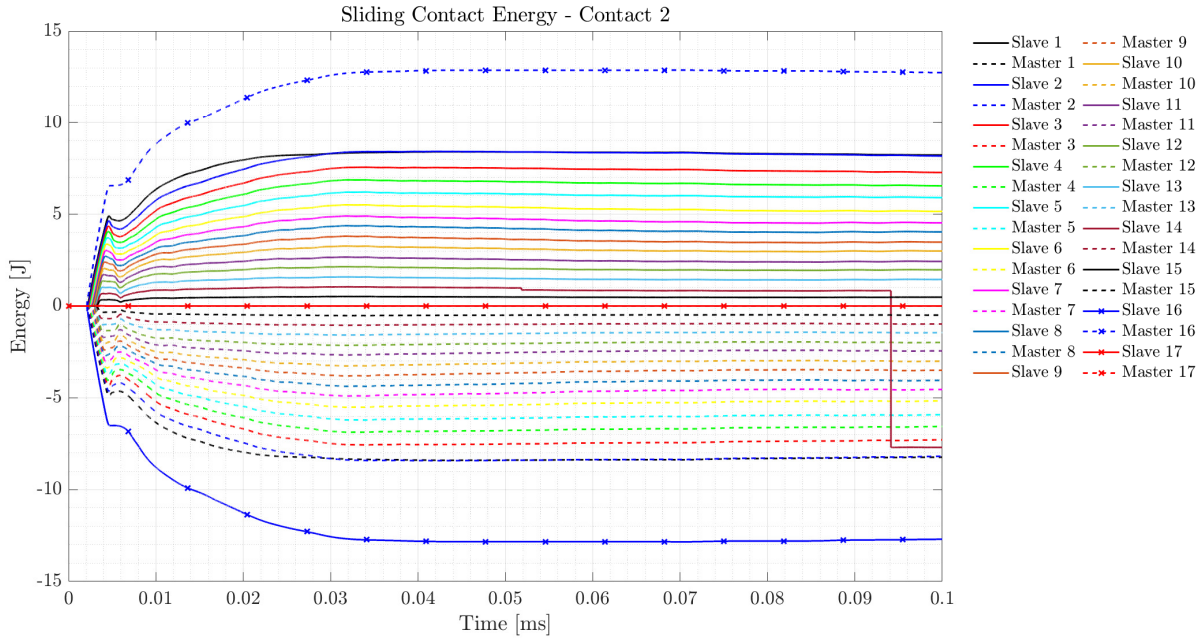

Figure 4.5: Sliding contact slave and master energies for model with modified contact algorithm (*CONTACT_AUTOMATIC_ERODING_SURFACE _TO_SURFACE for projectile-plies and *CONTACT_AUTOMATIC _SINGLE_SURFACE for interply contact)

4.3.3 Element formulation and Hourglass Algorithm

In this section, the element integration method and hourglass algorithm are examined. Hourglass energy, which is basically work done by the internal forces applied to resist hourglass modes, is dissipative in nature. In this regard, it is similar to damping except that it is nonphysical and so it should be kept to a minimum.

In Fig. 4.6, the internal, sliding and hourglass energy plots are shown for the reference model (AWG) and for different hourglass control techniques tested with the contact model developed in the previous section.

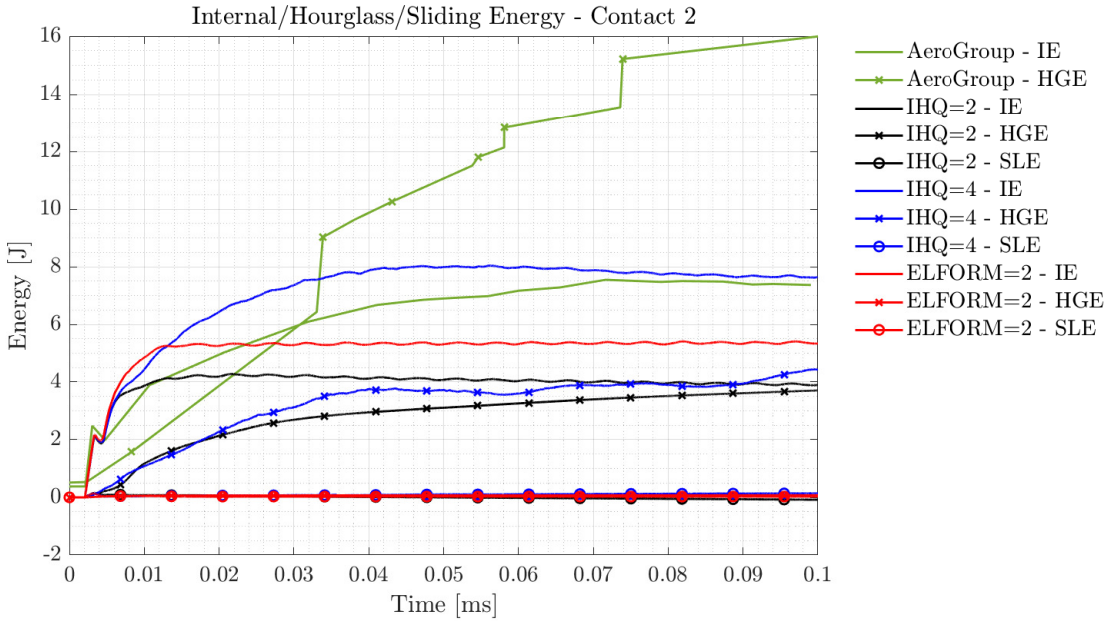

Figure 4.6: Internal, Hourglass and Sliding contact energy evolution. Comparison between results of reference AWG model [6] and present model with different element integration and hourglass configurations.

The green curves present the internal and hourglass energy evolutions predicted by the reference model [6] where clearly, the hourglass energy does not stay within a maximum of a 10% of the internal energy. Thus, the reference model shows a numerical limitation and should not be taken as the best approach. The rest of curves show the internal, hourglass and sliding energies for the new contact model and for different hourglass algorithms, viscous (IHQ=2) and stiffness (IHQ=4), and also for the case with fully integrated elements (ELFORM=2). The contact instability previously observed in the baseline case has been fixed by adjusting the hourglass forces scale coefficient from the baseline case, QM=0.1, to a lower value, QM=0.05.

The results for the last time step are tabulated and presented in Tab. 4.3 to ease the analysis.

Energy/ Element & Hourglass (ELFORM/IHQ)	Scale Factor QM	Internal, IE (J)	Δe IE (%)	Hourglass, HGE (% IE)	Sliding, SLE (% IE)	CPU time (min)
Reference: ELFORM=1 IHQ=2	0.1	4.74 -7.34	n/a	166- 216.67	n/a	16
ELFORM=1 IHQ=2	0.05	3.9	17.8	95.04	2.11	18
	0.01	4	15.84	74.33	1.00	23
ELFORM=1 IHQ=4	0.05	7.64	4.04	58.04	1.82	19
	0.03	**6.88**	**6.3**	**42.15**	**0.83**	**16**
	0.01	5.25	10.65	26.99	0.36	17
ELFORM=2	No HG	5.33	12.5	1.32	0.52	31

Table 4.3: Internal, hourglass and sliding energy in last time step. Comparison between reference AWG model [6] and present model with different element and hourglass formulations.

The results collected in Fig. 4.6 and Tab. 4.3 lead to the following conclusions:

- The stiffness hourglass control algorithm (IHQ=4) is recommended over the viscous (IHQ=2). For the viscous type, the work performed by the hourglass resisting forces is introducing unphysical effects in the the model. This unphysical behaviour can be seen in the under estimation of impact energy absorbed by the plate (global internal energy), where an artificial stiffness is introduced by the hourglass forces.

- Although the hourglass energy can be controlled by adjusting the scale factor (QM), the excessive reduction of this parameter can cause the presence of unwanted hourglass modes in the model. Thus, when adjusting the scale coefficient a thorough inspection of hourglass modes in the model should be done.

- The use of fully integrated elements (ELFORM=2) provides a good prediction of the internal energy (impact energy), the contact algorithm remains stable and most importantly, the hourglass modes are not longer present in the problem. However, when using full integrated elements, specially in the case of bending problems, the elements may experience locking. To check if there is locking a separate parallel model using a material orthotropic elastic formulation for the composite with reduced and fully integrated elements is created. The results presented a small over-stiffened behaviour, which together with the increase of computational time by a factor of 2 were enough motives to discard the use of fully integrated elements.

As a final conclusion, a **stiffness hourglass algorithm (IHQ=4)** is recommended for this case, as it provides a fair good reduction of the unphysical hourglass forces work while being computationally efficient and manageable in terms of time.

The scale factor choice is made by checking the presence of hourglass in the simulation, as shown in 4.8. In this figure, a top view of the first ply of the composite plate (impact surface) at the instant $t = 7.5E - 3ms$ is shown in order to check the appearance of hourglass modes in the simulation. The red shapes represent the deformed elements of the first ply, which has been studied separately from the rest. Note that, an erosion option is included in the material formulation, some elements are deleted and that is why there are blank spaces between the ply elements. In order to ease the visualization of spurious modes the displacements are scaled by a factor of 5.

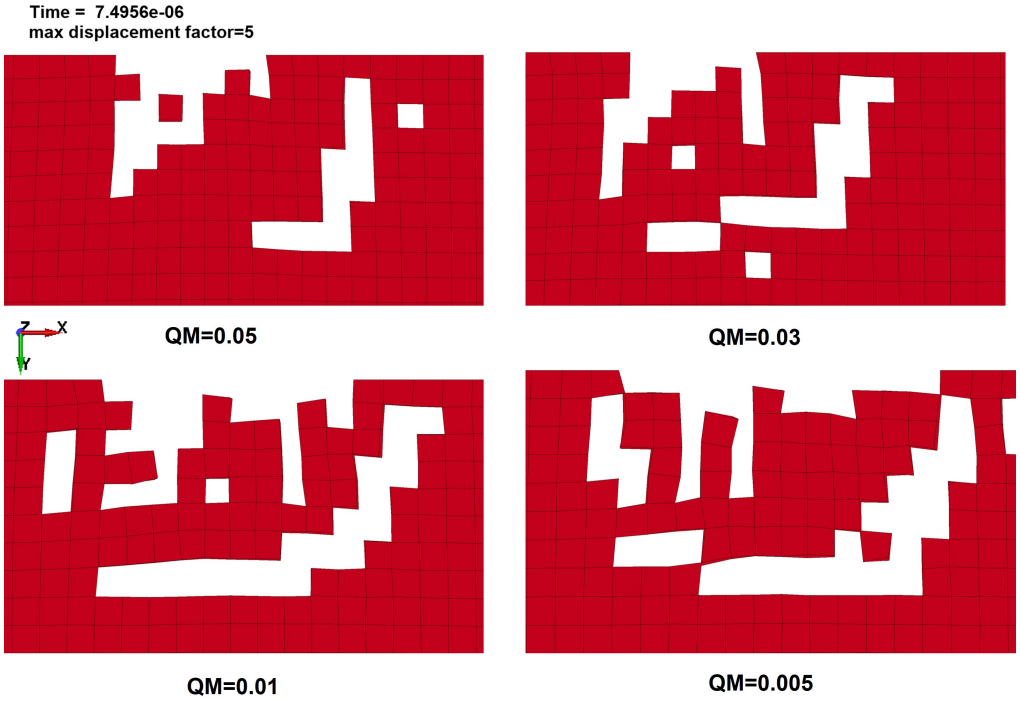

Figure 4.7: Hourglass modes presence check at the impact surface (ply 1) at a $t = 7.5e - 3$ ms (top view). Stiffness hourglass control (IHQ=4) for different scale coefficients: QM=0.05 (left, top), 0.03 (right,top), 0.01 (left,bottom) and 0.005 (right,bottom).

Figure 4.8: Hourglass modes presence check at the impact surface (ply 1) at a $t = 7.5e - 3$ ms (top view). Stiffness hourglass control (IHQ=4) for different scale coefficients: QM=0.05 (left, top), QM=QM=0.03 (right, top), QM=0.01 (left, bottom) and QM=0.005 (right, bottom).

After careful consideration, a **scale coefficient of** $QM = 0.03$ **was selected** for the next steps of the analysis. This coefficient is sufficiently high to effectively counteract the hourglass modes presence while reducing the unphysical effects introduced by the hourglass resisting forces with respect to the reference results. However, the hourglass energy is too high still (42% of the internal energy). That is why, in next section **??** the mesh is refined in the impact area.

Verification with Reference Model

The final numerical model was verified through the global kinetic energy and the projectiles' internal, kinetic energies and residual velocity (velocity after penetration) with the numerical results shown in [46] as shown in Fig. 4.9.

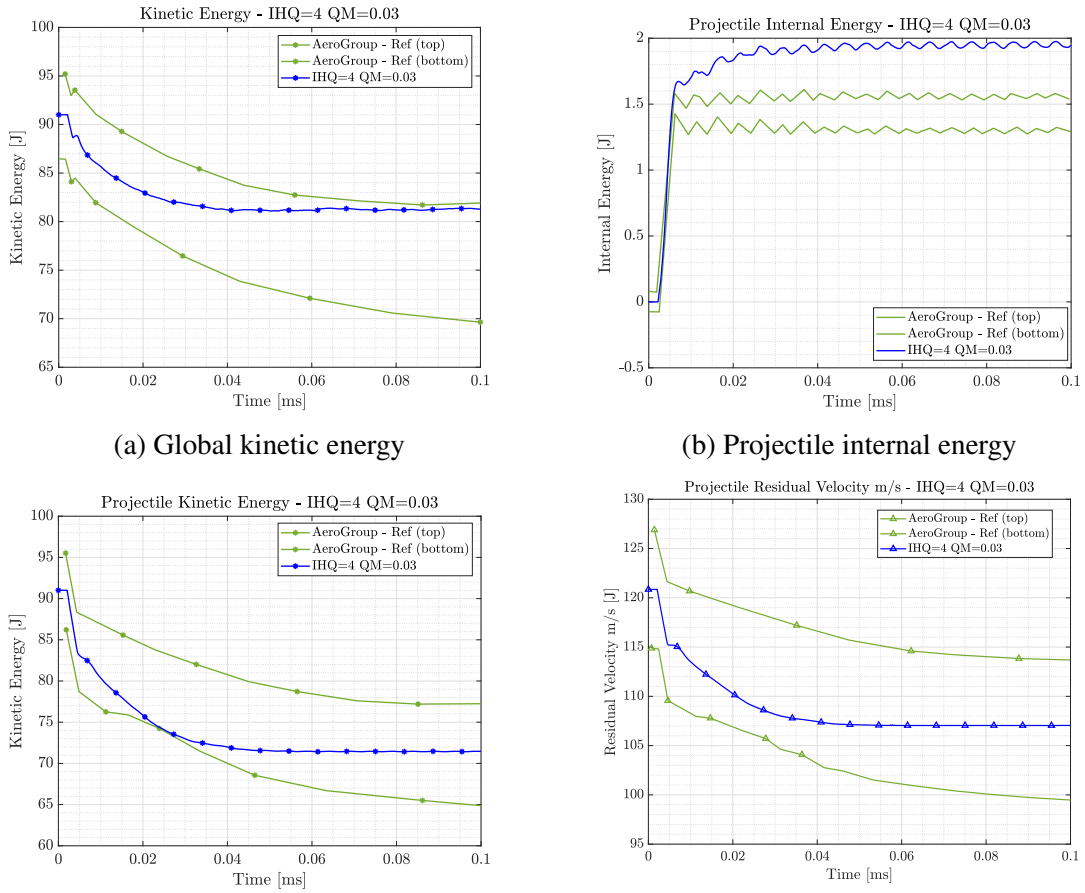

(a) Global kinetic energy

(b) Projectile internal energy

(c) Projectile kinetic energy

(d) Projectile velocity

Figure 4.9: Global kinetic energy and projectile's internal energy, kinetic energy and residual velocity evolution. Validation of present model (IHQ=4 QM=0.03) with reference numerical results [6].

The results at the last step of the simulation from this latest part of the numerical validation process have been collected in Tab. 4.4.

Parts /Energy	Internal, IE (J)		Δe	Kinetic, KE (J)		Δe	Hourglass,
	Aerogroup	Model	IE (%)	Aerogroup	Model	KE (%)	HGE (% IE)
Projectile	1.24-1.47	1.95	32	64.7-77.1	71.45	7.4	7
Plies (average)	Unknown	0.13	n/a	n/a	0.29	n/a	47

Table 4.4: Projectile and plies internal, kinetic and hourglass final energies. Validation of present model (IHQ=4 QM=0.03) with reference numerical results [6] .

In addition the internal, kinetic and hourglass modes for every ply was checked, as recommended in the LS Dyna support page [47]. The energies for all the plies have been averaged at every time step and the final results demonstrate coherence with global results. If every ply is checked separately the higher hourglass resisting forces work is performed in the middle plies (from ply 6 to ply 12). This must be specially taken into account when analyzing the physical behaviour of the ply, contact forces, displacement, failed elements, etc.

4.3.4 Mesh Analysis

The next part of the study consists in modifying the mesh density of the composite plate in order to achieve two different objectives. First, to **reduce the hourglass energy** below a 10% of the internal energy [46]. The second is to **study the convergence of the impact physical properties** e.g. impact energy, contact forces and velocity of the projectile. These results were also included in the reference [6] and are used as validation for this present model.

Four mesh distributions are used in the impact area of the plate, as shown in Fig. 4.10 and Tab. 4.5, where also the notation used to identify each case in the rest of the graphics of the manuscript is indicated. The refinement is only performed in the impact area mesh, which is the limited surface where the composite is to experience most of its deformation. This imposes a clear limitation on the mesh quality and may reduce in the accuracy of the results. The nodes from the refined area are connected to the rest of the plates by means of tying constraints.

Mesh Density/ Test case	Name	X (mm)	Y (mm)	Z (mm)	Aspect ratio	# Elements	Approx CPU time (min)
Mesh 1	M1	1.28	1.28	0.2	0.11	61448	17
Mesh 2	M2	0.64	0.64	0.2	0.31	71048	20
Mesh 3	M3	0.32	0.32	0.2	0.625	132488	40
Mesh 4	M4	0.16	0.16	0.2	0.8	3788348	140

Table 4.5: Mesh density study: Name, Element X, Y and Z size, aspect ratio, number of elements and approximate CPU time of each case.

After these two objectives have been carried out, the most adequate mesh distribution between the four models density is chosen in terms of:

- Absence of developed hourglass modes, checked in the final results by scaling the displacements in the most conflictive areas.

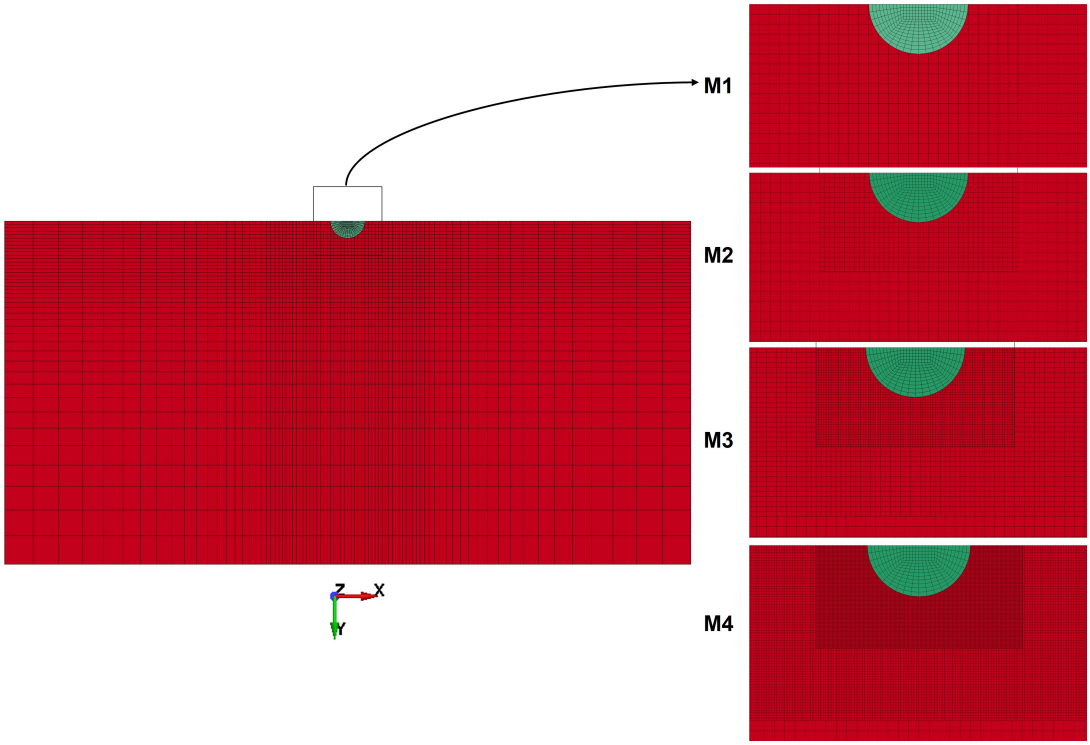

Figure 4.10: Mesh density models (top view): Mesh 1 (M1), Mesh 2 (M2), Mesh 3 (M3) and Mesh 4 (M4).

- Minimum work performed by the hourglass resisting forces, controlled via the hourglass energy in the global energy plot and the energies of each part of the system.

- Accuracy with respect to the reference results in [6], through the analysis of the contact force, impact energy, residual velocity of the projectile, absorbed energy per ply, etc.

- Computational efficiency, measured in minutes of simulation. By refining the mesh, the element size and the element time steps decrease, driving to larger computational times.

The composite plate chosen with the adequate mesh density will be employed for the physical parametrical study of this work carried out in the next section 4.4.

Following the same methodology as in the previous section, the first plot Fig. 4.11 shows systems' internal, hourglass and sliding energies for the different mesh distributions with the chosen hourglass algorithm (stiffness, IHQ=4, and scale factor, QM=0.03).

The internal, hourglass and sliding energy final results are also tabulated in Tab. 4.6. This table helps to compare the accuracy in the calculation of the internal energy, the work done by hourglass resisting forces (hourglass energy) and the stability of the contact

interactions (sliding contact energy) for the different mesh densities and hourglass scaling coefficients. The results are also compared with the reference results given in [6].

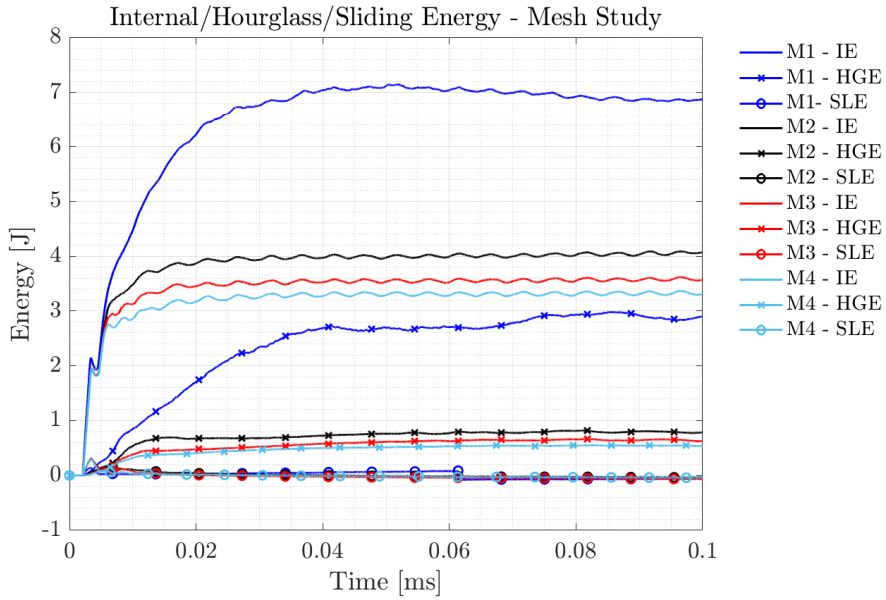

Figure 4.11: Internal, Hourglass and Sliding Contact energy evolution for different mesh densities: M1=1.3x1.3x0.2mm, M2=0.6x0.6x0.2 mm, M3=0.3x0.3x0.2 mm and M4=0.15x0.15x0.15 mm.

Energy/ Mesh	QM	Internal, IE (J)	Δe, (%)	HGE (% IE)	SLE (% IE)	CPU time (min)
Aerogroup Reference	0.1 (IHQ=2)	4.74-7.34	0	166-217	Unknown	Unknown
Mesh 2	0.03	4.07	14.14	19.20	0.86	20
	0.02	3.89	18.06	19.72	0.89	20
	0.01	3.84	19.08	16.56	0.69	20
	0.005	3.73	21.40	14.65	1.32	20
Mesh 3	0.03	3.58	24.66	17.48	1.82	40
	0.02	3.47	26.94	16.11	1.94	40
	0.01	3.42	27.90	14.64	2.62	40
	0.005	3.48	26.58	13.04	2.41	40
Mesh 4	0.03	3.31	30.06	15.20	1.3	142
	0.02	3.43	27	15.20	1.3	146
	0.01	3.31	30	14.60	1.7	158

Table 4.6: Internal, hourglass and sliding contact final energies for different mesh densities and hourglass scaling coefficients.

As the mesh is refined, the presence of hourglass modes decrease. Thus, the scale coefficient can be adjusted to a different value for each mesh distribution. In order to do

so, the presence of hourglass modes in the simulation needs to be examined further. In Fig. 4.12 and Fig. 4.13 the elements deformations are examined in the impact surface (ply 1). It must be remarked that the displacements have been scaled up by a factor of 4 in order to observe the presence of these spurious modes. If both mesh density cases are compared for the same scale factor, QM=0.01, there is a clear reduction in the apparition of hourglass modes of deformation for a finer mesh.

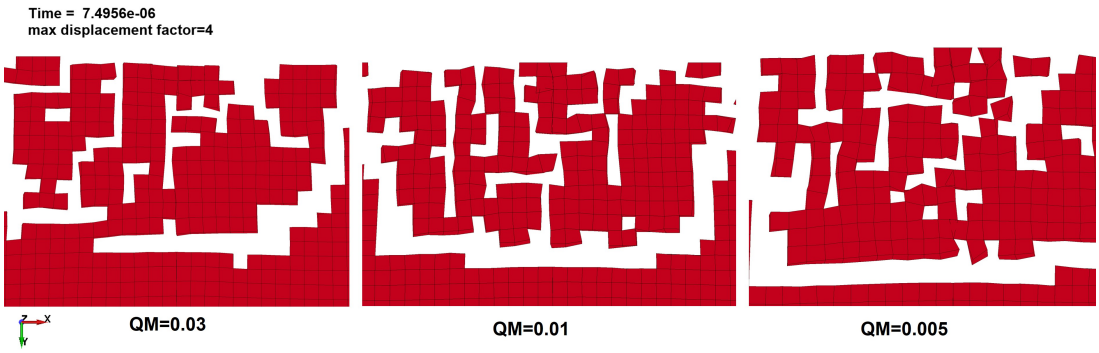

Figure 4.12: Hourglass modes presence (top view) in M2 (0.6x0.6x0.2 mm) for different scale hourglass force coefficients, QM: 0.03 (left), 0.01 (middle) and 0.005 (right).

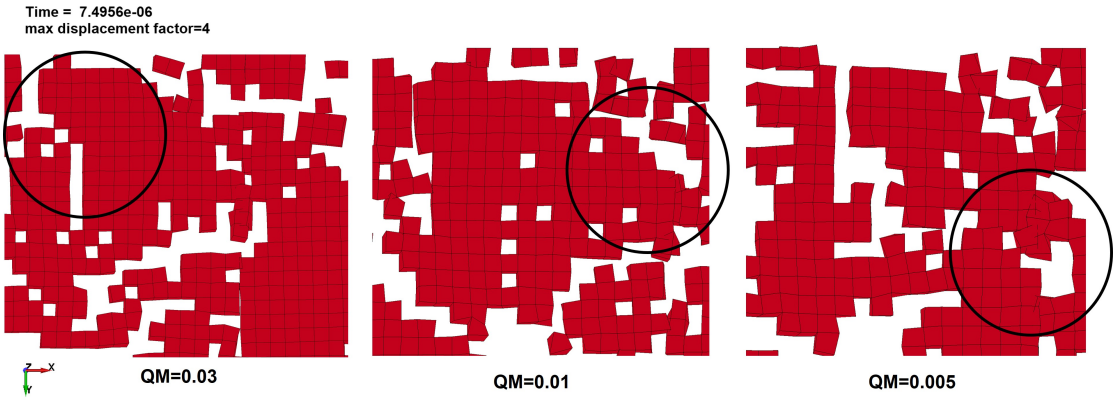

Figure 4.13: Hourglass modes presence (top view) in M3 (0.3x0.3x0.2 mm) for different scale hourglass force coefficients, QM: 0.03 (left), 0.01 (middle) and 0.005 (right).

The mesh convergence study for the plate physical properties is carried out next.

In Fig. 4.14, the energies for the different mesh densities and the selected hourglass configuration (IHQ=4, QM=0.03) are shown, and there is a slight convergence of the impact energy as the mesh is refined, though full convergence has not been reached yet. In this figure, the reference results from [6] are also presented. There is difference in the deforming rate of the plate, the reference model seems to absorb the internal energy more progressively and reaching a stable value later than in our model. This could be due to use of a different and less advanced material model in the present model. Remember that, the

reference study employed a strain-dependent progressive damage model while our model uses a simplified material approach based on a stress-based failure criterion and on some strain to failure parameters.

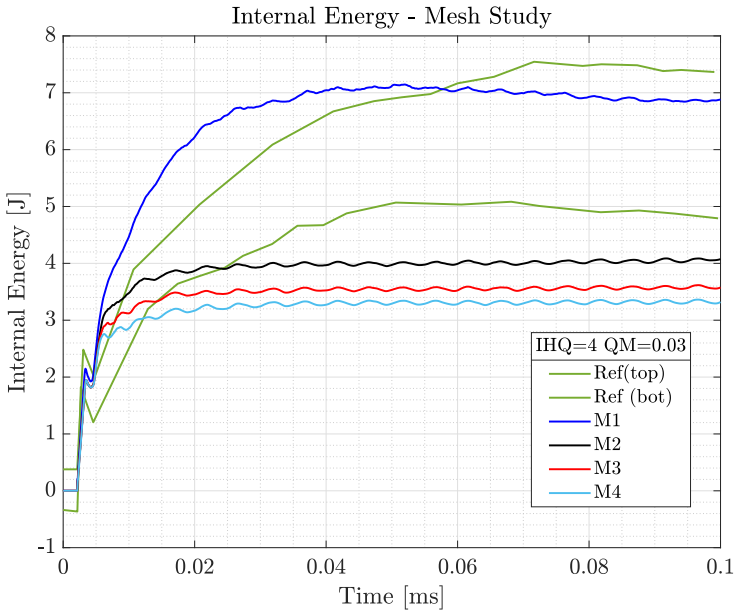

Figure 4.14: Internal energy evolution for different mesh densities. Validation with numerical reference results [6].

In 4.15 the impact energy for the different hourglass scale coefficients is shown. There is also a convergence on the impact energy as the hourglass scale coefficient decreases. This could be due to the reduction of unphysical energy in the model. From the third mesh distributions, the impact energy can be considered to be fully converged.

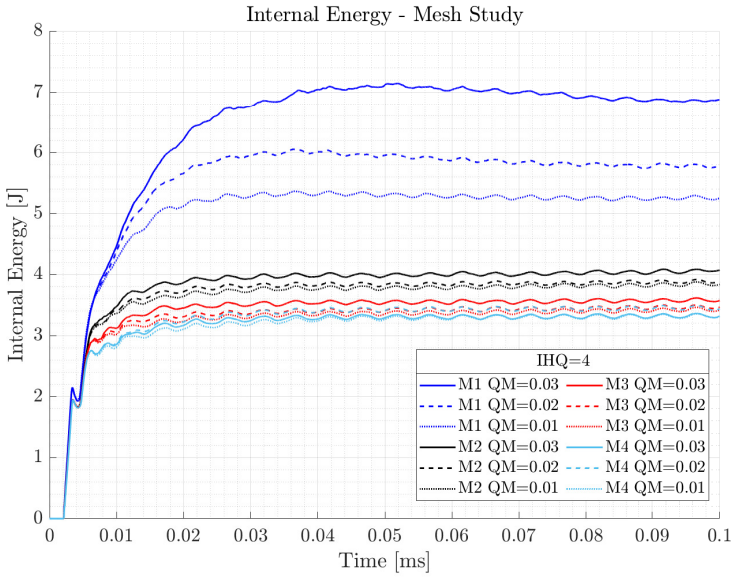

Figure 4.15: Internal energy evolution for different mesh densities and hourglass scale coefficients, QM: QM=0.03, QM=0.02 and QM=0.01.

Same method is applied to study the convergence of the projectile's velocity. This result is not only verified numerically, but also validated experimentally validated through the experimental results included in [39, 49]. The numerical validation shown in [6] is done by checking that the computed results remain within the range defined in [6] as shown in Fig. 4.16. It is evident that the residual velocity converges towards the higher velocity limit as the mesh is refined.

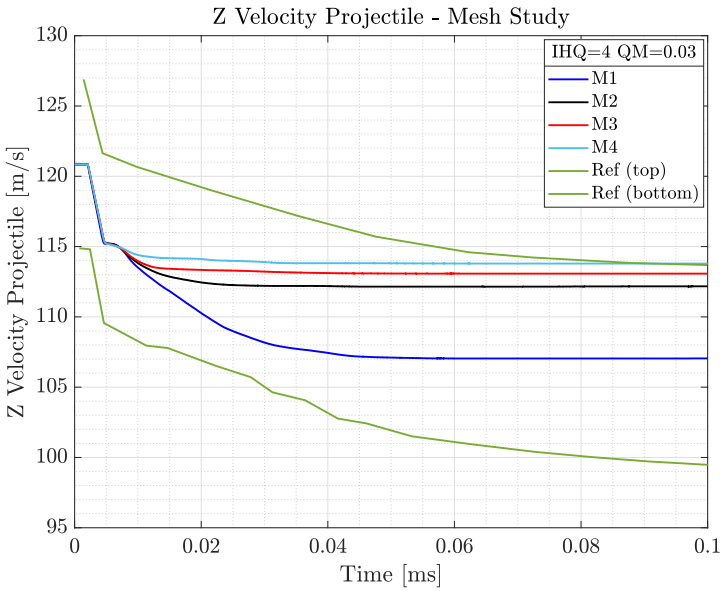

Figure 4.16: Projectile velocity evolution for different mesh densities. Validation with numerical reference results [6].

In Fig. 4.17 the effect of the hourglass forces scale factor on the residual velocity convergence is shown. As this coefficient decreases the final value of the residual velocity also converges towards the higher velocity limit, as it occurred with the impact energy.

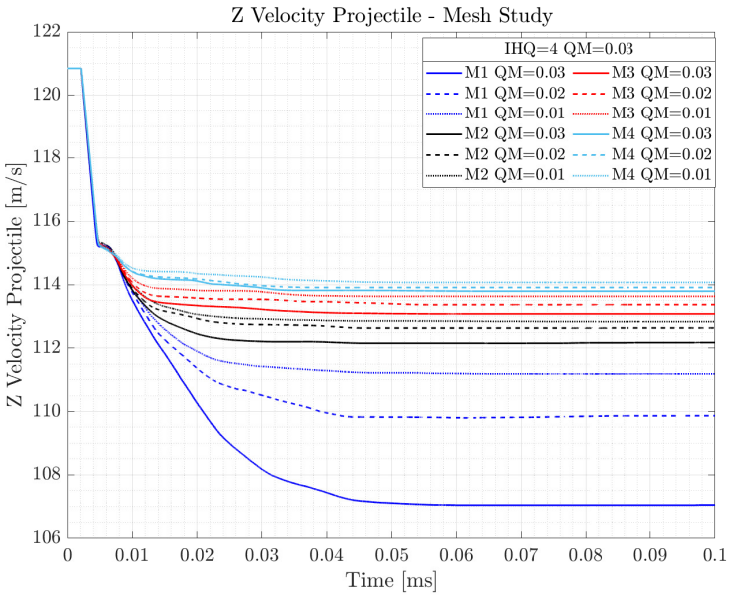

Figure 4.17: Projectile velocity for different mesh densities and hourglass scale coefficients: QM=0.03, QM=0.02 and QM=0.01.

For the residual velocity there is also experimental data available which was measured during the ballistic impact test developed by the authors [39, 49]. The final measurements are shown in Fig. 4.18, where they are compared with the numerical model developed by the reference authors and with the models developed in this work. The case of study is shown $v_{proj,i} = 120.85$ m/s and another test case with higher projectile's velocity $v_{proj,i} = 154$ m/s is also included for comparison.

As the mesh is refined the residual velocity converges but to a value slightly higher than the experimental one. The higher projectile's velocity case ($v_{proj,i} = 154$ m/s) shows better accuracy with the experimental data. Note that as velocity increases, the delamination failure mechanism becomes less relevant in the damage response of the plate as there is no time for its development. Moreover, the plate breaks in a more brittle manner as tensile fibre breakage is reached sooner for higher velocities, and the evolution of the rest of damage modes do not develop. This means that, the errors introduced by the poor delamination and material damage evolution models have less effect in the final ballistic response of the plate as velocity incresases.

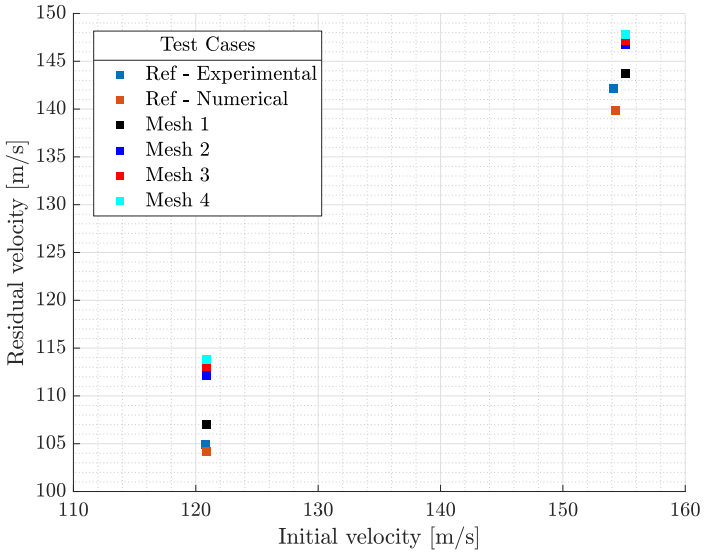

Figure 4.18: Projectile residual velocity validation. Experimental and Numerical results of the reference ballistic test case [39].

4.3.5 Conclusions

The final goal of this study was to construct a numerically stable and robust model to represent the response of the composite plate to a high velocity impact phenomenon. After analyzing all the relevant numerical values as well as the convergence of the impact parameters, the chosen numerical setup includes the modified contact algorithm along with the third impact area mesh refinement (M3: 0.16x0.16x0.2 mm) and a stiffness hourglass algorithm (IHQ=4) with a resisting forces scale factor of QM=0.03.

However, this final model has some important limitations that introduce some error in the prediction of the exit projectiles' velocity and impact energy of the system could be due to the same following reasons:

- The hourglass energy although being enormously reduced with respect to the reference model, is still over 10% of the internal energy of the system for any of the cases. In fact, the chosen final numerical model has a final HGE of 17% of the IE. This issue can affect to a certain degree the accuracy and reliability of the solutions.

- Poor representation of intralaminar progressive failure. Remember that, the strain to failure values were approximated as specified in 4.1 following the recommendations given in [57] and not calibrated through the necessary material testing procedures. In addition, the material model does not include a strength softening representation.

- There is some error introduced by mesh element distortion caused by refining only the impact area. The difference between the element sizes and poor element

connectivity causes some distortion that can affect the accuracy of the final results.

- Poor representation of the delamination phenomenon, although it is not that relevant for a high velocity model. Remember that in this case, the numerical technique to model delamination (OPTION=7) is only based on a failure criterion after which the tiebreak contact is disabled without following any progressive damage evolution of the properties.

As a final note, by validating the ballistic residual velocities of the projectile at the end of the simulation it was shown that the model enhances its accuracy for higher velocity cases. For an additional test, where the projectile impacts with a velocity of $v_{proj,i} = 154$ m/s the error on the residual velocity for the chosen configuration (M3, IHQ=4 and QM=0.03) is $e_{relative} = 3.54\%$ is half of the error of the initial case of study in which $v_{proj,i} = 120$ m/s, $e_{relative} = 7.78\%$.

4.4 Physical Parametrical Study

In this section, the selected numerical model (M3, IHQ=4 QM=0.03) is studied from a physical perspective. The final goal is to evaluate the effect of certain physical properties of the model on the response and damage suffered by the composite plate during a high velocity impact. The physical properties to be examined here are shown next and the nomenclature employed for interpreting the results is shown in Tab. 4.7:

- **Ply material constitutive law and strain to erosion parameters:** The damage and failure numerical parameters introduced in the composite material formulation are removed to see the effect on the plate's response.

- **Plate thickness:** The bending stiffness of the plate is modified through the thickness. More flexible and stiffer plates are modelled by reducing and increasing the number of plies to a 8-ply and 32-ply models respectively, thus modifying the total thickness of the plate.

- **Stacking sequence:** The fibre directional stiffness can also be modified by altering the stacking sequence. Considering that the initial stacking sequence is $[+45, 90, -45, 0]_{2s}$, the two additional configurations of $[+45, -45, 90, 0]_{2s}$ and $[0, +45, 90, -45]_{2s}$ are tested to observe the effect on the plate final stiffness. Note that, the modification of the mechanical properties of the laminate plate is a complex task, due to the directional-dependency of the material. By introducing a $+45\,\mathrm{deg}$ ply as the impact surface, the purpose is to increase the fibre-directional stiffness to tensile. As tensile fibre-breakage is the predominant source of failure in a high

velocity impact, as indicated in 3.2.2, this is the direction and the mode of interest. However, it must be acknowledged that impact is a complex loading mechanism that not only induces tension in the fibers.

Physical Study	Nomenclature	Material	N plies (thickness)	Stackup Sequence
Baseline case	Baseline	DFAILT=9e-3 DFAILC=8e-3 DFAILM=2.8e-2	16 ply (3.175 mm)	$[+45/90/-45/0]_{2s}$
Material Law - Only Failure	Mat - Only failure	DFAILT/C/M/S=0	16 ply (3.175 mm)	$[+45/90/-45/0]_{2s}$
Thickness	Thickness - 8 ply	DFAILT/C/M/S=0	8 ply (1.524 mm)	$[+45/90/-45/0]_{2s}$
	Thickness - 32 ply	DFAILT/C/M/S=0	32 ply (6.35 mm)	$[+45/90/-45/0]_{2s}$
Stackup Sequence	Stackup [+45/-45/90/0]	DFAILT/C/M/S=0	16 ply (3.175 mm)	$[+45/-45/90/0]_{2s}$
	Stackup [0/+45/90/-45]	DFAILT/C/M/S=0	16 ply (3.175 mm)	$[0/+45/90/-45]_{2s}$

Table 4.7: Physical study cases and nomenclature.

The effect of these physical parameters is evaluated by analyzing some important results in the behaviour of the plate and damage characterization.

- **Intralaminar failure:** Information about the status in each layer (integration point) and element can be plotted using additional integration point variables named history variables. These variables are included in the material formulation, as explained in 3.3.3. The objective is to identify the dominant failure mode and analyze the influence of the aforementioned physical parameters into the different damage modes of the composite material.
- **Impact energy:** The impact energy can be also identified as the energy absorbed by the plate. This property is interesting specially for the different thickness plates tested, to see if the energy absorbed per ply remains the same for different thicknesses.
- **Exit projectile velocity:** The residual velocity of the projectile at the exit of the plate is another important value for the ballistic analysis.

Note that, in the reference model [6] and other relevant sources [39, 49], numerical and experimental results for both the impact energy and the residual projectile velocity are included, for the baseline case but also for the different thickness values introduced (8-ply and 32-ply models). The results are going to be also used to validate the model as done previously for the baseline configuration in 4.3.

4.4.1 Intralaminar Damage: Material Parameters

This part is focused on examining the effect the erosion failure strains DFAILT, DFAILC, DFAILM and DFAILS introduced in the material formulation, explained in section 3.3.3, in the composite plate response and failure evolution.

As indicated in the theory, these parameters can be measured through coupon-level tests or one-element numerical simulations. However, most design allowables for material systems do not include any information about the strain to failure values, and even if they do these parameters are strongly dependent on numerical aspects such as the mesh size. Considering the resources and time limitations, the strain to failure parameters were adjusted for the previous numerical study following a very simplified approximation found in the literature [57, 44]. This simplification is not very accurate since it is recommended for simulating one-element tests, not full impact models. For this reason, **in this section the strain to failure parameters are removed from the material formulation** in order to observe the effect in the plate response.

The difference in the impact behaviour of the plate when employing a material formulation with and without strain to erosion parameters can be anticipated: the composite material elements would most likely be capable of absorbing more impact energy when only strength failure criteria is included in the material formulation. Remember from 3.3.3 that, by reaching the failure criteria, the elements are limited to carry more stress, but the stress distribution on them is not driven to zero unless the strain to failure parameters are introduced. Thus, the number of eroded elements is probably much lower for the called "Only Failure" material formulation. As a direct consequence, the removal of these parameters allows the plate to absorb higher energy during the impact.

In Fig. 4.19, the increased energy absorption capability of the plate allows the model to represent more accurately the reference numerical and experimental results [39, 57]. Thus, for the rest of the physical study, the strain to failure parameters have been removed from the material cards. From this section onwards, the composite material is only able to model the damage onset of the different failure modes.

In Fig. 4.20, the fringe plots representing the evolution of the different failure modes in the composite are shown for the baseline case and for the case with the only failure material model, at the time instant $t = 7.5E - 3$ ms. The contours represent the history variables included in the material formulation that quantify the different types of failure in the composite. The mathematical expressions for the history variables were shown in section 3.1.2 in Eq.(3.1), Eq.(3.2), Eq.(3.3), Eq.(3.4). In them, failure is computed in each element integration point (centroid) in a range between 0 to 1, where 1 corresponds to fully elastic and 0 to failed status.

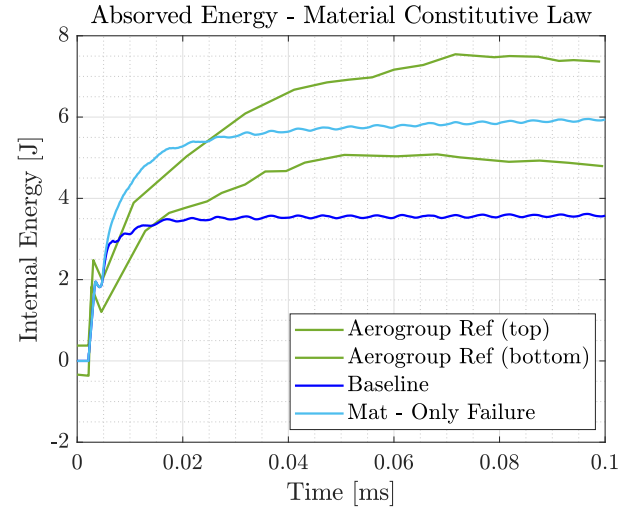

(a) Internal energy.

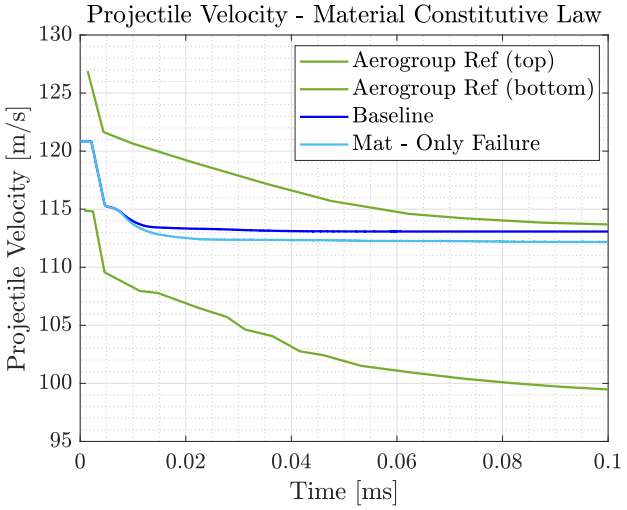

(b) Projectile velocity.

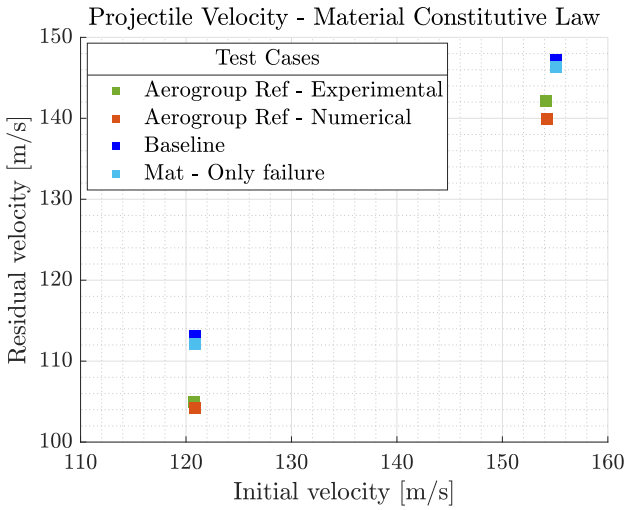

(c) Projectile residual velocity.

Figure 4.19: Internal energy, projectile velocity evolution and residual projectile velocity for baseline case and only failure material model (strain to failure parameters not included in material formulation). Validation with numerical and experimental reference results [6, 39].

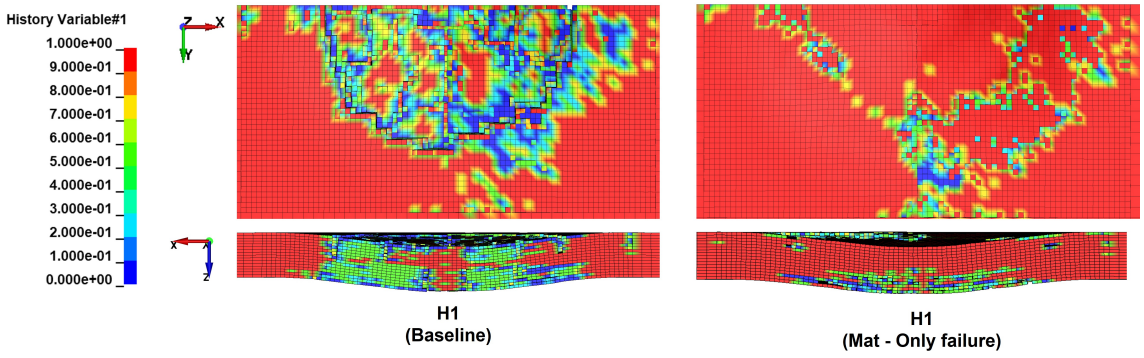

(a) Longitudinal (fibre) tensile failure (History variable #1)

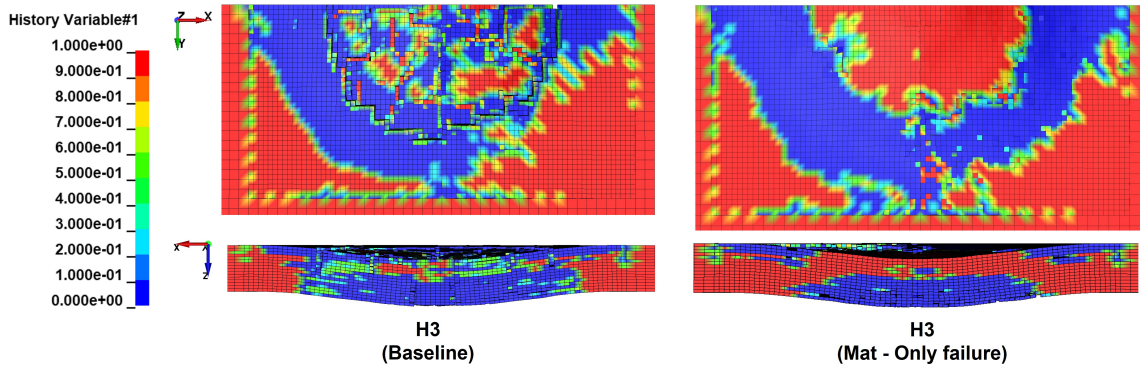

(b) Transverse (matrix) tensile failure (History variable #3)

Figure 4.20: History variables ($t = 7.5E - 3$ms) of the fibre (H1, left) and the matrix (H3, right) tensile cracking modes. Baseline case (left) and the only failure material formulation (right). For all subfigures the top (upper) and frontal (bottom) views are presented.

By examining the different plots, the composite failure mechanims background theory explained in 3.2 is demonstrated.

- The **earliest** failure mechanism is the **transverse tensile failure (matrix cracking)** (H3) as can be seen in the front view (top) of the History Variable #3 plot shown in Fig. 4.20b. In addition, the 16-ply plate response shows a flexible behaviour as failure starts due to bending deformation in the lowest ply of the plate, as can be appreciated thanks to the lateral view (bottom) of History Variable #3.

- In high velocity impacts, the critical failure mechanism is **fibre breakage** (H1). Note that, the tensile and compressive fibre failure modes can be represented via History Variable #1 and #2 respectively. In other words, penetration of the plate occurs when fibre breakage damage reaches its critical amount. As the history variables fringe plots are presented in a pretty early stage in the simulation, this may not be clearly visible in the picture. However, what should be noticed is that the penetration of the plate is dominated by the longitudinal failure mechanisms for the case of high velocity impact.

4.4.2 Thickness

The thickness of the plate was varied from the 16-ply baseline case, to a 8-ply and a 32-ply models, to modify the stiffness and observe the response to impact. Note that, for these thickness variations, experimental and numerical results available in the reference studies [39, 49] were used for validation of the present model.

Only the longitudinal (fibre) and the transversal (matrix) tensile crack modes are analyzed in this section (H1 and H3, respectively), as they proved to be the most relevant failure modes for the high velocity case. Thus, the fringe plots of the history variables #1 and #3 are shown in Fig. 4.21 at an intermediate time instant $t = 7.5E - 3$ms.

The **matrix tensile failure (H3)** is still the earliest source of failure to appear during impact. The stiffness effect is clearly observable: for lower thickness, less stiff is the target and the failure starts in the last ply (seen in 8-ply and 16-ply model), while for the a higher thickness, the plate shows a stiffer response, in which the failure seems to be starting in earlier plies. Remember that, for thin plates failure comes from the bending failure of the bottom layers. And as thickness increases, a higher energy is required to initiate damage in the lowest ply, until a maximum is reached. This maximum is considered to be the ”optimal thickness” in which failure starts simultaneously on the top and the bottom layers of the plate, giving the highest resistance to damage initiation. Above this optimal thicknesss, failure comes from high contact stresses in the top layer, and increasing the thickness only results in lower damage threshold energies.

About **fibre tensile failure (H1)**, this damage mode generally takes longer to develop. This can be observed as, for the chosen time stage this failure source is not as advanced as the matrix tensile failure, despite being the dominant source of failure in high velocity impact. The behaviour of this failure mechanism with thickness is quite similar to the matrix breaking mode. For lower thickness, the failure start is concentrated in the bottom plies as it is driven by bending loads in these layers. As thickness increases, the fibre damage onset seems to be moving to upper layers as a consequence of being more driven by contact stresses suffered in the upper plies.

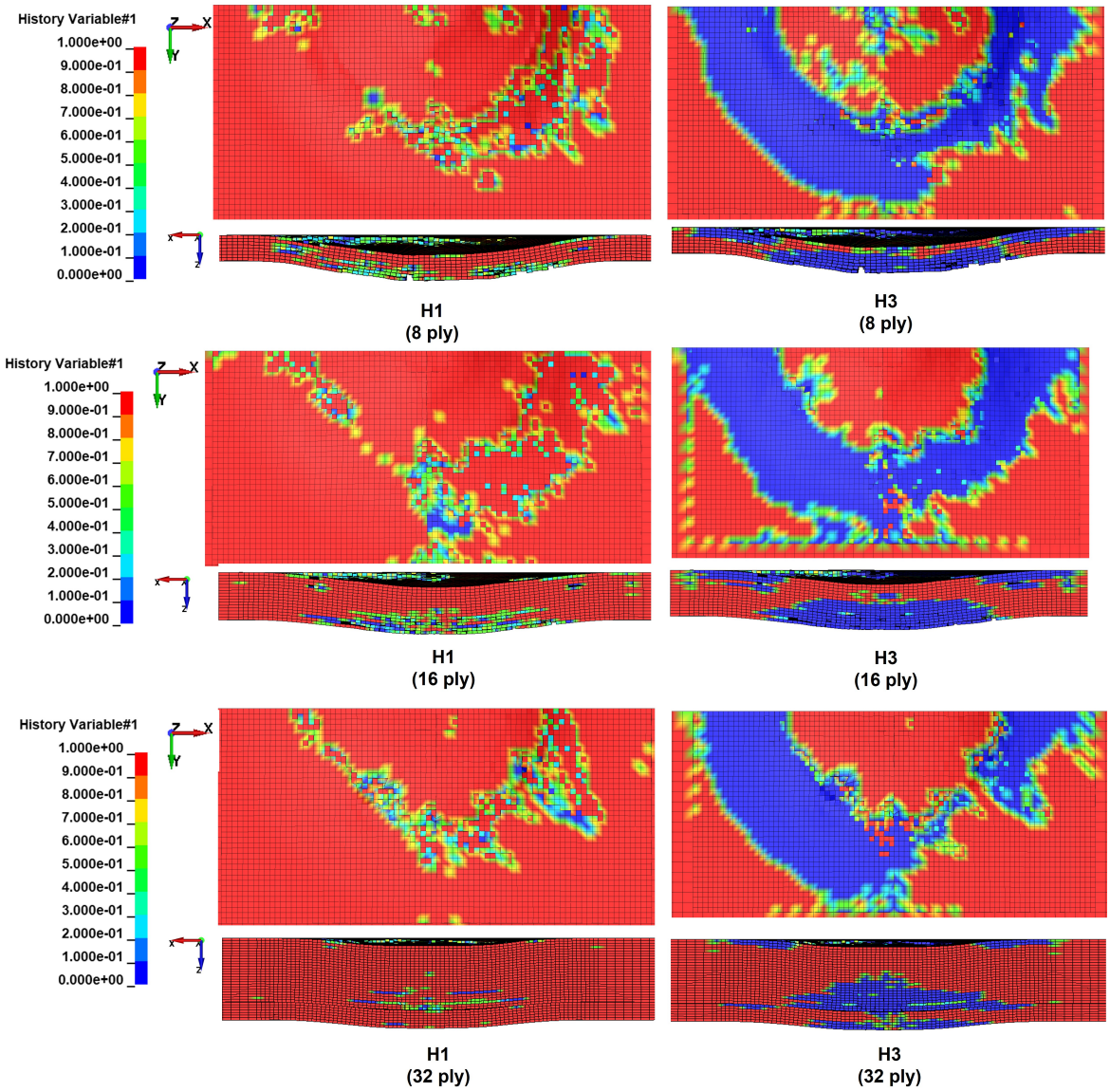

Figure 4.21: History variables ($t = 7.5E - 3$ms) of the fibre (H1, left) and the matrix (H3, right) tensile cracking modes for different plate thickness: 8-ply (top), 16-ply (middle) and 32-ply (bottom). For all history variable plots, the top (upper) and frontal (lower) views are presented.

4.4.3 Stackup Sequence

The stacking sequence is another physical property that determines the final stiffness of the plate. Apart from the baseline configuration, two other stacking sequences are considered in this study:

- Baseline $[+45/90/-45/0]_{2s}$: The initial configuration of the plate, for which experimental and numerical results are available.

- Stackup $[+45/-45/90/0]_{2s}$: By setting ± 45 as the fibre orientation for the first impact ply, stiffness in the fibre or longitudinal direction is introduced. This could be beneficial in the case of high velocity cases, as the dominant failure mode that drives to penetration is tensile fibre breakage in the impact plies. However, impact is a very complex loading phenomenon where tension is not the only mode involved. That is why, this is just a preliminar study on the effect of fibre orientation on the final response of the plate to impact.

- Stackup $[0/45/90/-45]_{2s}$: Using $0\,\mathrm{deg}$ as the fibre orientation angle for the impact ply is expected to provide the plate a more flexible response to impact. This ply orientation in the impact surface is also of interest, as a more energy absorption capability is searched.

The contour plots in Fig. 4.22 show the longitudinal (fibre) and the transversal (matrix) tensile cracking history variables (H1 and H3, respectively) for the baseline and the two modified stacking sequences sequences at an intermediate time instant $t = 7.5E-3$ms.

On the **matrix tensile damage** (H3) results, the failure pattern for the three stacking sequences is very similar in shape and extension through the plate thickness. This failure mode is the earliest and more advanced one as it has been previously mentioned in previous sections. As for the **fibre tensile breaking** failure (H1), it is clear that the third stacking sequence shows the least damaged status. This exhibits a higher energy absorption capability of the $0\,\mathrm{deg}$ compared to the $45\,\mathrm{deg}$ fibre-oriented layers.

4.4.4 Conclusions

To end this study, the main physical properties of the high velocity impact problem are shown and commented for the different configurations implemented through the whole physical analysis.

In Fig. 4.23, the internal energy absorbed by the entire plate and the absorbed per ply are shown for the different configurations tested in the physical parametrical study.

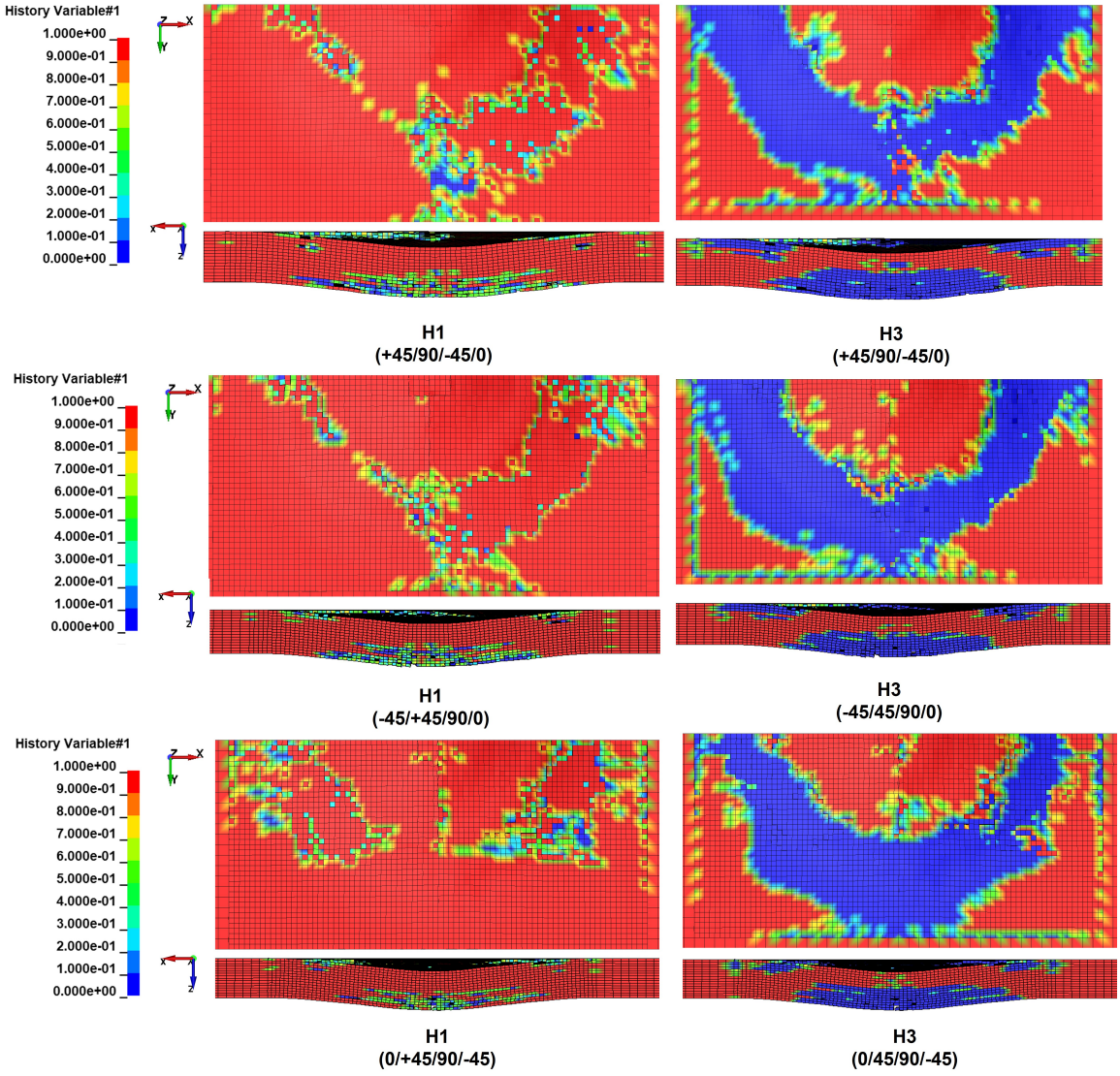

Figure 4.22: History variables ($t = 7.5E-3$ms) of the fibre (H1, left) and the matrix (H3, right) tensile cracking modes for different stackup sequences: [+45/90/-45/0] (top), [+45/-45/90/0] (middle) and [0/+45/90/-45] (bottom). For all history variable plots, the top (upper) and frontal (lower) views are presented.

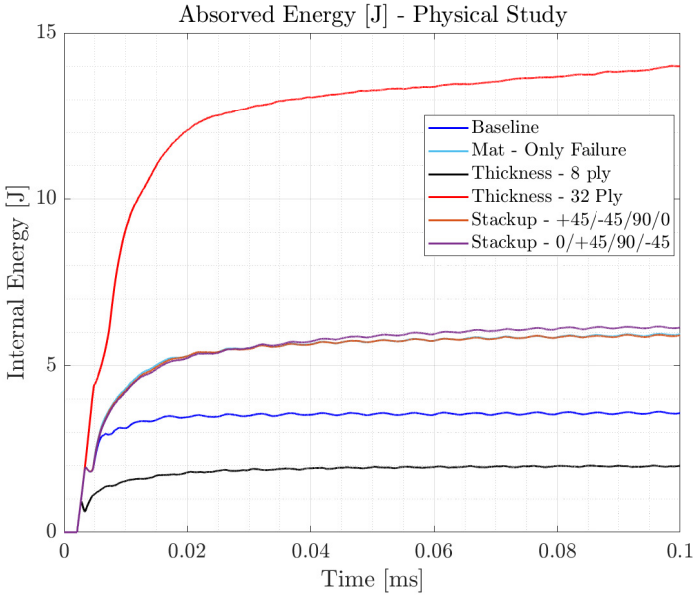

(a) Internal energy.

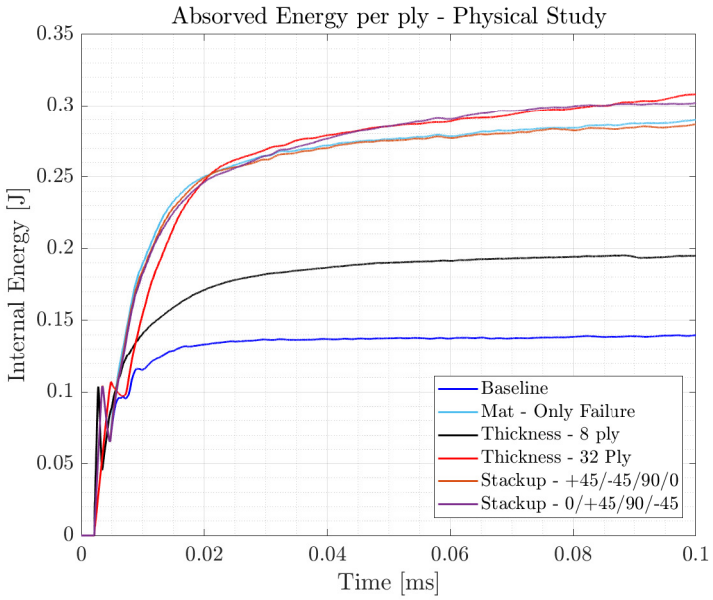

(b) Internal energy per ply.

Figure 4.23: Internal energy (total and per ply) evolution for the physical study test cases: 16-ply plate with material formulation with erosion strain parameters (Baseline), 16-ply plate without erosion strain parameters (Mat- Only Failure), 8-ply plate (Thickness - 8 ply) and 32-ply plate (Thickness - 32 ply).

It is clear from Fig. 4.23, that the plate with the more flexible stackup sequence, $[0/+45/90/-45]_{2s}$, is capable of absorbing more energy than the other two stackup sequences. On another note, Fig. 4.23b shows that the energy absorbed per ply is practically the same for the plate with 16 and 32 plies, while being lower for the smaller thickness plate, the 8-ply case.

In Fig. 4.24 shows the evolution during impact and the residual/exit value of the projectile's velocity. The residual velocities computed by the present model for all the different configurations employed in the physical study are compared with the experimental results recorded in the reference works [49, 39]. Two different impact velocities tests are shown. First, for the impact velocity employed during the whole study $v_{i,proj} = 120$ m/s and for a higher velocity case $v_{i,proj} = 154$ m/s, for which experimental tests were also available.

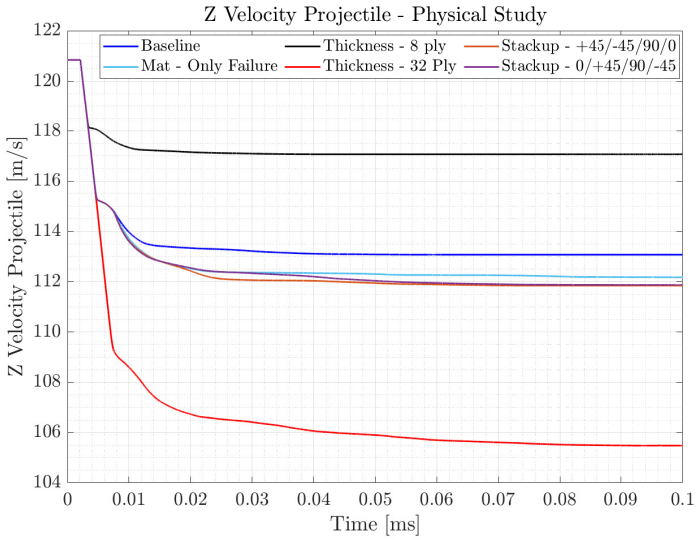

(a) Projectile velocity.

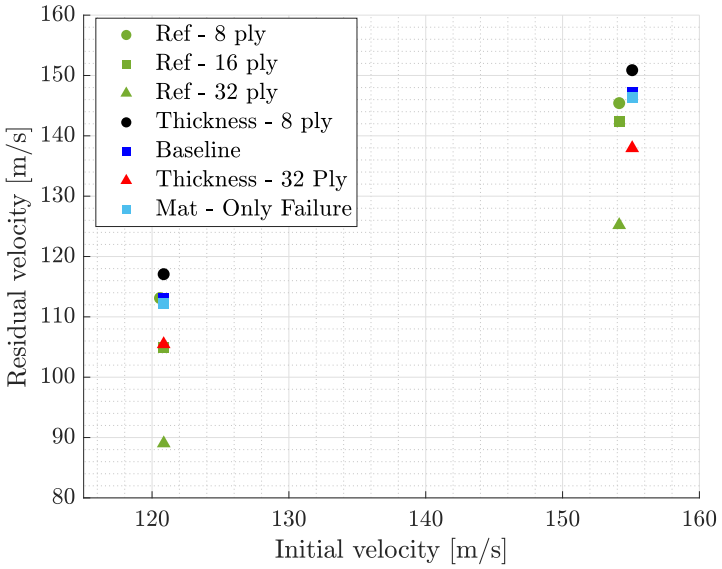

(b) Projectile residual velocity.

Figure 4.24: Projectile velocity evolution and residual velocity for the physical study test cases. Validation with experimental results from reference [39].

About the residual velocity, it should be noted that the projectile velocity Fig. 4.24a

follows a similar trend than the impact energy but reverse. The lower energy absorbed indicates a smaller transfer of the kinetic energy of the projectile to the plate. It should be noted that, the velocity of the projectile in the 32-ply model keeps decreasing unlike in the other cases. Since the composite plate in this case is much thicker, many elements pertaining mostly to the lower plies of the plate do not experience enough deformation to be eroded. Thus, even after penetration there is still an interaction between these remaining parts of the plies and the projectile, and the energy transference keeps going, as shown in Fig. 4.25.

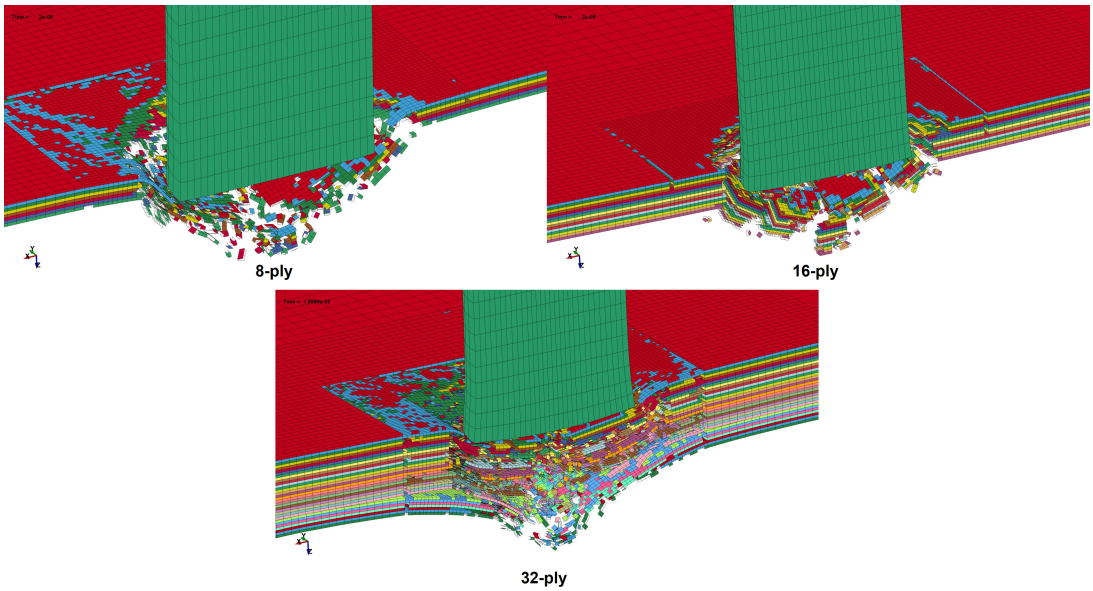

Figure 4.25: High Velocity Impact in a 8 (top, left), 16 (top, right) and 32-ply (bottom, middle) composite plates at a $t = 2e - 2$ ms.

In the last figure Fig. 4.24b, it is clear that the exit velocity for impact on the lower thickness plate (8-ply model) represented by the numerical model is the best compared to experimental results, while the higher thickness case (32-ply model) shows the higher difference between numerical and experimental. About the baseline thickness case (16-ply model), the model with the material formulation without the failure strains represents better the exit velocity of the projectile.

As a final conclusion, the limitations of the model, specially the ones coming from the material formulation, have an evident impact on the physical results. In fact, the error seems to increase as more plies are introduced into the model. However, these models have numerical robustness and serve as a proof of concept to represent the ballistic response of the plate to impact. The final goal of this study is not to provide the most accurate approach and override the reference studies found in the literature, but contribute to the research and construction of numerical solutions to the composite impact problem.

Chapter 5

Low Velocity Impact on a Composite Plate

In this chapter we describe and analyze the low velocity impact model on a composite plate. The model constructed is based on previous reference studies found in the literature [25, 36].

In the low velocity model, we followed a different structure than in the previous chapter. As was explained in 3.1.1, in a low velocity impact, delamination is one of the most relevant sources of damage. This is why, this interlaminar failure mechanism has been isolated in a preliminar model named ”Elastic Model”, in which the composite material is assumed to follow a orthotropic elastic constitutive law, and delamination is represented through tiebreak contact.

After building the ”Elastic Model”, the intralaminar failure of the plate is introduced into the problem in a new model named ”Failure Model”. The material formulation is modified to the same model employed in the high velocity case (*MAT_054), adjusting the mechanical properties to the fibre-matrix of interest for this case.

In this study, several material tests results were borrowed from the literature reference model [25]. These experiments were carried out to develop a cohesive material model for delamination in the plies interfaces and a continuum damage model for the ply intralaminar failure mechanism. Please refer to Appendix 8 for more details on the material experimental procedures carried out.

5.1 Model Characteristics

The reference studies [36, 25] are based on a Drop Tower test, for which a representative numerical model was constructed in LS Dyna. The reference numerical model is used as an initial configuration to represent the failure mechanisms of a composite during impact

for low ranges of velocity. However, some modifications were introduced to adapt their work to the scope of this project, and also, to enhance the delamination and interlaminar failure representation capabilities. The model layout is presented in Fig. 5.1.

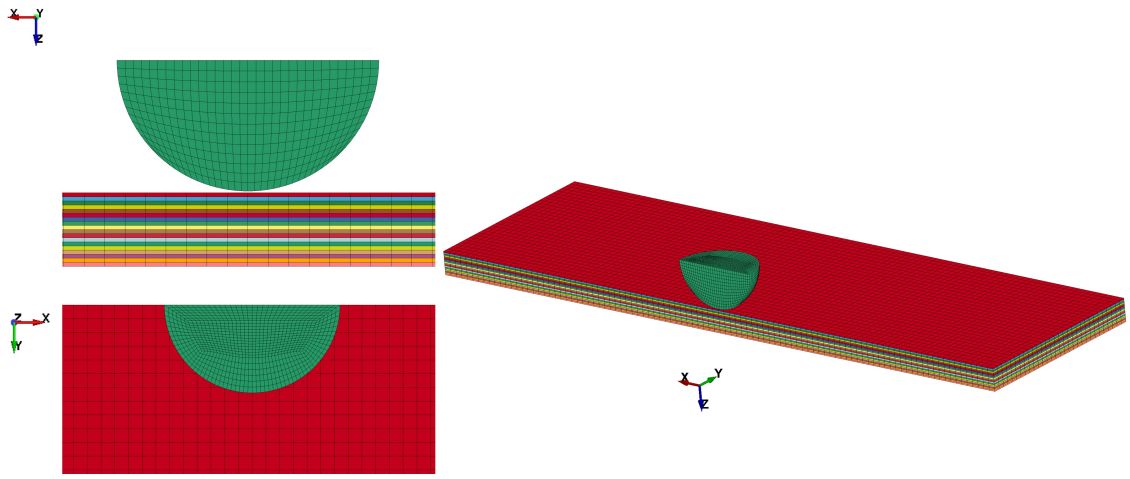

Figure 5.1: Low Velocity Impact on a Composite Plate model [36, 25]. Frontal (top, left), top (bottom, left) and isometric (right) views of the model.

The main physical characteristics relevant in this model are:

- The **composite plate** is rectangular, XZ-symmetric, and is made in T800S/M21 carbon-epoxy composite material. The plate counts with 18 plies following a $[-45, 45, 0, 90, 0, 0, -45, 45, 0]_s$ stacking sequence, as shown in Fig. 5.2, and has a total nominal thickness of 4.5 mm.

- The **projectile** used in the Drop Tower experiments was a cylinder with a hemispherical end, which has been simplified to a hemisphere in the numerical model with a velocity of $v = 4.17m/s$ and a mass of $m = 2.368kg$, in which the mass of the cylinder is included. The projectile was modelled through a rigid material law and bounded to move in the Z-direction only.

The main numerical aspects of the reference model, which was used as a baseline for this study, are compared with those of the adjusted present model in Tab.5.1. Note that, a mesh refinement on the impact area was introduced in the present model to improve the accuracy and numerical stability of the numerical reference model.

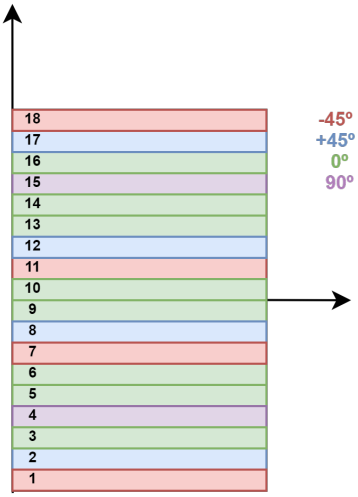

Figure 5.2: Stacking sequence of T800S/M21 composite plate employed in low velocity model.

Numerical Model	Description	Reference Model [36, 25]	Present Model
Mesh Density	Element size impact area	1.25x1.25x0.25 mm	0.75x0.75x0.25 mm
Element Type	Element type and integration	Hexahedron 1-point reduced integration (ELFORM=1)	Hexahedron 1-point reduced integration (ELFORM=1)
Material Formulation (Elastic/Failure)	Composite LS Dyna type	Elasic orthotropic (*MAT_002)	Elasic orthotropic (*MAT_002)
		Rate dependent progressive damage (*MAT_162)	Damage evolution by strength reduction, Erosion with failure strains (*MAT_54)
Hourglass Control	Resisting forces and scale factor (QM)	Stiffness forces (QM=n/a)	Stiffness forces (QM=0.03)
Contact Algorithm	Projectile-plies	Surface-to-surface eroding	Surface-to-surface eroding
	Interply	n/a	Single surface
	Delamination	Cohesive elements bilinear traction separation law (*MAT_138)	Tiebreak with no damage law (OPTION=7)

Table 5.1: Numerical characteristics of the low-velocity reference [36] compared to the present model.

5.2 Analysis methodology

Low velocity impact modelling requires longer simulation times to fully analyze the evolution of damage in the plate, since the deformation rate is much lower. This motivates the search for simplified techniques that optimize the computational effort while providing a representative solution of the problem. To do so, we developed two independent sub-models with the purpose of isolating the sources of complexity in the problem:

- **Delamination or "Elastic" Model:** The focus is to examine the delamination, so, an elastic orthotrophic law is used for the composite plate material. As a consequence, this model is not able to represent intralaminar failure inside of the plies. As was explained in section 3.1, delamination is one of the most influential failure mechanisms in low velocity impacts, so it is interesting to first evaluate its effect and refine its modelling methodology before tackling the intralaminar damage problem.

- **Intralaminar and Delamination or "Failure" Model:** The second sub-model includes the conclusions of the previous one to represent delamination and introduces intralaminar failure. The goal here is evaluating a complex material constitutive law, able to represent intra-laminar failure and element erosion, together with the tiebreak contact, that accounts for delamination.

The necessary material data for both the plies material constitutive law and the tiebreak contact parameters were obtained from the work of Muhammad in [25]. In this reference study, cohesive elements (*MAT_138) with a bilinear traction-separation progressive damage law able to account for mixed-mode loading are employed for delamination modelling. Besides, Muhammad's model used an advanced material formulation (*MAT_162) with a strain-rate sensitive progressive damage model for representing the intralaminar failure.

In this present work, these two parts of the numerical model have been simplified to reduce its complexity and adapt it to the available license. As shown in Tab. 5.1, the material formulation for the failure model is modified to the one employed in the high velocity case (*MAT_054). For **delamination**, the present model employs a tiebreak contact with OPTION=7 as a baseline approach. Nevertheless, since the reference model [25] employed cohesive elements to model delamination interfaces, the necessary fracture mechanics parameters are available and can be translated to other more advanced tiebreak contact options, OPTION=6 and OPTION=9. The results on delamination are compared in terms of accuracy and efficiency with the baseline (OPTION=7), to find the best approach.

5.3 Elastic Model: Only Delamination

This section studies the delamination damage mechanism, and can be divided into two main areas:

- **Construction of a stable and robust numerical model**: The element type and integration technique, the hourglass control method and the contact algorithm employed, particularly the tiebreak contact formulations, are examined. These are the main numerical parts of any impact mechanics problem that need to be checked to reach the numerical solution.
- **Validation with experimental data**: In the reference study [25], some C-scans were taken during the drop-tower test experiments. The C-scanner technology is one of the most common instruments to experimentally measure delamination. The results taken from these experiments are used here to validate the elastic model.

5.3.1 Material Formulation

Before explaining the different numerical parts of the model, the mechanical properties of T800S/M21, modelled with an elastic orthotropic law, are presented in Tab. 5.2.

Mechanical Properties T800S/M21	ρ (kg/m^3)	E_a (GPa)	E_b (GPa)	E_c (GPa)	ν_{ab}	ν_{ca}	ν_{bc}	G_{ab} (GPa)	G_{bc} (GPa)
	1550	157	8.5	8.5	0.35	0.35	0.53	4.2	2.2

Table 5.2: Elastic orthotropic mechanical properties of T800S/M21 plies.

Note that *a* represents the fibre or axial direction, *b* is the matrix or transversal direction and *c* is the normal direction to the ply.

5.3.2 Element Formulation and Hourglass Algorithm

The first part of the numerical analysis is the element integration technique and hourglass algorithm. As was concluded in the previous chapter, 1-point reduced integrated solid elements with a stiffness hourglass approach is a good compromise in terms of computational efficiency and robustness.

The stiffness-type hourglass resisting forces are, in general, more effective for structural parts than the viscous-type. In addition, in LS Dyna support page, [47] it is recommended to use a stiffness algorithm in the case of low velocity with an hourglass scale coefficient in the range of $QM = 0.03 - 0.05$, so as to minimize nonphysical stiffening of the response

and, at the same time, effectively inhibiting hourglass modes. This is why, this formulation is used as a baseline case in this study.

The internal, hourglass and sliding contact energy evolution are presented in Fig. 5.3, for a stiffness hourglass control method with different hourglass resisting forces scale coefficient.

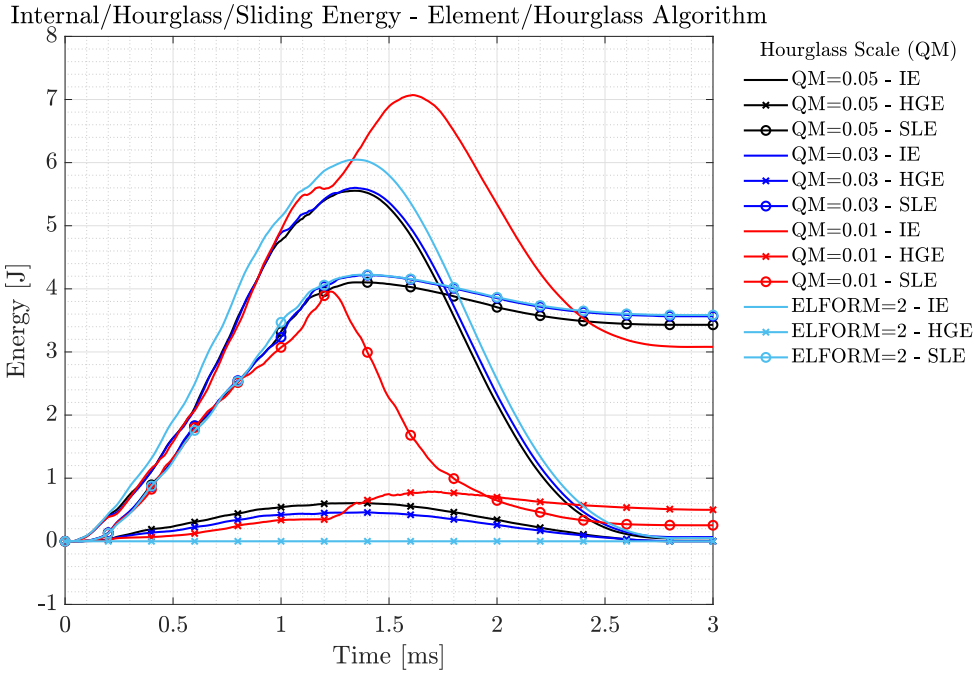

Figure 5.3: Internal, Hourglass and Sliding energy evolution for different element formulation and hourglass configurations. Reduced integrated elements (ELFORM=1) with different hourglass scale coefficients (QM=0.05, QM=0.03 and QM=0.01) and full integrated elements ELFORM=2.

The final values of these energies are also tabulated in Tab. 5.3 for a more clear comparison between the different scale factors.

Energy/ Hourglass Scale QM	Internal, IE (J)	Peak Internal, IE (J)	Hourglass, HGE (%IE)	Sliding, SLE (%IE)	CPU time (min)
0.05	0.0491	5.554	2.707	61.75	164
0.03	0.0667	5.601	1.707	63.66	171
0.02	0.0835	5.8	1.212	59.13	178
0.01	3.081	7.071	16.21	3.58	167
ELFORM=2	0.0513	6.047	0	59.28	284

Table 5.3: Internal, hourglass and sliding contact final energies for different element formulation and hourglass configurations.

As specified in LS Dyna Support recommendations [46], the hourglass energy checked

is with respect to the final internal energy and, the sliding contact energy with respect to the peak internal energy. In the case of the hourglass energy, it remains within the 10% of the internal energy, except for the lowest scale factor tested (QM=0.01). This might come as a surprise, as for lower scale factors one would expect that the hourglass resisting forces would not contribute as much to the work done by the system. However, it is interesting to keep this result in mind and move to the sliding contact energy analysis.

To choose the most adequate hourglass configuration, the presence of hourglass modes in the structure must be examined carefully. This is done in Fig. 5.4. Note that, in this plot, the displacements have been scaled by a factor of 3 to facilitate the vision of hourglass shaped modes. The most adequate hourglass algorithm must inhibit the presence of these spurious modes, while keeping the work done by the resisting forces under a certain limit. This is why, as long as hourglass energy respects its maximum limitation, the best hourglass algorithm is the one with highest scale factor, as it guarantees a lower probability of hourglass modes being present in the simulation.

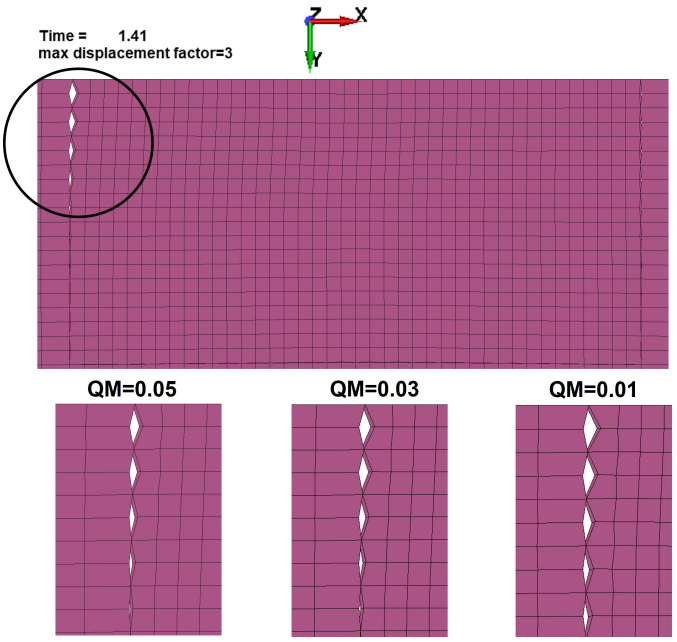

Figure 5.4: Hourglass modes presence for different scale coefficients (QM=0.05, QM=0.03 and QM=0.01). Top view of the ply #16.

In Fig. 5.4, although the displacements have been scaled by a factor of 3, which exaggerates the void between the nodes, a discontinuity in the nodal displacement field computed is observed. This discontinuity could be due to the poor mesh quality generated by connecting the impact area elements to the large aspect ratio elements from the rest of the plate. Another reason could be the lack of a failure criterion or damage law in the material formulation. This discontinuity must be taken into account when examining the

results as a limitation of the model, although being only observable in one ply of the plate when a displacement factor of 3 is introduced.

On the other hand, the **sliding contact energy** (SLE) presents a regular behaviour in most cases, as seen in Fig. 5.3. However, it should be kept in mind that this energy is an nonphysical artifact of LS Dyna, and its values should remain under a 10% of the peak internal energy, a rule of thumb [46] that is not respected for these first cases. There is a sudden drop of the sliding energy for the lowest scale factor (QM=0.01) case, which is also the case that presented the abnormality in the hourglass energy evolution. To further explore this issue, Fig. 5.5 shows the sliding energies for all the contact interfaces.

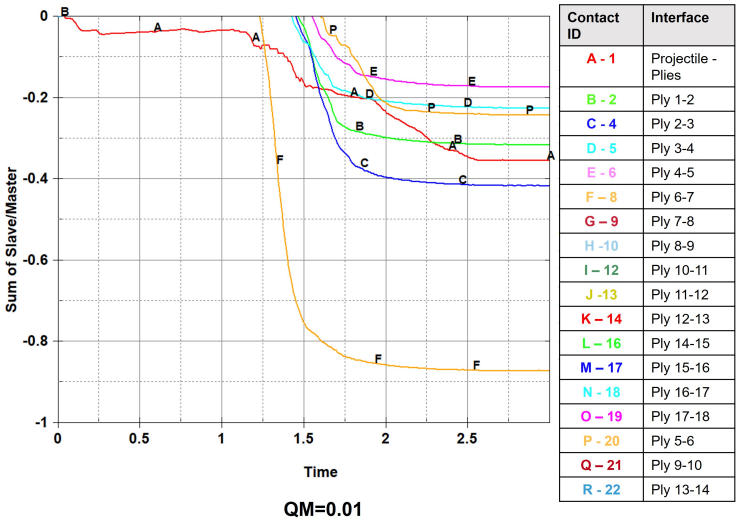

Figure 5.5: Negative sliding contact energies at every contact interface for chosen hourglass configuration (QM=0.03).

As explained in 3.3.4, LS Dyna computes for each contact interface two sliding contact energies, corresponding to the slave and the master parts. These energies, should have a similar evolution and opposite sign, and their net sum should remain close to zero (10% of peak internal energy) and always positive. Negative net contact energy is sometimes generated when contact parts slide relative to each other [46]. As specified in section 3.3.4, if the global internal energy mirrors the negative contact energy, it is possible that the problem is localized with low impact on the overall validity of the solution. In fact, the problem is very localized in contact interface between plies #6-#7, where the net sliding energy reaches a final value of $SLE_{6-7} = -0.87$ J (12.7% of the peak internal energy). There are other contact interfaces that also present negative net sliding energies, but that respect the limit.

To solve this issue, the contact model would need to be refined. However, as the model shows good behaviour for the other scale coefficients and as these values provide a higher reassurance on the elimination of the hourglass modes, the chosen scale coefficient for the

rest of the analysis is going to be **QM=0.03**. Keep in mind that the model shows still large values of the contact sliding energy, an issue that would be solved in the next section by working on the contact algorithm.

In this case, given the already long computational times and the fact that the hourglass energy seems to be below the limit value for all cases, the mesh size is considered to be sufficient to represent the physics of the problem. However, a possible enhancement of this model could be a mesh refinement in the impact area.

5.3.3 Contact Algorithm

This section focuses on refining of the contact algorithm and its effect on the impact solution. There are two mainaspects of the contact algorithm that can be enhanced:

- The **sliding contact energy** needs to be lower. The sliding contact energy is an unphysical artifact in the simulation and it is on our best interest to keep it to a minimum to preserve the accuracy of the model.

- The second enhancement is to **introduce a damage law in the tiebreak contact** interactions. As explained in 3.3.4, the baseline tiebreak option (OPTION=7) does not incorporate a model to describe the evolution of damage after the failure onset is predicted. The other options described in this section include linear (OPTION=6) and bilinear (OPTION=9) laws to model interlaminar damage growth. These options can only be implemented providing the necessary material test parameters. Thanks to the extensive work carried out by Muhammad in [25], these parameters can be introduced into the material formulation. For more detail on how these material experimental parameters were obtained, please refer to section 8.1.1 in Appendix 8.

Untied same fibre-oriented plies

The first refinement is achieved by modifying the contact model between same fibre-oriented plies. This modification is based on the principle theory basics explained in section 3.1, which state that delamination can only occur between plies which have different fibre orientation. As it can be observed in Fig. 5.2, the interfaces between plies #5-#6, #9-#10 and #13-#14, are regions with a lower probability of developing delamination damage. This allows the contact model to be simplified and to assume a classical surface-to-surface contact formulation between these set of plies.

This modified configuration, named **"Untied" model**, is compared to the previous model, in which all plies are connected through tiebreak contacts. In Fig. 5.6, the internal, hourglass and sliding contact energies from both approaches are compared. The sliding

energy final value is 11.63% of the peak internal energy for the ”Untied” model, while for the initial model, it was a 63.67%. This provides higher reliability and solves the issue shown in previous section.

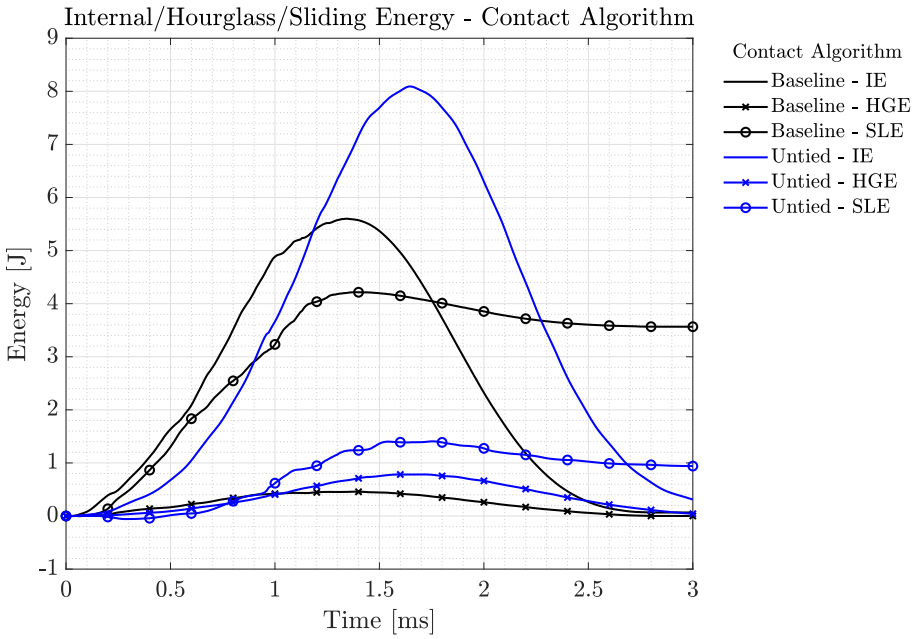

Figure 5.6: Internal, hourglass and sliding contact energies evolution for different contact algorithms: Baseline (all plies interact with tiebreak contact), Untied (only plies with different fibre orientations interact with tiebreak contacts).

As a final recommendation, the global sliding net energy should be checked separately for every contact interface. Although the global value of the sliding contact energy shows a better behaviour, it must be kept in mind that this value is computed through the sum of the interfaces' net contact energy. In other words, the behaviour of some of the contacts interactions could be erroneous but the values of the sliding energies could compensate each other and give a seemingly good value.

Tiebreak contact option: Interlaminar damage law

The second contact modification consists in introducing a damage model in the tiebreak contact formulation. The multiple damage options were explained in detail in 3.3.4.

The baseline model was constructed using the simplest option, OPTION=7, which does not include a damage law after tiebreak failure is detected. When the failure criterion is met, the tied contact is deactivated and replaced by a classical surface-to-surface penalty based formulation. The other more advanced options, OPTION=6 and OPTION=9, incorporate a linear and bilinear damage evolution laws respectively.

The necessary parameters that must be provided for each alternative are indicated in Tab. 5.4, and have been obtained from the experimental tests carried out in [25]. Please refer to Appendix 8 for more detail on the test procedures carried out to compute these delamination characteristics of the composite.

Contact Tiebreak Option/Parameters	Description	OPTION=7	OPTION=6	OPTION=9
NFLS	Normal failure stress (MPa)	60	60	60
SFLS	Shear failure stress (MPa)	60	60	60
PARAM	Friction angle, ϕ (rad) Critical distance, CCRIT (mm) Damage model exponent, α	0	0.025	1
ERATEN	Normal energy release rate (J/m^2)	765	765	765
ERATES	Shear energy release rate (J/m^2)	1250	1250	1250
CT2CN	Ratio tangential to normal stiffness	n/a	n/a	1
CN	Normal stiffness (kN/mm^3)	n/a	n/a	100

Table 5.4: Tiebreak contact options parameters definition and values implemented in the numerical model.[25]

Each contact option is introduced along with the two contact configurations explained previously: the **baseline configuration** refers to the case where all plies are assumed to interact through a tiebreak contact, and the **untied model** is the case where the same fibre-oriented plies (#5-#6, #9-#10 and #13-#14) interact through a classical penalty contact.

The internal, hourglass and sliding contact energies final values are tabulated in Tab. 5.5 and their evolution is shown in Fig. 5.7.

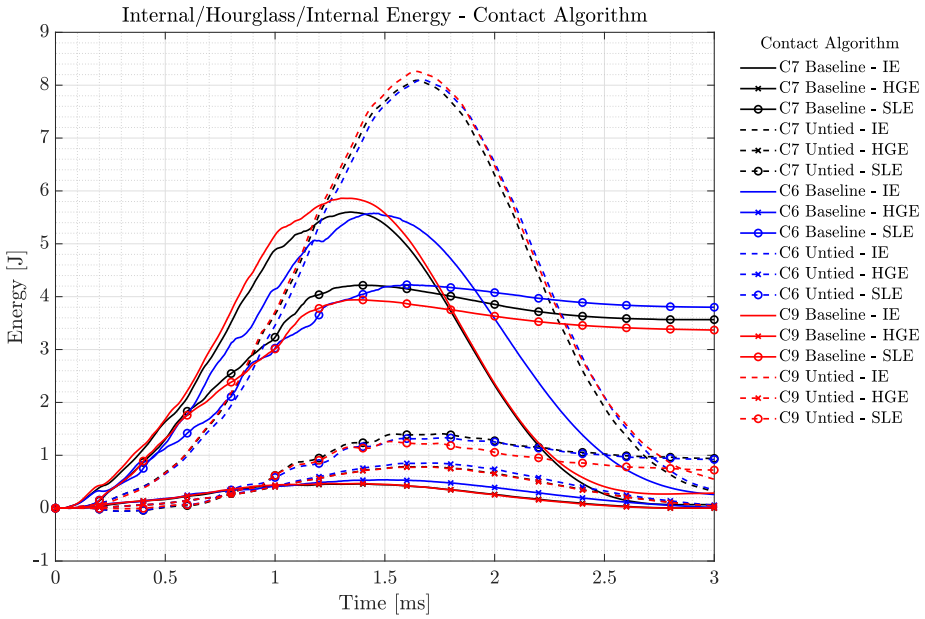

Figure 5.7: Internal, hourglass and sliding energies for different contact configurations: Baseline (all the plies interact with tiebreak contact), Untied (only plies with different fibre orientations interact with tiebreak contacts), C7 (Tiebreak contact with no damage law, OPTION=7), C6 (Tiebreak contact with linear damage law, OPTION=6) and C9 (Tiebreak contact with bilinear traction separation law with mixed loading capability, OPTION=9).

Energy/ Tiebreak Option	Contact Plies Conf.	Internal, IE (J)	Peak Internal, IE (J)	Hourglass, HGE (%IE)	Sliding, SLE (%IE)	CPU time (min)
OPTION=7	Baseline	0.0667	5.601	1.70	63.67	171
	Untied	0.3108	8.092	13.87	11.63	173
OPTION=6	Baseline	0.2582	5.577	5.58	68.14	167
	Untied	0.3400	8.109	16.56	11.37	163
OPTION=9	Baseline	0.2849	5.861	0.53	57.48	192
	Untied	0.5466	8.263	7.45	8.716	184

Table 5.5: Internal, hourglass and sliding contact final energies for the different contact configurations.

Both Tab. 5.5 and Fig. 5.7 show that the untied contact configuration provides better numerical results than the baseline configuration, since the global net sliding contact energies decrease from values around the 50-60% to 8-12% of the peak internal energy. On another hand, the hourglass energy escalates from 1-5% to 7-14% of the final internal energy when removing the tiebreak from the same-oriented plies. As a compromise must be made between the control over sliding contact, hourglass energies and computational effort, **OPTION=9 seems to be the optimal choice.**

Next, the effect of the different contact models on the physical delamination results is considered. The main physical results that are analyzed and compared to the reference experimental and numerical results [25] are:

- **Z Displacement of the bottom ply (Ply 18)**: The last ply is one of the most dangerous areas when examining delamination behaviour, in particular for flexible plates as explained in the theoretical part of this manuscript.

- **Resultant Contact Force:** The average of the resultant normal contact forces in all the contact interfaces is analyzed. The normal contact force is computed for each contact interface at every timestep during the simulation. To evaluate the behaviour of the entire plate, the resultant normal contact forces developed in all the interfaces are averaged at every time step. The final contact force shown is, thus, not only the force between the projectile-plies, but also between the plies connected through tiebreak contacts. This average operation is performed to compare the results of the present model to the reference [25, 36]. Note that, higher values of the contact force indicate a stiffer behaviour of the composite plate.

- **Delamination area:** In the reference study [25], some C-scans were collected during the experimental tests and are available for comparison with our model. Besides, the localization and amount of delamination predicted by the different tiebreak contact options is examined.

There is a clear enhancement on the accuracy of the results when employing the untied model, as was to be expected from the previous Fig. 5.6.

In Fig. 5.8 and Fig. 5.9 the displacement and the contact force evolution during the simulation are represented respectively. All the different tiebreak options provide good results for the untied configuration. The relative errors in peak contact forces are reduced to 0.25-3%, and the error in the peak displacement drop from values of 40-50% of error to 20%.

The present model could be considered as a robust first approach in terms of numerical stability and serve as an approximate solution of the delamination problem in a low velocity impact problem. However, there are some clear differences between the present developed model and the experimental data. The main source of error resides in the material formulation and mesh distribution and are further described in the conclusions of this section 5.3.4.

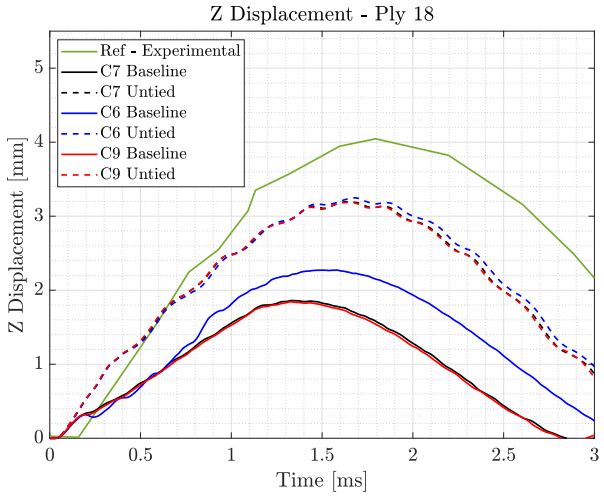

Figure 5.8: Displacement in the Z-axis of the bottom ply (Ply 18) evolution for different contact configurations.

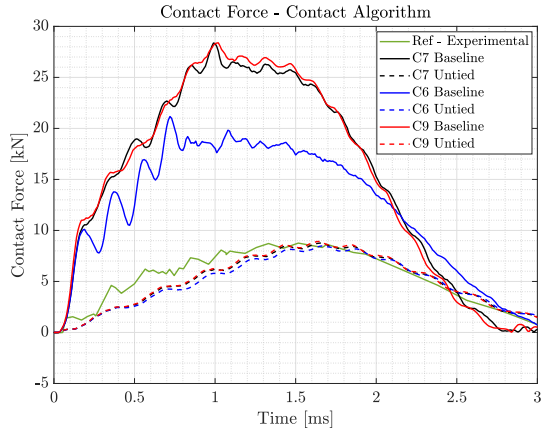

(a) Contact force

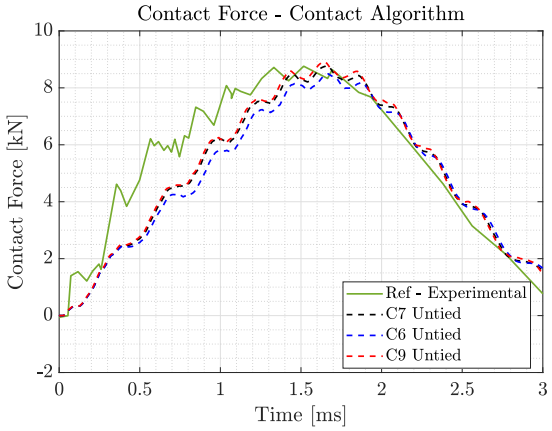

(b) Contact force zoom

Figure 5.9: Normal contact force average of all contact interfaces at each time step for different contact configurations.

Finally, the delaminated area was obtained experimentally through C-scans in the reference study [25] for the different contact interfaces. The experimental results are be compared with the predicted by the present model.

The delaminated area at the last stage of the impact in the impacted surface (ply #1) for this case is **25x29mm** as shown in Fig. 5.10.

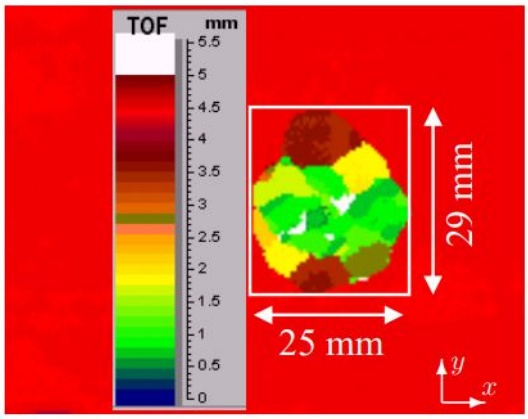

Figure 5.10: Top view of delaminated area in impacted surface (ply 1), from C-Scan measurements during Drop Tower Tests. [25]

The delamination area in this study is obtained by plotting the elements belonging to the failed tiebreak contacts. The failure of the tiebreak means the deactivation of the artificial tensile spring that is representing the delamination phenomenon numerically.

This deactivation is performed at different points of the stress profile, depending on the option chosen to model damage after the failure criterion is reached, as it is shown in section 3.3.4. The spring is removed right after the failure criterion is met for OPTION=7 (no damage law). Instead, for OPTION=6 and OPTION=9, which include a linear and bilinear damage laws respectively, this occurs when the damage variable reaches the value of 1.

The OPTION=9 is the most expensive option, not only because it allows to represent separately the damage evolution of the two main delamination modes of (opening and shear), but because it also allows to represent mixed mode loading cases, through the introduction of an internal parameter (α), which is given in the reference model [25] $\alpha = 1$[1].

The elements belonging to the failed contact interfaces can be represented through a variable name ”Contact Gap”. The ”contact gap” on the slave side of the tiebreak is a damage variable ranging from 0 (not-damaged interface) to 1 (fully damaged interface, tiebreak contact released). The delaminated areas for plies #1 and #18, the impacted and

[1]LS Dyna Material Models Manual [32] recommends that α is set to a value between 1-2.

non-impacted surfaces at the instant $t = 1.41$ ms of the simulation, are presented in Fig. 5.11.

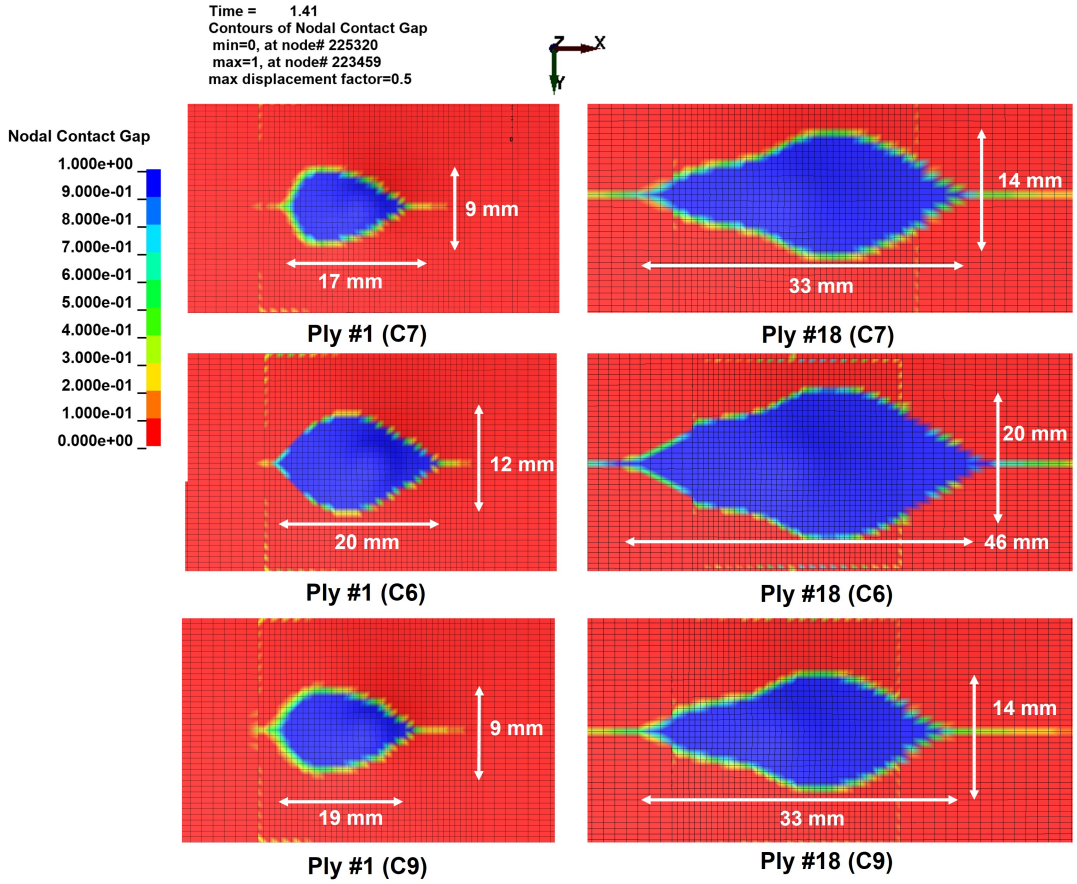

Figure 5.11: Top view of delaminated area in impacted surface (ply 1) and non-impacted surface (ply 18) for different tiebreak contact option.

The areas predicted for the different contact options are quite similar, which shows consistency of the present method, independently of the contact option used. However, there is a difference with the experimental values obtained in the C-scan, Fig. 5.10. This could be due to the limitations of the present model which are discussed in the conclusions 5.3.4. Moreover, the application of the XZ-symmetry obviously does not accurately represent in the real delaminated area.

5.3.4 Conclusions: Elastic Model

The difference in the physical results presented between the present model and the experimental tests could be due to some limitations of the present model, that could be enhanced by:

- **Material experimental tests** (Double-Cantilever Beam, End Notched Flexure etc.),

should be carried out in LS Dyna to refine the numerical parameters that conform the damage model for interlaminar failure. These parameters are highly sensitive not only to the material behaviour during damage, but also to numerical aspects such as the element size. Thus, the necessary experiments to characterize the delamination in the composite panel should be developed numerically along with a mesh independence study.

- **Mesh refinement of the impact area and element aspect ratio enhancement** are other adjustments for future developments of this model. These recommendations may be introduced including another symmetry condition in the YZ plane, which will also introduce some error in the representation of the delaminated area but reduce the CPU time.

5.4 Failure Material Model

In this section, the material formulation employed in the high velocity model (*MAT_ENHANCED _COMPOSITE_DAMAGE or *MAT_054) is introduced in the low velocity case to account for intralaminar failure along with the previously developed model for delamination.

From the previous section, the tiebreak contact options were reviewed and **OPTION=7** has been selected for this part, as it simplifies the model in terms of modelling the interlaminar failure, and enables us to put more emphasis on the intralaminar failure of the ply. Moreover, some numerical stability issues were encountered when introducing the other two tiebreak options (OPTION=6 and OPTION=9). These are left for future developments of the low velocity model.

The main goal of this section is to review on the numerical parts of the model: material constitutive law, element and hourglass formulations, and the mesh density. The contact algorithm is not further investigated for this case, as it was done previously through the elastic model. For this model, another symmetry condition has been applied on the YZ plane, to reduce the CPU effort. Thus, the impact energies are computed only for a quarter of the plate.

5.4.1 Material Formulation

The material formulation chosen for the ”Failure Model” is the same as the one employed in the high velocity model (*MAT_054). Note that, the reference study material model (*MAT_162) is not compatible with the current author’s LS Dyna license. This is why, the parameters obtained in the reference [25] through standard and non-stardard material

testing and calibration procedures need to be adapted to the formulation of the present model.

The material formulation chosen introduces an unavoidable source of error in the model, since the effect of strain rate and strength progressive softening during failure are not modelled. Instead, the chosen material formulation is able to represent the onset of damage (failure criterion), the strength softening process and finally, the erosion of the element due to strain failure as explained in section 3.3.3.

First, the mechanical properties and failure strength values, necessary to model the **intralaminar failure onset**, are shown in Tab. 5.6 and have been obtained from experimental tests carried out in the reference study [25].

Mechanical Properties T800S/M21	ρ (kg/m^3)	E_a (GPa)	E_b (GPa)	E_c (GPa)	ν_{ab}	ν_{ca}	ν_{bc}	G_{ab} (GPa)	G_{bc} (GPa)
	1550	157	8.5	8.5	0.35	0.35	0.53	4.2	2.2
Failure Parameters	X_T (GPa)	X_C (GPa)	Y_T (GPa)	Y_C (GPa)	S_C				
	2.2	1.2	0.045	0.28	0.045				

Table 5.6: Mechanical properties of composite failure model for T800S/M21. [25]

The strength softening parameters (YCFAC,FBRT) were not specified in the reference study [25]. The lack of representation of the progressive softening of the composite material is strong limitation, specially in low velocity impact. Besides, these parameters cannot be measured by tests but only through trial and error [20]. Consequently, the choice of damage parameters for each mode is still an open issue for the case of impact of brittle materials such as composites.

Finally, the strain to failure parameters (DFAILT/C/M/S), have been obtained from the experimental testing procedures carried out in [25] and are shown in Tab. 5.7.

Failure ϵ / Ply Angle	Description	± 45 deg	90 deg	0 deg
ϵ_T^f DFAILT (%)	Fibre tension	2	0.6	1.557
ϵ_C^f DFAILC (%)	Fibre compression	-7	-3.3	-1.05
ϵ_M^f DFAILM (%)	Matrix tension/ compression	7	3.3	1.05
ϵ_S^f DFAILS (%)	Shear	3.5	0	0

Table 5.7: Strains to failure parameters inside material formulation (*MAT_054) for the present model.

For more information on the experimental tests procedures on this section please refer to the Appendix 8 dedicated exclusively to the description of the material properties and calibration procedures for each model.

In Fig. 5.12, the internal, hourglass and sliding contact energy evolution during the impact are presented for a material formulation with and without strain erosion parameters included (DFAILT/C/M/S). By including eroding strains in the material formulation, the plate is able to absorb more energy and fail in a less brittle form. Note that, the removal of the strain to failure parameters had the same effect in the high velocity impact model 4.4.1.

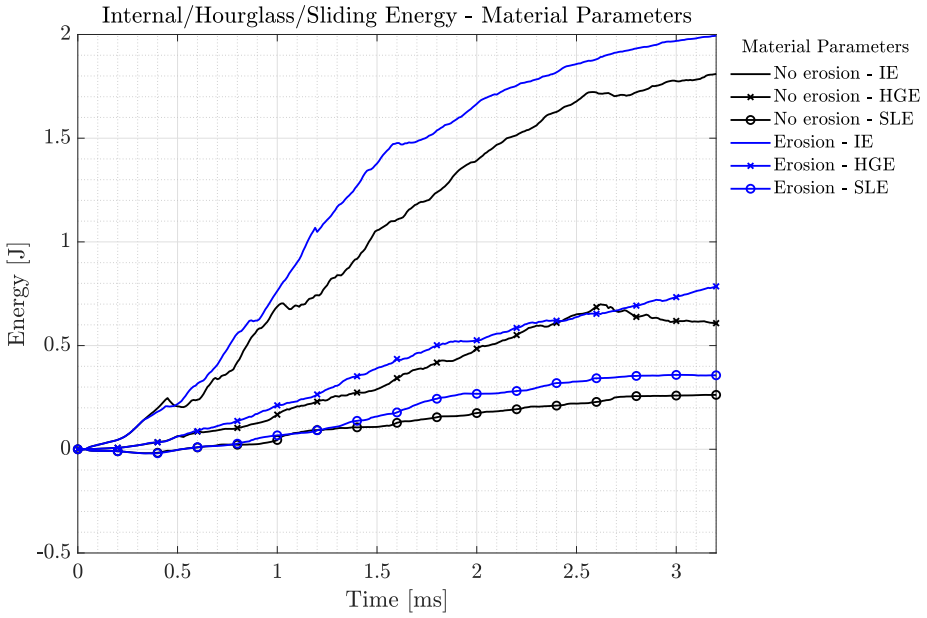

Figure 5.12: Internal, Sliding and Hourglass energy evolution for different material formulations with (Erosion) and without (No Erosion) failure strain parameters.

In Fig. 5.13, a top (upper) and lateral (bottom) views of plate are shown and the matrix tensile failure history variable (H3) is computed at the last stage of the simulation ($t = 3$ms).

As it is known from the theory, apart from delamination, the matrix tensile is the dominant source of damage during a low velocity impact. The introduction of the strain to failure damage parameters allows some failed elements to still be present in the simulation. This indicates that, the critical strain values are reached later than the stress failure criterion is met, allowing for the elements to experience some kind of ”plasticity” in terms of degradation. This also explains the higher internal energy absorption capacity.

As a conclusion, the introduction of failure strains reduces the brittle response of the composite to impact, and allows to represent its damage more smoothly, thus, in all the next steps the erosion parameters are implemented in the model. Note that, this behaviour is opposite as the one that the high velocity model plate presented when the

failure strains were removed from the material formulation 4.4.1. Consequently, the effect of this parameters needs to be examined for each individual case of study.

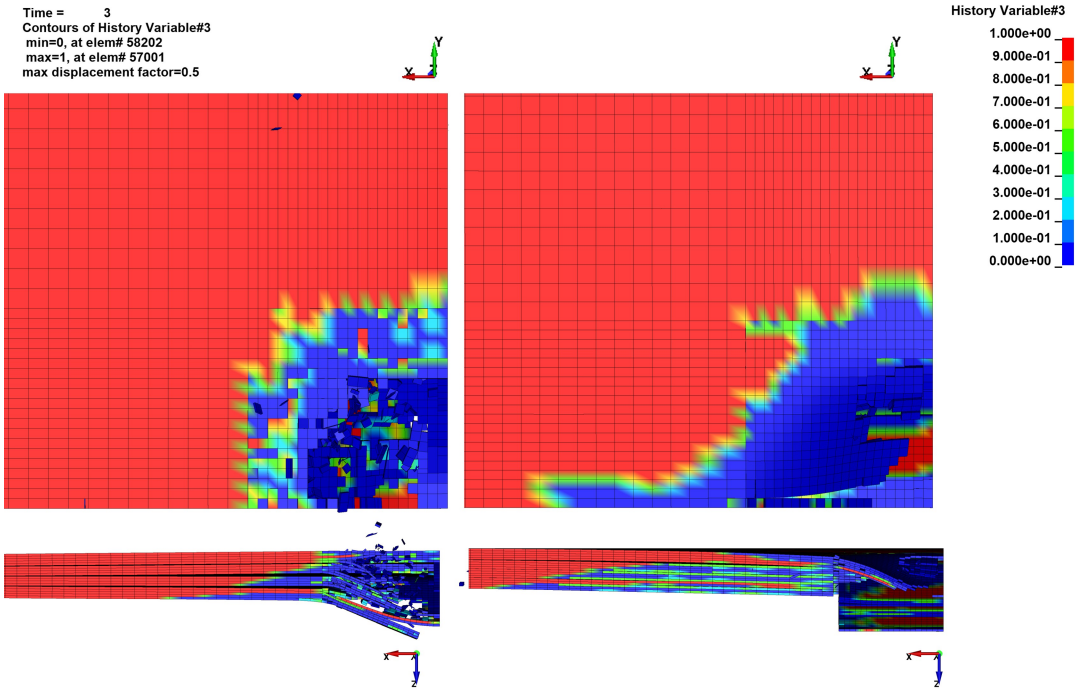

Figure 5.13: Matrix tensile failure history variable (H3) at $t = 3$ ms, for different materials formulations: no strain to erosion parameters (left) and with strain to erosion parameters (right). Top view (upper) and frontal view (bottom).

5.4.2 Element and Hourglass Formulation

In this section, the effect of element formulation and the hourglass algorithm are chosen for the ”Failure Model”.

Fig. 5.14 presents the internal, hourglass and siding energies for different numerical configurations. The first two, use a 1-point reduced integration technique with stiffness hourglass resisting forces scaled by factors of QM=0.03 and QM=0.01, respectively. The third, uses full-integrated elements for the plate.

To keep the CPU time to a minimum while representing the plate damage process accurately a reduced 1-point integration technique (ELFORM=1) with a hourglass resisting forces scale factor of QM=0.01 seems like the best option (blue curve). This scale factor reduces the unphysical effect of hourglass resisting forces while preventing the appearance of hourglass modes (checked in the model final stage for the ply 16).

However, since the hourglass and sliding contact forces energies are still over 10% of the internal energy, the next step will be to refine the mesh in the impact area, to try reducing the effect of these unphysical forces in the final solution.

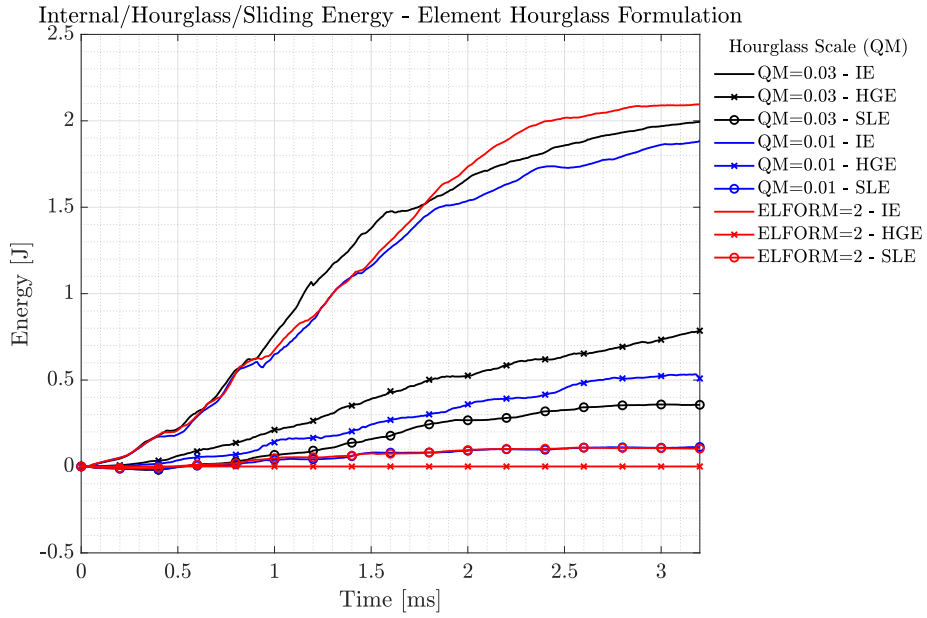

Figure 5.14: Internal, Sliding and Hourglass energy evolution for different element formulations and hourglass control algorithm.

5.4.3 Mesh density

In this section, the mesh on the impact area is refined as shown in Fig. 5.15. The main goal is to reduce work done by the hourglass resisting and sliding contact forces. Moreover, it is desirable to study the convergence of some physical results relevant during impact. Following our methodology, the convergence will be studied on: the impact energy, the resultant contact forces and the displacement of the non-impacted surface (Ply 18).

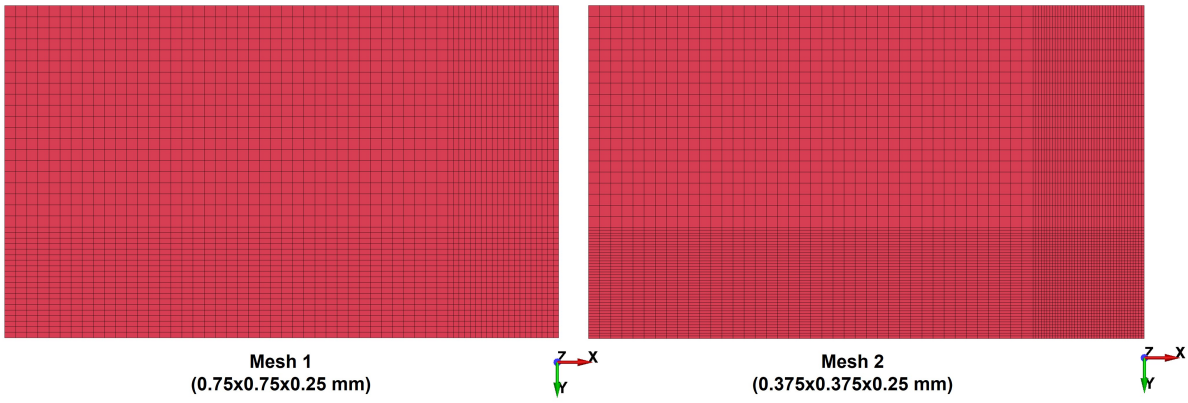

Figure 5.15: Mesh refinement for low velocity impact failure model (top view).

Although the selected hourglass resisting forces scale factor in the previous section is 0.01, the two relevant coefficients (QM=0.03 and QM=0.01) are tested to determine

the best configuration for this mesh distribution. Moreover, the fully integrated element solution is also included for comparison.

In Fig. 5.16, the internal, hourglass and sliding energy evolution for the different mesh densities, element and hourglass configurations are presented. In addition, the final values of these energies are are tabulated in Tab. 5.8 to ease the comparison between the different configurations.

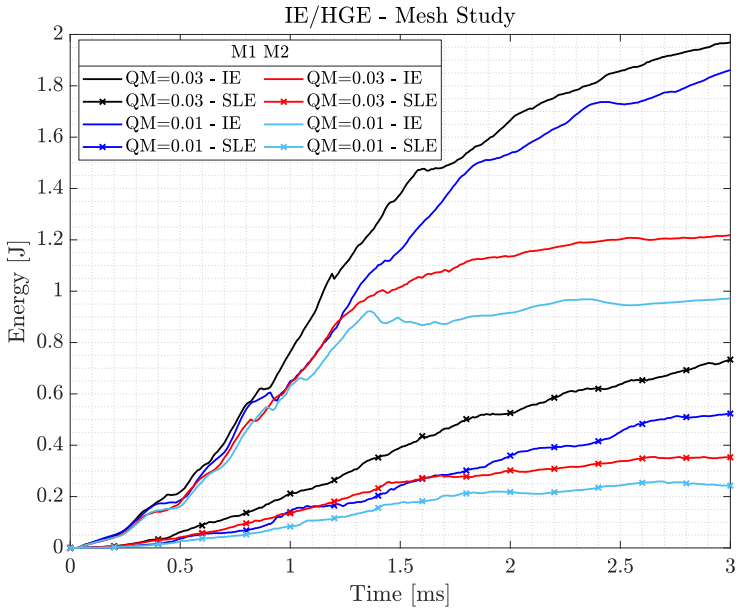

(a) Internal and Hourglass energy evolution

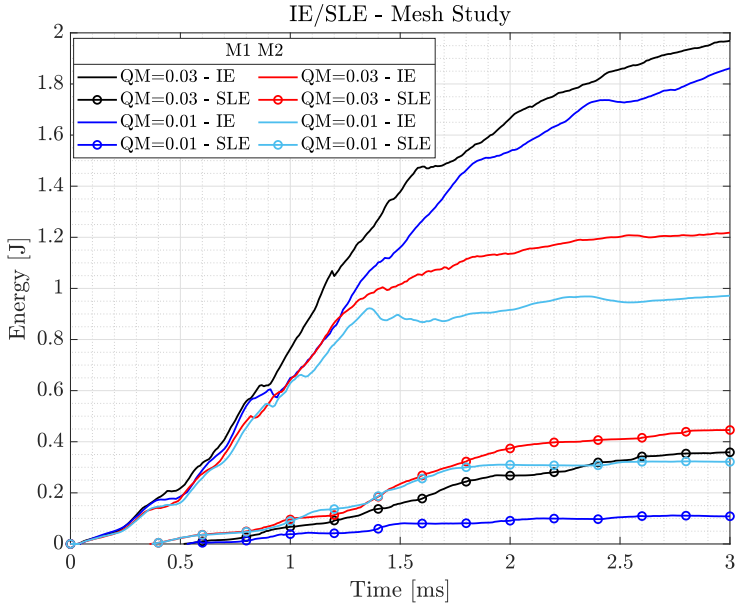

(b) Internal and Sliding contact energy evolution

Figure 5.16: Internal, hourglass and sliding contact energy evolution for different mesh densities and hourglass algorithm.

Energy /Test Cases	Material Parameters	Element Hourglass Form	Internal IE (J)	Hourglass (%IE)	Sliding (%IE)	CPU Time
M1	No erosion DFAIL=0	Reduced int QM=0.03	1.8193	33.1453	14.5161	170
	Erosion (from ref)	Reduced int QM=0.03	2.0013	39.7469	17.8629	154
		Reduced int QM=0.01	**1.9003**	**24.9874**	**6.1967**	**149**
		Full int	**2.0996**	**0**	**4.8933**	**337**
M2	No erosion DFAIL=0	Reduced int QM=0.03	1.3837	53.0956	30.1595	378
	Erosion (from ref)	Reduced int QM=0.03	1.2181	28.9951	36.6006	278
		Reduced int QM=0.01	0.9717	24.9708	33.0800	273
		Full int	1.13	0	11.8	534

Table 5.8: Internal, hourglass and sliding energies for different mesh densities and hourglass algorithms.

In terms of hourglass energy, the results do not show a great improvement on the hourglass energy for a reduced mesh density. The hourglass energy keeps being over the 10% limit even for low values of the scale factor.

Besides, the refined model shows an increase on the work done by sliding contact forces and although, the sleout file was checked and all the individual energies remain below the limit, the total sum of the net sliding energies is higher than for the first mesh density. This shows a numerical limitation, that could be due from the lack of accuracy of the material formulation parameters.

As a conclusion, the recommendation is to use the first mesh density (M1:0.75X0.75X0.25) mm with either the full integration method, obviously sacrificing some computational efficiency, or the reduced integrated model with the stiffness hourglass forces and QM=0.01.

The **second objective** of this section is to evaluate the main impact physical results for different mesh sizes. In addition, the physical results are compared with the experimental measurements performed during the reference study [25].

Fig. 5.17 shows the evolution of the resultant normal contact force (average of the normal contact forces developed in all the different interfaces at every time step) in the first part of the impact ($t = 0 - 1$ ms), for the different mesh densities and hourglass control configurations.

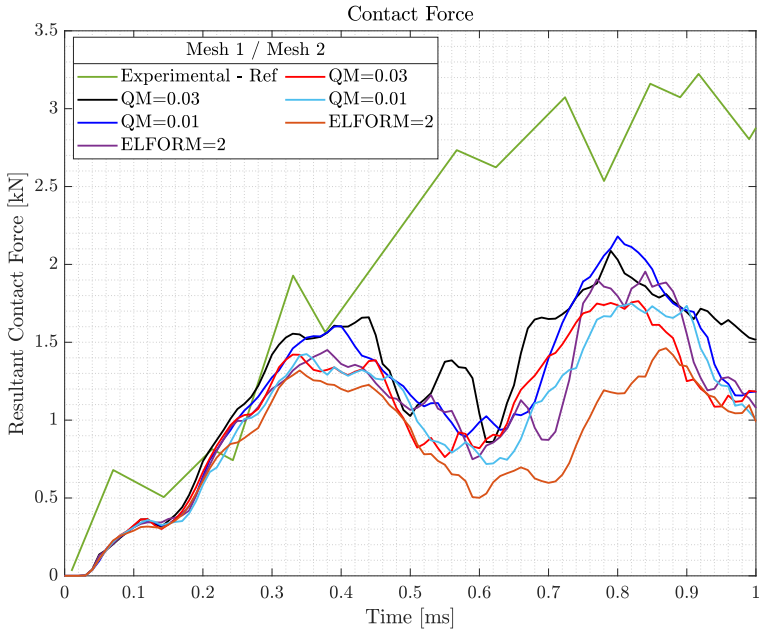

Figure 5.17: Resultant average contact force for different mesh densities and hourglass control algorithm, during the initial state ($t = 0 - 1$) ms. Validation with experimental reference results [25].

The resultant contact force does not show a clear trend, and the numerical model exhibits a brittle behaviour of the plate when compared to the experimental results. The contact force oscillations represent the delamination of the between the plies of the model, which clearly have a strong impact on the solution, as explained in the theory. However, the error on the contact force results most probably comes from the intralaminar failure model, since the results for the fully elastic model were much more close to the behaviour of the real plate.

The same can be said about the displacement of the non-impacted surface (ply 18) shown in Fig. 5.18. There is not a visible convergence of the results for different mesh densities. In fact, the only two models that seem to converge in this property are the reduced (QM=0.01) and the full integration cases. The behaviour recorded during the reference model experiments [25] is less brittle than the behaviour predicted by our mode. The last ply is supposed to bend back and recover some of its initial shape, while the displacement evolution of the our model indicates that the plate gets finally penetrated by the projectile.

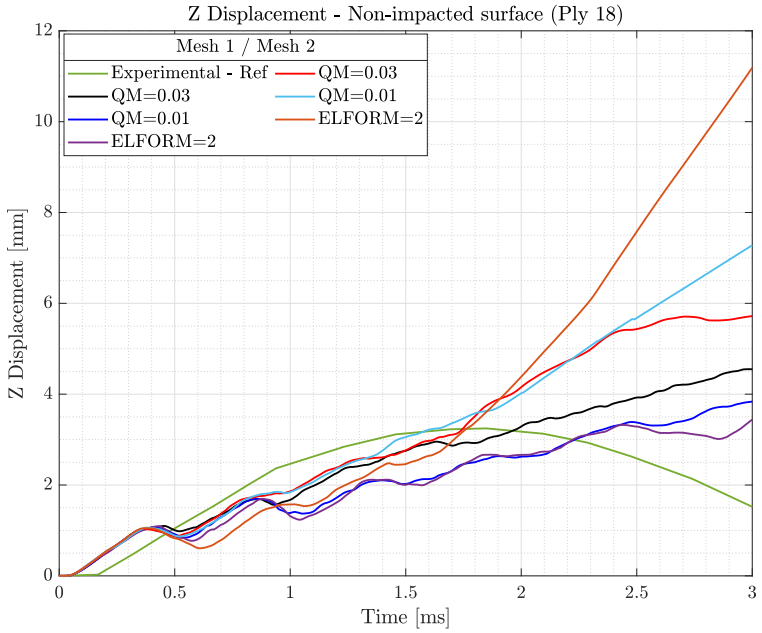

Figure 5.18: Displacement non-impacted surface (Ply 18) evolution for different element formulation and hourglass configuration. Validation with experimental reference results [25].

The lack of consistency is due to the limitations discussed at multiple points of this chapter, and that will be summarized again in the conclusions. However, the most relevant limitation for this model is the simplified material model. In low velocity impact modelling, where the strain rate is much lower, the strength-softening and strain to failure parameters of the composite material formulation need to be more precise. To this end, calibration with standard and non-standard material testing data is crucial. Furthermore, these parameters are also highly sensitive to the mesh size of the target, and this explains the divergence of the results such as the impact energy or the displacement.

Fig. 5.19 shows the matrix tensile cracking history variable (H3) at the end of the simulation $t = 3$ ms, for the full integrated elements case and the reduced integration technique with the chosen scale factor (QM=0.01). By comparing these two models, it is clear that the full-integrated plate breaks in more brittle pattern. This proves the introduction of artificial stiffness (locking) on the plate, which is more visible in Fig. 5.20 where the lateral view (bottom) is shown.

The fringe plots show the penetration of the plate by the projectile, which does not correspond to the behaviour seen in the experimental tests, where the plate deformed but then recovered some of its initial shape and bended back. As a conclusion, perhaps the error is mostly introduced by the strain to failure of the fibre tensile breakage (DFAILT) since this is the failure model that leads to penetration. However, due to the complex

behaviour of composites during impact failure and to the lack of resources to carry out the necessary experimental tests, this can only be stated as a hypothesis.

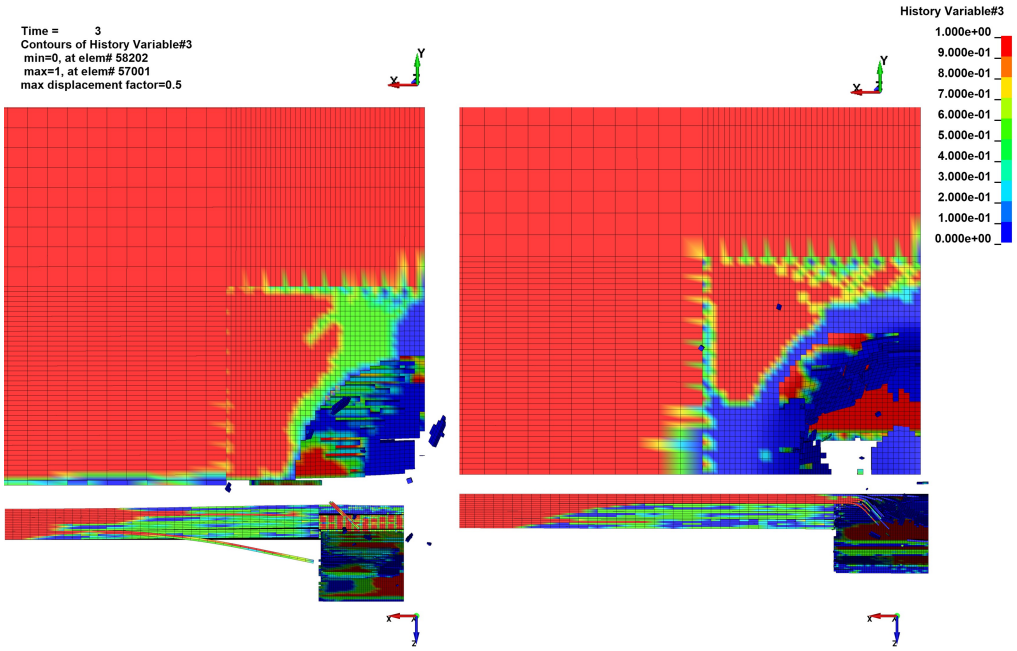

Figure 5.19: Top (upper) and frontal (bottom) view of matrix tensile failure history variable (H3) at time $t = 3$ ms, for different element formulations: full integration (left) and reduced integration with hourglass scale factor 0.01 (right)

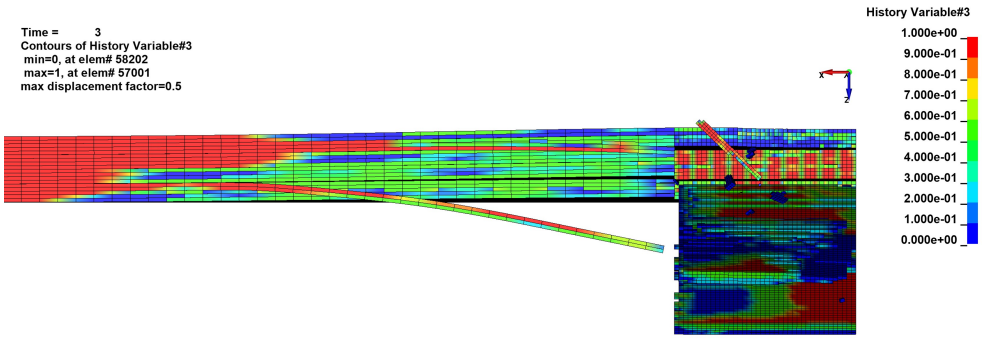

Figure 5.20: Frontal view of matrix tensile failure history (H3) at time $t = 3$ ms for full integration model.

Chapter 6

Conclusions and Future Work

In this chapter, the main objectives, conclusions extracted and limitations.for both models are included. At the end of the chapter, a final remark on the future work that could be done in this line of research is summarized.

6.1 General Objectives

Before enumerating the conclusions extracted from both models, the main purpose of developing both high and low velocity impact models is explained. In addition, a common assumption made for both models is explained before analyzing the final conclusions.

The usefulness of the **high velocity model** is to predict the ballistic response of a composite structure as well as the location and distribution of the main sources of damage, to later enhance its resistance properties. The model carried out in this project contributes to the numerical research of high velocity impact studies, enabling to model this phenomenon without the need of expensive and almost always destructive experiments. Moreover, the methodology developed for the numerical and physical parametrical studies can be applied in future FOI models for more complex components, such as fan blades subjected to bird strike.

Damage examination of **low velocity** impacted specimens is not always possible through visual inspection, and that is the main drive of investing effort on developing reliable numerical models. Note that, while low velocity impact damage on metallic components usually starts from the impacted surface, on composite targets, significant amount of permanent damage in the form of subsurface delaminations, matrix cracking and fiber breakage may be present without being detectable by "outside" visual inspection. These damages can result in a significant strength reduction, compromising the safety of the structure and constituting the most difficult challenge on composite material design.

A important assumption made in both models is that carbon fibres are often thought

of as being strain rate independent [50]. Another important limitation that affects both models is the number of through thickness integration points per ply. When using 1-point reduced integrated solid element layers for each ply, there is a lack of accuracy particularly in bending deformation. In order to solve this issue, the introduction at least 3 additional integration points through thickness is recommended for future enhancements of the model (each ply should be represented by 3 layers of solid elements with its correspondant integration point in the middle).

6.2 Conclusions

The main conclusions that came from the **High Velocity Impact model** numerical and physical analysis carried out of the results are:

- The **contact algorithm** from the reference configuration (*CONTACT_AUTOMATIC _SINGLE_SURFACE), which defined all the contact interactions present in the impact in the same option, is divided in two simple contact interactions, to account separately for the contact between the projectile-plies and the contact between different plies. This adjustment provided better results in terms of computational effort, numerical stability thorough the simulation, and work performed by the hourglass resisting forces.

- The **element and hourglass control method** chosen were 8-node solid elements with 1-point integration (centroid) together with a stiffness control hourglass algorithm (IHQ=4) with a scale factor of $QM = 0.03$.

  The use of viscous resisting hourglass forces was completely discarded due to the large unphysical effects introduced in the model. This was visible in the impact energy absorbed by the plate, which was clearly underestimated due to the artificial stiffness.

  Fully integrated elements were also discarded as an option. Although the contact algorithm remains stable and the presence of hourglass modes is no longer an issue, full integrated elements introduced ”locking” and the computational effort was doubled for this configuration.

- The **mesh refinement study** proved that, as the mesh is refined, the presence of hourglass modes decrease. Thus, the scale coefficient (QM) needed to be adjusted to a different value for each mesh distribution.

  The impact energy and the projectile's velocity evolution start to converge for finer mesh densities, and also with the reduction of the hourglass scale factor. However,

full convergence was not reached for the four mesh refinements introduced in the impact area. There is also a difference in the deforming rate of the plate from the present and reference models. The reference model's plate deforms in a less brittle manner, absorbing internal energy more progressively.

The residual velocity of the projectile was measured through tests in [39] and compared with the present model results. It was shown that, as the mesh is refined the residual velocity converges but to a value slightly higher than the experimental one. The accuracy of the model increases for higher impact velocities of the projectile. As the velocity increases, the impact is shorter and the plate damage develops in less time. As a consequence, the error introduced by the poor intra and interlaminar failure models has less influence over the final results.

- The removal of the **strain to failure (or erosion) parameters** (DFAILT, DFAILC, DFAILM and DFAILS) results in higher impact energy absorbing capability of the plate. Remember that, these strains were roughly approximated as recommended in [57] for tensile and compressive loading tests.

  When composite elements reach the failure criteria (stress based), they are unabled to carry higher stresses. However, the stress distribution on them is not driven to zero, i.e. these elements are not removed from the simulation, until the strain to failure is reached. In this particular case, the failure strains decreased the absorbing capability of the composite. Thus, by removing these parameters, the number of eroded elements is much lower, and the plate is able to absorb more energy representing better the actual response in reality.

- The **thickness of the plate** was varied from the 16-ply baseline case, to a 8-ply and a 32-ply models, to modify the stiffness and to estimate the response to impact. The energy absorbed per ply is practically the same for the plate with 16 and 32 plies. This indicates that the total energy absorbed capacity of the plate is directly proportional to the number of plies.

- The **stackup sequence** was also varied in order to examine the effect of fibre orientation on the response. By introducing replacing the $+45\,\mathrm{deg}$ fibre oriented ply by a $0\,\mathrm{deg}$ fibre oriented ply in the impact surface (ply 1) the composite plate is able to absorb a slightly higher impact energy showing a slightly more flexible behaviour.

However, the results were influenced by some limitations of the model that must be highlighted to understand its weak points:

- The **material formulation** employed in the reference [6] is an advanced progressive damage composite material model, which requires a commercial license not available

for the author. As a consequence, the parameters from the reference material formulation were translated to a an option compatible with the author's license.

The material formulation employed has been previously described in section 3.3.3 and is the *MAT_054 in LS Dyna database [32]. The chosen formulation is able to model the initiation of damage through stress-based criteria, the strength-softening of the composite (not introduced in the present case), and the erosion of elements through some failure strains parameters. This last feature introduces an additional source of error, since these strains were roughly approximated as recommended in [57] for 1D tensile and compressive loading tests.

- The **poor quality of the mesh** in terms of connectivity. The four different mesh refinements were only implemented in the impact area of the plate, which is the limited surface where the plate experiences most of its deformation. This imposes a clear limitation on the mesh quality and reduces the accuracy of the results. The nodes from the refined area are connected to the rest of the plates by means of tying constraints.

In the **Low Velocity Model**, delamination failure is one the most relevant damage mechanisms. That is why it is strongly recommended to perform an independent sub-model to solve the delamination problem, removing the intralaminar failure part of the material model, as performed in this present work under the name of **"Elastic Model"**. The main conclusions extracted from this sub-model are:

- On the **contact algorithm** development it was found that, by removing the tiebreak contact interaction between the same fibre-oriented plies, the model is optimized in terms of CPU time. Moreover, the unphysical effects introduced by the work done by the normal contact forces is reduced and, thus, the results are more reliable. This was observed on the analysis of the main physical quantities of the impact problem e.g. the displacement of the non-impacted surface (ply 18), the total normal contact force evolution. The removal of this unnecessary tiebreaks reduces the artificial stiffness introduced in the model and allows the plate to absorb more impact energy.

- The **delamination model** based on tiebreak contacts was also analyzed in depth. In terms of numerical robustness, the OPTION=9 is the best approach. This option employs a bilinear traction-separation law to represent the delamination damage evolution. The physical results, such as the displacement of the non-impacted surface, the normal contact force or the delaminated area, proved consistency in the present numerical method independently of the contact option used. The delaminated area was also compared with experimental C-Scans from the reference model. Some clear differences where encountered between the experiments and the numerical results.

However, the ”Elastic Model” developed in this work has some important restrictions:

- Elastic behaviour of the composite plate which is clearly not realistic, as the composites do fail in a brittle manner.

- The discontinuity in the nodes displacement field which appears when checking the hourglass deformation modes present in the model. The cause for this discontinuity is open for discussion, as it comes from a bug on the present model. However, it could be due to the poor mesh quality generated by connecting the impact area elements to the large aspect ratio elements from the rest of the plate, or the lack of a failure criterion inside the material formulation.

Once the delamination model is optimized and the consistency of tiebreak contacts is proved, the material formulation employed in the high velocity model (*MAT_ENHANCED _COMPOSITE_DAMAGE or *MAT_054) is introduced in the low velocity case to account for intralaminar failure along with the previously developed model for delamination. As a result from this sub-model named **”Failure Model”**:

- On the **composite material formulation**, the introduction of failure strain parameters in the model (DFAILT, DFAILC, DFAILM and DFAILS), which were obtained through experimental tests carried out in the reference study [25], reduces the brittle response of the composite to impact, and allows to represent its damage process more smoothly.

- The **element formulation and hourglass algorithm** recommended is the reduced 1-point integration solid (ELFORM=1) with stiffness hourglass control algorithm with a scale factor of QM=0.01. However, the hourglass resisting and contact forces work are still very high so, it is convenient to refine the mesh in the impact area.

- From the **mesh refinement** study it can be concluded that numerically, the hourglass resisting forces work is not greatly reduced, for a refined mesh. Moreover, the mesh refined model shows an increase on the work done by sliding contact forces.

  About the physical analysis, there is not a clear convergence in any of the physical results, which shows that the model has some important numerical limitations. The difference between the reference experimental contact force and the numerical model exhibits a brittle behaviour of the plate when compared to the reality. Also, the displacement plot shows that the last ply which is supposed to bend back and recover some of its initial shape, indicates that the plate gets finally penetrated by the projectile.

The limitations of the low velocity impact "Failure Model", able to model intralaminar and interlaminar behaviour are clearly specified in this last part:

- For this mode, another symmetry was introduced into the YZ-plane. This mostly affects the reliability of results such as the delamination area, which clearly does not have a perfectly symmetric shape.

- Once again, the reference study material model (*MAT_162) is not compatible with the current author's LS Dyna license. This formulation is more advanced and allows to model the effect of strain rate and strength progressive softening during failure. The parameters necessary for this option were obtained through calibration with standard and non-stardard material testing procedures in the reference study [25], as detailed in the Appendix 8.

  These parameters were introduced into the present material formulation (*MAT_054) to model the failure onset and strain to failure phenomena. The translation of these parameters from the reference material formulation to the present one is approximated, and thus, introduces a relevant source of failure in the model.

  The strength softening parameters (YCFAC, FBRT), were not specified in the reference study [25]. The lack of representation of the progressive softening of the composite material is probably the most critical limitation of the model. However, it is known the high difficulty to obtain the physical softening response of most quasi-brittle materials including fiber-reinforced composites. The softening response heavily depends on the set-up and test machines, which can lead to very scattered results. Consequently the choice of damage parameters for each mode is still an open issue for the case of impact of brittle materials such as composites.

6.3 Future Developments

There are some of future lines of work in this research field. The first line is directed towards the EleFanT project direction, and the second focuses on the evaluation of the impact response of composite structures and intra and interlaminar impact damage characterization models.

First, in the frame of the EleFanT project, the next step would be to transport this methodology, particularly the high velocity impact model, to represent a foreign object impact (FOI) on their designed composite fan blade. In this future line of work, there are several aspects of the present work that could be useful:

- The representation of the blade geometry and assigning the material fibre orientation for every ply on LS Dyna is a quite complex procedure, specially when employing

solid elements. It is recommended to first define the direction of the plies on t-shell elements (TSHELL_BETA), which is a more intuitive and direct process, and then transform the t-shell elements to solid orthotropic elements (SOLID_ORTHO) [35]. The orthotropic solid elements will keep the assigned directions in the t-shells and are more reliable, particularly for representing delamination.

- The final goal is to develop a complete bird strike model on the EleFanT designed blade, for which a separate study, only focused on the representation of the bird, must be conducted. In fact, one of the first parts of the development of an accurate soft-projectile (bird) is to perform a preliminar model of the impactor on a rectangular plate. In this step, the developed high and low velocity models constructed in this work, along with the methodology employed to evaluate its numerical stability and physical reliability, are of great help.

On the evaluation of the response to impact and damage mechanisms developed during impact on composite structures, there is also additional work that could be done in the following areas, in order to enhance the accuracy and robustness of the presented models.

- The available material model MAT54 ”Enhanced Composite Damage” in LS-DYNA is more often used to simulate damage progression in dynamic failure simulations because it requires a reduced number of experimental input parameters compared to damage mechanics-based material models, and is available for all licenses [20].

  The main inconvenient of this formulation is that it is sensitive to changes in model parameters, which are either non-physical (i.e. are purely mathematical), or cannot be measured experimentally. These include element size, contact definition, load–penetration curve, and crush front softening parameter, among others. This issue appears in this work and to enhace the accuracy if these models the following recommendations are given on the intralaminar failure model:

  - Development of numerical procedures to calibrate the strength softening parameters (FBRT and YCFAC), which cannot be measured experimentally [20] and need to be determined by trial and error. A study of their sensitivity with respect to the numerical aspects of the model is recommended.
  - The four failure strains parameters (DFAILT, DFAILC, DFAILM and DFAILS) need to be measured through coupon-level tests or one-element numerical simulations.
  - Numerical calibration of the SOFT parameter, or crush front reduction factor, which is a mathematical expedient used to reduce the strength of the elements

immediately ahead of the crush front. This parameter cannot be measured experimentally and needs to be callibrated through trial and error.

- The characterization of the interlaminar failure of the composite plates in the present work is also based on reference model experimental data, as explained in more detail in the Appendix 8. Although the delamination model (”Elastic”) developed in this work provides rather good results when compared to the experimental data, the fracture toughness acquisition process could be refined. By developing the necessary experiments and numerical models of the Double Cantilever Beam (DCB) and the End Loaded Split (ELS), the normal/shear fracture toughness, failure tractions and stiffness values could be refined, and delamination through the tiebreak contacts would be more representative of the reality of the impact phenomenon.

- As a final recommendation, shell elements could be introduced to represent the intra and interlaminar damage in the composite. It would be interesting to compare these results with those obtained through solid elements in this project. The use of shell elements could reduce the computational effort and give flexibility to the model.

  However, it must be acknowledged that some accuracy, particularly in the representation of delamination, is probably compromised by using a shell element layup structure. In this type of element configuration some plies would be represented by integration points and not by element layers. This is why, this adjustment is recommended only for the high velocity impact model, where this failure mechanism is not predominant.

Bibliography

[1] Serge Abrate. Impact on laminated composite materials. 1991.

[2] Serge Abrate. Modeling of impacts on composite structures. *Composite structures*, 51(2):129–138, 2001.

[3] Anonymus AC09036782. *Standard test method for mode I interlaminar fracture toughness of unidirectional fiber-reinforced polymer matrix composites*. ASTM Internat., 2007.

[4] Adi Adumitroaie. *Initiation and Evolution of Matrix Cracking in Non-Symmetric Laminates under in-Plane and Flexural Loading*. West Virginia University, 2012.

[5] GKN Aerospace. GKN AEROSPACE TO LEAD DEVELOPMENT OF ELECTRIC FAN THRUSTER FOR ELECTRIC AIRCRAFT. https://www.gknaerospace.com/en/newsroom/news-releases/2021/gkn-aerospace-to-lead-development-of-electric-fan-thruster-for-electric-aircraft/, 2021. [Online].

[6] LS Dyna Aerospace Working Group. Test case id awg-erif-7 ballistic impact on composite plate. https://awg.ansys.com/QA+test+example+7, 2023. [Online].

[7] Leye M Amoo. On the design and structural analysis of jet engine fan blade structures. *Progress in Aerospace Sciences*, 60:1–11, 2013.

[8] AA Baker, R Jones, and RJ Callinan. Damage tolerance of graphite/epoxy composites. *Composite Structures*, 4(1):15–44, 1985.

[9] Suri Bala. Tie-break contacts in ls-dyna. *Livemore Software. USA*, 2007.

[10] M. Bruyneel. Mechanics of composites. classical lamination theory. University of Liège, Liège Belgium, 2021.

[11] The Arup Campus. Introduction to Composites Modelling in LS-DYNA. https://www.oasys-software.com/dyna/wp-content/uploads/2019/03/6_Composites_Modelling_LS-DYNA_Galal-Mohamed-IN.pdf, 2018. [Online].

[12] Wesley J Cantwell and John Morton. The impact resistance of composite materials—a review. *composites*, 22(5):347–362, 1991.

[13] FK Chang. A progressive damage model for laminated composites containing stress concentration. *J. Compos. Mater.*, 21:809–833, 1987.

[14] Yen Chian-Fong. Ballistic impact modeling of composite materials. In *Proceedings of the 7th international LS-DYNA users conference, Detroit, Michigan*, pages 15–25, 2002.

[15] LJ Deka, SD Bartus, and UK Vaidya. Damage evolution and energy absorption of frp plates subjected to ballistic impact using a numerical model. In *9th International LS-DYNA Users Conference*. Dearborn, MI, 2006.

[16] Fatih Dogan, Homayoun Hadavinia, Todor Donchev, and Prasannakumar S Bhonge. Delamination of impacted composite structures by cohesive zone interface elements and tiebreak contact. *Central European Journal of Engineering*, 2:612–626, 2012.

[17] Wolf Elber. The effect of matrix and fiber properties on impact resistance. *Tough Composite Mater.*, 1984.

[18] FAA. 14 CFR 33.76 - Bird ingestion. https://www.govinfo.gov/app/details/CFR-2011-title14-vol1/CFR-2011-title14-vol1-sec33-76/summary, 2011. [Online].

[19] AC FAA. Ac 20-107b, composite aircraft structure. *US Department of Transportation Federal Aviation Administration*, 2009.

[20] Paolo Feraboli, Bonnie Wade, Francesco Deleo, Mostafa Rassaian, Mark Higgins, and Alan Byar. Ls-dyna mat54 modeling of the axial crushing of a composite tape sinusoidal specimen. *Composites Part A: applied science and manufacturing*, 42(11): 1809–1825, 2011.

[21] Jacob Fish and Ted Belytschko. *A first course in finite elements*, volume 1. Wiley New York, 2007.

[22] Bazle Z Gama Haque. A progressive composite damage model for unidirectional and woven fabric composites. *MAT162 user manual*, 10, 2015.

[23] Zvi Hashin. Fatigue failure criteria for unidirectional fiber composites. *Journal of applied mechanics*, 47(4):329–334, 1980.

[24] Sebastian Heimbs, Sven Heller, and Peter Middendorf. Simulation of low velocity impact on composite plates with compressive preload. In *Proceedings of The 7th German LS-DYNA Forum*, 2008.

[25] Muhammad Ilyas. *Damage modeling of carbon epoxy laminated composites submitted to impact loading*. PhD thesis, Université de Toulouse, 2010.

[26] ASTM International. Standard d7136 - standard test method for measuring the damage resistance of a fiber reinforced polymer matrix composite to a drop weight impact event. http://dx.doi.org/10.1520/D7136.

[27] G Kay, D Urabe, A Shields, and S DeTeresa. Characterization of bms-8-212 for use in penetration simulations. Technical report, Lawrence Livermore National Lab.(LLNL), Livermore, CA (United States), 2007.

[28] Keith T Kedward. Large composite fan blade development for modern aeroengines. In *Proc. 11th Int. Conf. on Composite Materials*, volume 1, pages 200–217, 1997.

[29] PPM Lemmen and GJ Meijer. Failure prediction tool theory and user manual. *TNO Report*, 769, 2001.

[30] Dahsin Liu and Lawrence E Malvern. Matrix cracking in impacted glass/epoxy plates. *Journal of Composite Materials*, 21(7):594–609, 1987.

[31] AN ANSYS COMPANY LIVERMORE SOFTWARE TECHNOLOGY (LST). *LS-DYNA® KEYWORD USER'S MANUAL - VOLUME I*. LIVERMORE SOFTWARE TECHNOLOGY (LST), AN ANSYS COMPANY, .

[32] AN ANSYS COMPANY LIVERMORE SOFTWARE TECHNOLOGY (LST). *LS-DYNA® KEYWORD USER'S MANUAL VOLUME II - Material Models*. LIVERMORE SOFTWARE TECHNOLOGY (LST), AN ANSYS COMPANY, .

[33] Jorge López-Puente, Ramón Zaera, and C Navarro. The effect of low temperatures on the intermediate and high velocity impact response of cfrps. *Composites Part B: Engineering*, 33(8):559–566, 2002.

[34] LSTC. Modeling of composites in ls-dyna. https://ftp.lstc.com/anonymous/outgoing/jday/composites/mat_comp.pdf, .

[35] LSTC. Composites preprocessing. https://ftp.lstc.com/anonymous/outgoing/support/FAQ_kw/composites/composite_preprocessing, .

[36] Djilali Beida Maamar and Zenasni Ramdane. Characterization of the mechanical behaviour of carbon fiber composite laminate under low velocity impact. *Periodica Polytechnica Mechanical Engineering*, 60(3):142–151, 2016.

[37] Pankar K Mallick. *Fiber-reinforced composites: materials, manufacturing, and design*. CRC press, 2007.

[38] George Marsh. Aero engines lose weight thanks to composites. *Reinforced Plastics*, 56(6):32–35, 2012.

[39] Grama Praveen Matti Loikkanen and David Powell. Simulation of ballistic impact on composite panels. In *10th International LS-DYNA Users Conference*. DYNAlook, 2008.

[40] E Moncayo, H Wagner, and K Drechsler. Benchmarks for composite delamination using ls-dyna 971: Low velocity impact. In *Proceedings of the German LS-DYNA Forum, Frankenthal, Gemany*, pages 11–12, 2007.

[41] Ph.D Morten Rikard Jensen. Specification of directional depended materials in ls-dyna®. chrome-extension://efaidnbmnnnibpcajpcglclefindmkaj/https://ftp.lstc.com/anonymous/outgoing/support/PRESENTATIONS/orthotropic-materials-draft-mrj.pdf, 2011. [Online].

[42] Salah A Muflahi, G Mohamed, and Stephen R Hallett. Investigation of delamination modeling capabilities for thin composite structures in ls-dyna. In *Proceedings of the 13th International LS-DYNA Users Conference, Detroit, MI, USA*, pages 8–10, 2014.

[43] John O.Hallquist. *LS-DYNA® THEORY MANUAL*. LIVERMORE SOFTWARE TECHNOLOGY (LST), AN ANSYS COMPANY.

[44] Morgan Osborne. *Single-element characterization of the LS-DYNA MAT54 material model*. University of Washington, 2012.

[45] Emily Owen. Webinar: LS-DYNA Introduction to contacts. https://www.oasys-software.com/dyna/training/webinars/ls-dyna-intro-to-contacts/, 2020. [Online].

[46] LS DYNA Support page. Contact. https://www.dynasupport.com/howtos/contact/soft-option, 2003. [Online].

[47] LS DYNA Support page. Hourglass (HG) Modes. https://ftp.lstc.com/anonymous/outgoing/support/FAQ_docs/hourglass.pdf, 2003. [Online].

[48] LS DYNA Support page FAQ. Energy Balance. https://ftp.lstc.com/anonymous/outgoing/support/FAQ/energy_balance. [Online].

[49] David Powell, Tarek Zohdi, and George Johnson. Impact and delamination failure characterization of bms 8-212 composite aircraft material. 2008.

[50] MOW Richardson and MJ Wisheart. Review of low-velocity impact properties of composite materials. *Composites Part A: Applied Science and Manufacturing*, 27 (12):1123–1131, 1996.

[51] Ralph R Roe Jr. Standard materials and processes requirements for spacecraft. *NASA Technical Standard. NASA-STD_6016A*, 2016.

[52] SNA Safri, MTH Sultan, N Yidris, and F Mustapha. Low velocity and high velocity impact test on composite materials–a review. *Int. J. Eng. Sci*, 3(9):50–60, 2014.

[53] Karl Schweizerhof, K Weimar, Th Munz, and Th Rottner. Crashworthiness analysis with enhanced composite material models in ls-dyna–merits and limits. In *LS-DYNA world conference*, pages 1–17, 1998.

[54] KN Shivakumar, W Elber, and W Illg. Prediction of low-velocity impact damage in thin circular laminates. *AIAA journal*, 23(3):442–449, 1985.

[55] Youchao Sun, Yuemei Zhang, Yadong Zhou, Haitao Zhang, Haijun Zeng, and Kun Yang. Evaluating impact damage of flat composite plate for surrogate bird-strike testing of aeroengine fan blade. *Journal of Composites Science*, 5(7):171, 2021.

[56] Stephen W Tsai and Edward M Wu. A general theory of strength for anisotropic materials. *Journal of composite materials*, 5(1):58–80, 1971.

[57] Bonnie Wade, Paolo Feraboli, and Morgan Osborne. Simulating laminated composites using ls-dyna material model mat54 part i:[0] and [90] ply single-element investigation. *FAA JAMS: Baltimore, MD, USA*, 2012.

[58] Vladislav Yastrebov. *Computational contact mechanics: geometry, detection and numerical techniques*. PhD thesis, École Nationale Supérieure des Mines de Paris, 2011.